NUNO EDUARDO BUXO CARINHAS

# SYSTEMS BIOTECHNOLOGY OF BACULOVIRUS-PRODUCING INSECT CELLS

**SUPERVISORS:**
Dr. Paula Maria Marques Leal Sanches Alves
Dr. Rui Manuel Freitas Oliveira

Dissertation presented to obtain the Ph.D degree in *Ciências da Engenharia e Tecnologia, especialidade Biotecnologia*

Instituto de Tecnologia Química e Biológica, Universidade Nova de Lisboa
OEIRAS, SEPTEMBER, 2011

## ACKNOWLEDGEMENTS

Dr. Paula Alves and Prof. Rui Oliveira, my co-supervisors, for the confidence, availability and support along the years of this thesis and before. Paula for her stewardship in the world of animal cell technology, her practical side and her decisive presence during the determinant moments. Rui for introducing me into modeling in systems biology, the enticing discussions and critical guidance along the way. Both have contributed enormously for me to grow as a scientist and as a person.

Prof. Manuel Carrondo, whose words I eagerly conserve and which have the strange peculiarity of bottoming inside my brain over time: each conversation bears the fruit for something yet to come.

Dr. Vicente Bernal, whom I can consider my every-day guide during a great part of this thesis. His intelligence and knowledge have made a difference to this work. His support and friendship have made a difference to me.

Dr. Paul Jenö, who not only gave me the opportunity to be at his lab but also made me feel a part of it. Paul and Suzette are the nicest people and they absolutely love what they do.

Dr. Ana Teixeira, my first mentor, with whom I have learned and shared so much during these years. Her so many qualities as a scientist and as a person make her a unique person in my life.

All the colleagues from the Animal Cell Technology Unit, past and present, a dynamic group of people making things happen every day.

To my brother and my friends.

To my parents, who have contributed for most of who I am, for their love and everything else.

## SUMMARY

A critical step in the biopharmaceutical industry is the capacity to properly manufacture biological products in animal cell cultures. The ability to exploit the full potential of the underlying “cellular factories” is essential to reduce manufacturing costs and improve yield and product quality, thus freeing up resources to pursue other added value activities, such as clinical development and pharmacovigilance of new products. Bioprocess optimization efforts have mostly relied on empirical experience and rational, hypothesis-driven studies, rather than by fully leveraging the knowledge of how complex cells behave in culture. Despite the vast amount of information available on different cellular features, specific productivity improvements have been essentially incremental. The relatively recent developments in Systems Biology and computational methodologies present a paradigm-shifting opportunity to develop biotechnology processes with high efficiencies in a consistent, systematic way.

The present thesis focuses on optimizing baculovirus vectors (BV) production in *Sf*9 insect cell cultures, where a significant bioprocess challenge is the tendency for specific product yields to decrease when cell cultures are infected at later stages of growth, the so-called cell density effect. Given the complexity of the biological system under study, there is a need to address this issue from a fundamental, integrated perspective.

In chapter I, the basic bioprocess parameters affecting BV production are assessed in serum-free medium, analyzing how productivity is affected by varying cell concentrations and infection conditions. The results confirm a cell density effect, which can be partly overcome by replacement of the medium upon infection. However, metabolic substrate limitations were not observed, suggesting a more complex phenomenon. To explore this further, a stoichiometric model of the central energetic metabolism of *Sf*9

cells is developed in Chapter II to investigate physiological adaptations incurred along culture growth and as a response to infection. It is shown that cells undergo a progressive inhibition of their central metabolism when grown to high cell densities, and that an up-regulation of their central energy metabolism occurs at low cell concentrations after infection (CCI); nevertheless, this up-regulation fails to occur or is inhibited at high CCI when compared to uninfected cultures. To test the hypothesis that the energetic status of the cells is a key determinant of system productivity, we screened the effect of culture supplementation with a variety of nutrients and energetic intermediates of their central metabolism (Chapter III). Since productivity is independent of the availability of nutrients in the medium, it was not significantly improved upon addition of amino acids, lipids or complex nutrient mixtures; on the other hand, specific BV yields could be increased up to 7 fold after supplementation of pyruvate and α-ketoglutarate at the time of infection. These results represent a rational and cost-efficient strategy for high cell density production of recombinant BVs, confirming that more complex mechanisms underlie the cell density effect.

Though based on a rational study, this early work does not represent a systematic means to optimize bioprocesses since our model could not explicitly account for product formation, being based instead on empirical inspection. In Chapter IV, we attempt to demonstrate how a more global quantitative understanding of cell function can be translated into predictable bioprocess benefits. For this, a hybrid framework combining the same stoichiometric model with a statistical sub-model able to bridge the estimated metabolic fluxes with measured productivities is developed. Based on the data accumulated in the previous chapters, the importance of the same determinant pathways for viral replication is highlighted by using

an unbiased subset of preliminary experiments, while the productivity of independent cultures was predicted within experimental error.

Finally, chapter V describes the first proteomic survey of the *Sf*9 cell line, an attempt to explore the application of omic technologies as high-throughput, hypotheses generating tools in this system. In order to circumvent the lack of a complete genome sequence and annotation, a database was constructed with available sequences of related species, followed by a homology-based computational search. A thorough statistical analysis of biological replicates allowed us to confidently discriminate differentially expressed proteins due to culture growth and BV infection. Our findings suggest a possible mechanism for the cell density effect that is related with the differential accumulation of BV-encoded proteins detected during the initial stages of infection, which is influenced by the cell physiological state. While the results presented here have revealed deeper insight into the basis of this phenomenon, it is likely that a complete understanding can only come from an integrated view of the complex cell, a fundamental scientific goal that has yet to be accomplished.

In conclusion, a case-study is presented of how existing bioprocesses can be greatly improved with Systems Biology approaches that decode biological complexity beyond traditional R&D efforts. It is expected that Systems Biotechnology will follow the fields of biomedicine and drug discovery into this paradigm shift.

## SUMÁRIO

Um dos passos críticos na indústria biofarmaceutica é a capacidade de manufactura de produtos biológicos em culturas de células animais. A possibilidade de explorar completamente o potencial destas "fábricas celulares" é essencial para reduzir custos de produção, melhorar o rendimento e a qualidade do produto, desta forma libertando recursos para outras actividades de valor acrescentado, como o desenvolvivmento clínico e a fármaco-vigilância de novos produtos. A optimização de bioprocessos tem assentado principalmente em conhecimento empírico e estudos racionais dirigidos por hipóteses, mas pouco alavancado numa compreensão da complexidade celular e do seu comportamento em cultura. Apesar da vasta informação gerada a diferentes níveis celulares, a melhoria no rendimento de produtos biológicos tem sido apenas incremental. Neste sentido, os desenvolvimentos recentes em Biologia de Sistemas e métodos computacionais constituem uma oportunidade para mudar o paradigma actual e desenvolver processos biotecnológicos altamente eficientes de uma forma consistente e sistemática.

A presente tese foca-se na optimização da produção de vectores de baculovirus (BVs) em células de insecto (*Sf*9), em que um importante desafio a nível de bioprocesso é a tendência para o rendimento específico diminuir substancialmente quando a infecção é efectuada a alta densidade celular, o chamado efeito da densidade celular. Tendo em conta a complexidade do sistema biológico em estudo, existe uma necessidade de abordar esta questão através de uma perspectiva fundamental e integrada.

No Capítulo I, os parâmetros de bioprocesso básicos que afectam a produção de BVs, tais como concentração celular e condições de infecção, são analisados em meio sem soro. Os resulados confirmam um efeito negativo da densidade celular na produtividade, o qual foi possivel

minimizar recorrendo a uma troca de meio de cultura no momento da infecção. No entanto, não se verificaram quaisquer limitações de nutrientes no meio antes da troca, o que sugere tratar-se de um fenómeno de maior complexidade. Por conseguinte, desenvolveu-se no Capítulo II um modelo do metabolismo energético central das células *Sf*9 para investigar as adaptações fisiológicas que ocorrem ao longo do crescimento celular e em resposta à infecção. É mostrado que as células sofrem uma inibição progressiva do seu metabolismo central quando cultivadas até elevadas concentrações, e, quando infectadas a baixa concentração, o metabolismo energético é estimulado. Em contrapartida, esta estimulação não acontece após infecção a elevadas densidades celulares, ocorrendo mesmo uma inibição quando comparado com células não infectadas. Para testar a hipótese de que o estado energético é um determinante chave da produtividade neste sistema biológico, efectuou-se um rastreamento de diferentes suplementos nutricionais e intermediários do metabolismo energético central (Capítulo III). Uma vez que a produtividade é independente do nível nutricional disponível no meio de cultura, não foi possível ser significativamente melhorada pela adição de aminoácidos, lípidos ou uma mistura complexa de nutrientes. Pelo contrário, o rendimento específico de BVs aumentou até 7 vezes depois da suplementação de piruvato e α-cetoglutarato juntamente com a infecção. Estes resultados representam uma estratégia racional e eficiente para produção de BVs recombinantes a alta densidade celular, confirmando que mecanismos mais complexos estão na base do efeito da densidade celular.

Apesar de baseado num estudo racional, o trabalho até aqui efectuado não representa uma forma sistemática de optimizar bioprocessos porque o modelo desenvolvido não considera explicitamente a formação de produto, sendo por isso essencialmente empírico. No Capítulo IV, propomo-nos

demonstrar como um conhecimento quantitativo global do funcionamento celular pode ser traduzido, de forma preditiva, em benefícios para o bioprocesso. Para isto, estabeleceu-se uma metodologia matemática híbrida que assenta no mesmo modelo estequiométrico aqui proposto e combina uma componente estatística visando estabelecer a "ponte" entre fluxos metabólicos estimados e produtividades medidas. Baseado nos dados previamente obtidos, foi possível determinar a importância das mesmas vias metabólicas para a replicação viral usando apenas um sub-grupo imparcial de experiências preliminares, enquanto a produtividade de culturas independentes foi prevista dentro do error experimental.

Finalmente, o Capítulo V descreve o primeiro estudo proteómico em larga escala de células *Sf*9, numa tentativa de explorar a aplicação de novas tecnologias "ómicas" como ferramentas geradoras de hipóteses. De forma a obviar a inexistência da sequência genómica completa para este organismo, foi construída uma base de dados com sequências disponíveis de espécies de insectos relacionadas, as quais foram usadas para pesquisa computacional baseada em homologia. A análise estatística de replicados biológicos permitiu distinguir várias proteínas diferencialmente expressas em resposta ao crescimento em cultura e à infecção por baculovirus. Os resultados obtidos sugerem um mecanismo para o efeito da densidade celular relacionado com a acumulação diferencial de proteínas codificadas pelo próprio baculovirus durante a fase inicial após infecção, a qual é influenciada pelo estado fisiológico da célula. Apesar destes resultados revelarem um importante contributo para o aprofundamento deste fenómeno, é provável que a sua completa resolução dependa de um conhecimento integrado da complexidade celular, um objectivo científico fundamental ainda por alcançar.

Em conclusão, nesta tese é apresentado um caso de estudo em que se demonstra como um bioprocesso típico pode ser melhorado e compreendido aplicando uma abordagem de Biologia de Sistemas que foca a complexidade biológica para além da tradicional I&D. Espera-se que a disciplica emergente de Biotecnologia de Sistemas siga o caminho das áreas de Biomedicina e da descoberta de novos medicamentos no sentido desta mudança de paradigma.

## THESIS PUBLICATIONS

1. Carinhas N, Bernal V, Yokomizo AY, Carrondo MJT, Oliveira R, Alves PM (2009) Baculovirus production for gene therapy: the role of cell density, multiplicity of infection and medium exchange. *Appl Microbiol Biotechnol* **81**: 1041-1049

2. Bernal V/Carinhas N, Yokomizo AY, Carrondo MJT, Alves PM (2009) Cell density effect in the Baculovirus-Insect Cells system: a quantitative analysis of energetic metabolism. *Biotechnol Bioeng* **104**: 162-180

3. Carinhas N, Bernal V, Monteiro F, Carrondo MJT, Oliveira R, Alves PM (2010) Improving baculovirus production at high cell density through manipulation of energy metabolism. *Metab Eng* **12**: 39-52

4. Carinhas N, Bernal V, Teixeira AP, Carrondo MJT, Alves PM, Oliveira R (2011) Hybrid metabolic flux analysis: combining stoichiometric and statistical constraints to model the formation of complex recombinant products. *BMC Syst Biol* **5**: 34

5. Carinhas N, Robitaille AM, Moes S, Carrondo MJT, Jenoe J, Oliveira R, Alves PM. Quantitative proteomics of *Spodoptera frugiperda* cells during growth and baculovirus infection (*in revision*)

## GENERAL CONTENTS

## LIST OF FIGURES

# LIST OF TABLES

# INTRODUCTION

# TABLE OF CONTENTS

# 1. ANIMAL CELL TECHNOLOGY IN THE BIOPHARMACEUTICAL MARKET

Animal cell culture is currently the prime technology for the production of complex biopharmaceuticals such as therapeutic proteins, vaccines and gene delivery vectors. Its key advantage over competitor microbial cell factories lies in the ability to correctly process recombinant products, including structural and chemical alterations at the protein level, essential for therapeutic efficacy. The increased interest in complex biopharmaceuticals that have to be produced in animal cells derives mainly from 1) the need to address unmet medical needs and 2) diversification of the Big Pharma business model to participate in a high margin, rapidly growing market. Cultured cell lines derived from animal organisms are well positioned in this biotechnology revolution, a market globally valued at $US 99 billion in 2009 (Walsh, 2010).

A central concern in biopharmaceutical R&D is the capacity to properly manufacture complex biologicals in animal cell cultures, i. e., the ability to deliver enough product quantity at the right quality per unit volume of cell culture (Butler, 2005). In particular, if the productivity of a given biological can be improved, then resources can be used to pursue other activities such as development of new biological entities and clinical testing. However, the lengthy and expensive regulatory path for approval of a new market candidate significantly constrains the timeline and spending for process development. In addition, once manufacturing approval has been granted, changing the process may require new clinical trials to assure product safety. As a result, this often leads to production processes being run far below their maximum performance potential (Sommerfeld and Strube, 2005). Obviously, the need to have platforms for fast and efficient

development of production processes is a critical need for the biopharmaceutical industry.

The ability to tap the full potential of the underlying biological system would be even more relevant if recombinant products were a commodity-like business. In fact, for many of the initially marketed biologics, patent expirations are glooming the landscape for several companies, with an estimated $US 33.2 billion worth of biopharmaceuticals loosing patent protection by 2016 (Walsh, 2010). This is backed up by a continuous pipeline of innovative and potentially lucrative new products, either internally or externally developed, but concurrently opens the way for a large biosimilars market. In this business, the operational strategy must necessarily be different than the previous one, justifying a bigger emphasis on achieving productivity levels able to substantially reduce the cost per dose of the final copycat products (Hoe et al., 2011).

## 2. IMPROVING CELL CULTURE PERFORMANCE: FROM CLASSICAL TO RATIONAL APPROACHES

For recombinant monoclonal antibodies, volumetric yields above 5g/L are achievable today (Birch and Racher, 2006). Compared with a typical process in the mid 80's, with an average yield around 50mg/L, this represents at least a 100 fold increase (Wurm, 2004). Certainly, this accomplishment has alleviated capacity pressures and increased cost-efficiency of today's manufacturing processes. However, as pointed out before, the corresponding increment in per cell productivity accounted for less than half the overall volumetric increase, the majority of which resulting from a massive improvement in the accumulated viable cell number. In fact, specific productivities in 2004 were of the same magnitude

as during the early 90' for a mAb-producing myeloma cell line (Wurm, 2004). It seems therefore clear that the classical methods used to obtain high-producing cell clones have not changed materially in the past decades. These include gene selection and amplification techniques, while improvements in transfection, molecular biology of expression systems and clone screening have led primarily to an increased proportion of stable, high producer clones generated in much shorter time periods, rather than step improvements in per cell protein yields (O'Callaghan and James, 2008).

In order to improve cell culture performance, a great amount of effort has been given to the design of media formulations able to support high cell densities and, to a lesser extent, improved cell specific productivities. Media optimization is usually performed on an individual basis for each cell line; often, more than one formulation is used at different phases of the manufacturing process, typically including medium designed for growth and for production. Such knowledge has accumulated over many years of experience and empirical trial-and-error, culminating with the breakthrough of complete removal of undefined medium components (such as serum and hydrolisates) in several processes. The current state of the art, however, is simply a more elaborate form of trial-and-error, design of experiments (DoE), whereas the long development times required for this step remain a bottleneck.

A general approach to directly increase specific productivity is to alter the growth phenotype of the cell line, namely by impairing proliferation after reaching a desired cell density in order to shift resources to productivity. Several methods of manipulation have been used for this purpose, including reduced temperature (Yoon et al., 2004), hyper-osmolarity (Ozturk and Palsson, 1991), the addition of cell cycle inhibitors (Carvalhal

et al., 2003) or proliferation inhibitors (Balcarcel and Stephanopoulos, 2001). However, strategies to halt or reduce proliferation, though leading to increased productivities on a per cell basis, result in less impressive volumetric titers owing to limited cell growth. Other straightforward strategies to directly increase specific productivity at the expense of growth include the supplementation of dimethyl sulfoxide (Rodriguez et al., 2005), thought to assist protein folding and processing in the cell, or sodium butyrate (Jiang and Sharfstein, 2008), a histone deacetylase inhibitor. Apart from culture manipulation, cell engineering has been used to either prolong the lifespan of cultured animal cells by preventing apoptosis or, as in the previous examples, genetically halting growth (reviewed in Gòdia and Cairó, 2002). While successful results have been achieved for specific cell lines, there is still a difficulty in predicting the effects of a given engineering strategy (Mastrangelo et al., 2000); in one example, the outcome of manipulating single genes to induce growth arrest was the induction of apoptosis (Mazur et al., 1998). This is explained by limited knowledge of these complex pathways and the varying genetic backgrounds of individual cell lines.

A substantial body of work on the rational improvement of cell culture performance demonstrates the potential of Metabolic Engineering. These efforts have relied mainly on assessing and optimizing central metabolism to reduce overflow by-product secretion (lactate and ammonia) through either bioprocess (Cruz et al., 2000; Lee et al., 2003a) or cell (Chen et al., 2001; Irani et al., 1999) engineering approaches. Again, the major outcome has been an increased overall production associated with the generation of more productive biomass and prolonged viability rather than increasing specific productivity itself. Concurrent with the engineering of central metabolism, some rational studies have been directed towards the engineering of protein secretory pathways (Dinnis and James, 2005).

In summary, most of what has been done comes from empirical experience and hypothesis-driven studies rather than by knowing how the complex cell functions in culture (O'Callaghan and James, 2008). Despite the long accumulated knowledge on specific cellular aspects, significant productivity improvements have come mainly as result of increased cell growth and viability. There is still great pressure to reduce manufacturing costs by increasing specific product yields through effective redesign of producer cells. In particular, this could lead to the establishment of high producer "mother" cell lines that would then be transfected with the desired recombinant gene. Owing to outstanding technological advances, the molecular traits associated with high producer cells are coming to light. In what follows, a brief overview of the application of the "omics" in biotechnology is given.

## 3. THE CURRENT STATUS OF SYSTEMS BIOLOGY IN ANIMAL CELL CULTURE

Systems biology is the endeavor to organize in a comprehensive and actionable manner the data generated through high-throughput omic technologies covering the entire cellular landscape. Precursor disciplines debated with questions that are now globally addressed by the systems biologist: what are the functions of the genes sequenced in the Human Genome project? – Functional Genomics; what enzyme(s) should be manipulated to increase the production of a particular compound? – Metabolic Engineering. When applied to animal cell culture, only timid advances have been reported so far, significantly lagging the development already witnessed for industrial microorganisms (Lee et al., 2005; Otero and Nielsen, 2010; Stephanopoulos et al., 2004). This is mostly because of the unavailability of databases for biotechnologically relevant animal cell

lines, namely the lack of complete genome sequences and annotations, whereas accumulated knowledge on pathway and enzymatic activities is also scarcer (for instance, see: BRENDA – The Comprehensive Enzyme Information System, www.brenda-enzymes.org).

The most widely used omic technology in animal cell culture has been transcriptomics, the quantitative analysis of gene expression at the mRNA level (Jaluria et al., 2008). Interestingly, applications reported to date have focused on investigating the global effects of many of the traditional tools used to improve cell culture performance described above, including butyrate treatment (Gatti et al., 2007), hypothermic cultivation (Baik et al., 2006), osmotic shock (Shen and Sharfstein, 2006), metabolic shift (Korke et al., 2004), amongst others. A striking example of the lag in systems biotechnology development of animal cells is that transcriptomic surveys of the unsequenced CHO cell line have been based on a constructed library of expressed sequence tags (ESTs), or alternatively performed against the mouse genome sequence (Griffin et al., 2007), the pitfalls of which are illustrated in Gatti et al. (2007).

The prevalence of transcriptomics in cell culture studies can be attributed to the convenience of exploiting the microarray technology, which enables covering the entire genome in a single experiment. However, such surveys only give information at a basal regulatory level within the complex cell. Molecular signatures can be explored at other levels of information that are more close to its phenotypic portrait, namely expressed proteins (proteomics) and metabolites (metabolomics). In particular, proteomic studies can give qualitative and quantitative information on the effector molecules that govern cellular processes, including gene expression, metabolic reactions and cell regulation. Though somewhat limited to date, examples exist of the application of proteomics to evaluate the effects of

animal cell culture manipulations (Baik et al., 2006; Lee et al., 2003b; van Dick et al., 2003) and metabolic shift (Seow et al., 2001). One particularly interesting work explores how parental B cells develop into antibody-secreting plasma cells, therefore gaining insights into what makes a hyper-producer cell line (van Anken et al., 2003). These studies, however, are far from being “omic”, given the considerable lower coverage of the classical 2D-gel electrophoresis technology when compared with transcriptomic microarrays. More recently, breakthrough technological advances have been accomplished that put proteomics side-by-side with transcriptomics in giving a closer to genome-wide quantitative coverage of the cell (Ong and Mann, 2005). Unfortunately, these gel-free approaches have had virtually no application in animal cell biotechnology, with only one exception known from the literature (Seth et al., 2007a).

The main result from these omic studies is the high-throughput generation of hypotheses on how to manipulate cells to achieve a better production phenotype. Amongst others, genes/proteins involved in protein folding and secretion, cytoskeletal reorganization, growth control, energy metabolism and redox balance are consensually found (Seth et al., 2007b). The key question is how to exploit the data to design more productive cells and processes. Given the observed complexity, a dilemma exists over finding, if they exist, a few master regulators that could elicit system-wide responses or, alternatively, engage in the manipulation of complete pathways or networks. For instance, the existence of a reduced number of master regulators seems congruent with the concept of “metabolite hub” connecting different modules in metabolic networks (Guimerà and Amaral, 2005) and the existence of “global metabolite reporters” crosstalking to regulatory processes in the cell (Grüning et al., 2010). However, the complexity of phenotypes arising from the integration of multiple molecular layers of information makes the identification of such central molecules

extremely difficult. Thus, the integration of cellular data in a mathematical formalism can provide superior systems insights with consistent benefits for biotechnology.

## 4. INTEGRATION OF CELLULAR INFORMATION IN PREDICTIVE MODELS

Beyond the state-of-the-art of Systems Biotechnology, systems biologists today ponder how to: 1) measure the complete molecular state of the cell (molecular concentrations), 2) measure physical interactions between cell components (molecular networks), 3) model concentrations and interactions, and 4) integrate different layers of information (Ideker and Lauffenburger, 2003; Sauer et al., 2007). The major goal is to be able to predict how the complex cell responds to environmental or genetic perturbations, going an enormous step forward from the empirical hypotheses-driven approaches currently prevailing in bioprocess optimization.

Metabolic models play an important role in our understanding of biological systems as they are more closely connected with cell behavior. For instance, the growth and productive phenotypes are a direct output of metabolic flows within the cell. However, protocols for metabolome assessment and enzyme characterization have substantially lower throughput than other “omic” technologies. This is in part due to the wide range of concentrations and chemical properties of metabolites, while enzyme assays are inherently metabolite specific. For this reason, most metabolic models are based on steady-state assumptions, such as in classical metabolic flux analysis (MFA). Here, intracellular fluxes are calculated by closing intracellular metabolite balances and measuring a

number of extracellular consumption/production rates (Stephanopoulos et al., 1998). To increase flux resolution, $^{13}C$ labeling experiments have been conducted (Sauer, 2006), and optimization algorithms were developed to identify larger scale metabolic models (Kauffman et al., 2003).

The past decade has witnessed an exponential growth in metabolic reconstructions in microorganism, accompanying the surge in genome sequences available (Oberhardt et al., 2009). The practical effects of this investment are materialized in the innumerous applications of such models for *in silico* metabolic redesign of microbial strains (Blazeck and Alper, 2010; Boghigian et al., 2010). As expected, examples for animal cells are much scarcer, including the large-scale reconstruction of hybridoma cells (Sheikh et al., 2005) and human (Duarte et al., 2007) metabolic networks. In addition, several smaller scale models were also developed for animal cell lines under bioprocess-relevant conditions (see Quek et al., 2010 for a review); however, these have been mostly restricted to the evaluation of optimal conditions for cell growth and metabolic efficiency rather than leading to pronounced improvements in per cell productivity. Indeed, the complexity associated with the engineering of complex, multi-genic phenotypes, such as improving the yields of recombinant proteins, is much larger than for microorganims producing small molecules. Clearly, currently available metabolic models, either small-scale or genome-scale, do not embrace all layers of information that confer the cell phenotype, in particular detailed biosynthesis mechanisms. Nevertheless, metabolic networks provide convenient scaffolds to integrate different types of cellular data and mathematical formalisms. Efforts in this direction have included constraining metabolic fluxes with gene expression (transcription, translation) and regulation at multiple levels (Covert et al., 2008; Lee et al., 2008).

## 5. THE BACULOVIRUS-INSECT CELL SYSTEM

Insect cell lines, in particularly those derived from lepidopteran species, constitute an attractive alternative to mammalian cells for recombinant protein expression. This status is given by their susceptibility to baculovirus infection, a diverse family of arthropod pathogens containing large DNA genomes reaching up to 180 kbp (Okano et al., 2006). As happens with other viruses, not all genes are essential for viral propagation in cell culture; this has led to the technological achievement of the baculovirus expression vector system (BEVS) in the 1980's (Smith et al., 1983). The BEVS technology is commonly based on the replacement of the gene coding for a protein named polyhedrin by the gene coding for the desired recombinant protein (O'Reilly et al., 1994). In nature, polyhedrin makes up a protective matrix in which newly formed virions are stacked just prior to release from the infected insect, conveying resistance to harsh environmental conditions. Given its importance in assuring the horizontal transmission of baculoviruses, the genetic promoter of the polyhedrin gene is very strong, leading to substantial accumulation of the expressed proteins, which can be as high as 25-50 % of the total cellular protein (Ramachandran et al., 2001). Even though average volumetric productivities attained by animal cell cultures are far lower than those reported for microbial cultures, protein yields using the BEVS can be 20-250 times higher than those reported for some mammalian cell cultures, often reaching titers above 500 mg of protein per liter (Palomares et al., 2006).

The best characterized baculovirus is the *Autographa californica* multiple nuclear polyhedrosis virus (*Ac*MNPV), which has been primarily used in biotechnology to direct gene expression in cells derived from the *Spodoptera frugiperda* (fall armyworm) species. The first cell line to be widely used was the *Sf*21 clone (Vaughn et al. 1977), originated from *S.*

*frugiperda* ovaries. *Sf*9, a clonal isolate of *Sf*21, has progressively replaced its parent in the research and industrial fields owing to its improved growth and production characteristics. Several other cell lines exist that are derived from the lepidopteran *Trichoplusia ni*, namely *Tn*5 and its clonal isolate High-Five, commercially available from Invitrogen. The later is known to permit higher specific recombinant protein production than *Sf*9 cells, probably due to their larger cell size. However, this is largely compensated by the higher cell densities achieved by *Sf*9 cells (Aucoin et al., 2010), which can be easily grown to around $10\times10^6$ cells/mL in shake flasks using serum-free medium.

One of the most distinctive aspects of physiology of insect cell lines relates to their particular central metabolism: in mammalian cells, accumulation of lactate and ammonia are the main causes for poor culture performance, which has been tackled by fed-batch, medium design or cell engineering strategies; on the contrary, insect cells do not significantly accumulate lactate or ammonia, which has been attributed to a more active tricarboxylic acids (TCA) cycle in culture (Neermann and Wagner, 1996), while the primary overflow metabolite, alanine, is not known to cause growth inhibition. From a product quality viewpoint, insect cell lines provide an animal eukaryotic environment for protein processing, including folding, modification, trafficking and secretion of polypeptides. However, the complexity of such processing mechanisms is not at the same level as in mammalian cells. In terms of glycosylation, insect cells are naturally defective in galactosyltransferases and sialyltransferases, both enzymes being involved in the complex N-glycosylation pathway of higher eukaryotes (Kost et al., 2005). Nevertheless, the humanization of glycosylation pathways in insect cells has already been dealt with (Hollister et al., 2002), and a commercially modified *Sf*9 cell line is available (Mimic

*Sf*9, Invitrogen), opening the way for the production of therapeutic glycoproteins.

Due to the attributes described above, a wide repertoire of recombinant products has been expressed in insect cells using the BEVS (Summers, 2006). Besides the expression of proteins for academic research, quite a few therapeutic proteins have also been produced (reviewed in Palomares and Ramirez, 1998). In addition, the large genomic capacity and versatility of the BEVS has allowed the production of multi-subunit complexes such as Virus-Like Particles (VLPs) for vaccination (Maranga et al., 2002; Noad and Roy, 2003) and viral gene therapy vectors (Urabe et al., 2002). Currently, two biopharmaceuticals produced with this system are in the market: a human papiloma virus vaccine produced in High-Five cells (Cervarix, GlaxoSmithKline) and a seasonal influenza vaccine produced in *Sf*9 cells (FluBlok, Protein Sciences Corp.). More recently, an increasing number of investigators have tackled the use of the baculovirus vector (BV) itself for gene therapy applications (Airenne et al., 2009; Hu, 2006; Vicente et al., 2009).The manufacturing of modified BVs able to direct gene expression in mammalian cells represents a safer alternative over classical mammalian viruses. Apart from bioprocess issues, the validation of this approach still requires generating knowledge on the mechanisms governing tissue targeting, gene delivery, and host immunological responses to the engineered BVs.

## 6. STANDING BIOPROCESS CHALLENGES IN THE BACULOVIRUS-INSECT CELL SYSTEM

Although insect cell lines and the BEVS constitute a promising eukaryotic environment for recombinant protein production, significant bioprocess

challenges remain to be addressed. An inherent bottleneck of this technology is that it is a lytic system. Protein production takes place within a limited time-span during which the cell is already deteriorating from viral infection. Therefore, to increase process productivity, it is desirable to infect an insect cell culture at later stages of growth, when higher cell densities can lead to higher accumulation of product. However, early on investigators have come to the conclusion that recombinant protein yields decrease in batch cultures infected at later stages of growth (Caron et al., 1990; Reuveny et al., 1993), a bottleneck common to different biological systems and especially relevant in animal cell bioprocesses (Ferreira et al., 2005; Henry et al., 2005).

Despite multiple speculations regarding the reasons behind this so-called "cell density effect" (nutrient limitation, exhaustion of precursors, accumulation of toxic compounds, cell-to-cell contact inhibition, autocrine/paracrine secreted factors), the fundamental mechanisms remain elusive (Doverskog et al., 1997; Taticek and Shuler, 1997). A number of strategies have been attempted to overcome this phenomenon, ranging from improving medium composition, total or partial replenishing of medium at infection, nutrient supplementation schemes, fed-batch processes and perfusion cultures (Ikonomou et al., 2003). However, these have only led to modest and/or cost inefficient improvements. Although the literature related to the production of BV vectors is much scarcer, early works demonstrated similar effects of cell density on the yields of wild type viruses in a *Trichoplusia ni* cell line (Stockdale and Gardiner, 1977; Wood et al., 1982). Accordingly, Klöppinger et al. (1990) found that the production of *Ac*MNPV using a *S. frugiperda* cell line was inhibited at a cell density of $1.5\times10^6$ cells/mL.

Another significant factor influencing productivity is the multiplicity of infection (MOI), i.e., the number of infectious particles (IP) per cell added to a culture. More specifically, the interplay between MOI and the cell concentration at infection (CCI) is of utmost importance for the design of efficient infection strategies and to better understand the baculovirus-insect cell system. Reports addressing this issue agree that, in batch cultures, recombinant protein titers are relatively insensitive to MOI when the cells are infected during the early exponential phase, whereas from middle to late exponential phase a positive correlation exists between the two so that productivity can be maintained up to a certain cell density (Licari and Bailey, 1992; Power et al., 1994). Information on how the MOI and CCI interplay affect BV yields has not been systematically studied.

## 7. THESIS SCOPE AND OVERVIEW

The central objective of the present thesis was to develop novel cell culture strategies to overcome or mitigate the cell density effect in the baculovirus-insect cell system. This overall goal can be broken down into two parts. The first is to understand the mechanisms underlying the cell density effect at the physiological level. The second is to design and validate strategies to overcome it in real culture conditions. Our focus was on the production of BV vectors for gene therapy purposes, for which knowledge is most scarce. Given the complexity of the biological system under study, the approach followed in this work stems from previous work performed on protein production by first evaluating the basic process parameters affecting BV production, and then progressively evolving through rational and systems biology approaches. A brief description of the thesis chapters and the main conclusions resulting thereof follows.

In chapter I, the basic bioprocess parameters affecting BV production were assessed. *Sf*9 cells were cultured and infected in serum-free medium, and the patterns of production were analyzed under varying CCI and MOI conditions. The results confirm a cell density effect on production, with a high MOI "delaying" the drop in productivity to higher cell densities. Medium replacement was also tested as this is a classical strategy previously attempted to improve protein expression in animal cells, leading to higher BV titers and specific yields at high CCI. Substrate limitations were not observed in infected cultures, even without medium renewal, thus an alternative cause for the cell density effect has to be identified.

In chapter II, a stoichiometric model of the central metabolism of *Sf*9 cells was developed to investigate the metabolic basis for this phenomenon. The main pathways of carbon and nitrogen flow were included, as well as cellular growth and energetics. MFA revealed that *Sf*9 cells undergo a progressive inhibition of central metabolism when grown to high cell densities, mainly associated with a down-regulation of the TCA cycle and glycolysis. The combined output of these alterations was a progressive depression of the energetic state with increasing cell densities, as measured by the steady-state production of adenosine triphosphate (ATP) molecules. Following BV infection and cell growth arrest, central energy metabolism was significantly up-regulated at low CCI, but this failed to occur or was even inhibited at high CCI. The results obtained in this chapter led to the hypothesis that the cellular energetic state was a key determinant of system productivity, as it correlated well with the decrease in BV production at high CCI.

In chapter III, this hypothesis was evaluated by the application of metabolic engineering techniques. The main challenges were i) how to specifically manipulate the energetic state of the cells and ii) how can this be made feasible in real bioprocess conditions. To avoid the high costs and

development times associated with classical cell genetic engineering approaches, we opted to supplement the culture medium with TCA intermediaries not usually used as carbon sources, such as pyruvate or α-ketoglutarate. Consumption of these energetic metabolites at the time of infection resulted in up to 7 fold higher specific BV yields at high CCI when compared to un-supplemented cultures. This consequently pushed volumetric titers to levels higher than those obtained for low cell density infections. Furthermore, the quantitative analysis of intracellular fluxes confirmed a direct stimulation of carbon flow through the TCA cycle and increased ATP generation. These results represent a rational and cost-efficient strategy for high cell density production of recombinant BVs. Importantly, supplementation of amino acids, lipids or complex nutrient mixtures did not significantly improve production, confirming that nutrient exhaustion is not the primary cause of the cell density effect.

Chapter IV represents a leap from the rational bioprocess studies undertaken in the previous chapters to an approach more closely connected to the current Systems Biology trends. Here, it is attempted to demonstrate how a global quantitative understanding of cell function can lead to predictable bioprocess benefits. As mentioned before, a standing bottleneck is that current stoichiometric models, such as the one developed in Chapter II, cannot explicitly consider the synthesis pathways of recombinant proteins or viruses. Hence, the metabolic engineering approach performed in Chapter III was driven by a rational hypothesis but was not a result of model prediction. Given our still rudimentary knowledge of the mechanistic link between complex product biosynthesis and central metabolism, a hybrid framework was developed combining classical MFA with projection to latent structures (PLS) to bridge estimated metabolic fluxes with measured productivities. The main result from this study was the quantitative prediction of the effect of the metabolic manipulations applied

in Chapter III for the optimization of BV production, namely the supplementation of energy-generating metabolites. Also, the developed framework should be directly applicable to other production systems for the design of customized optimization strategies.

Finally, in chapter V, we attempt to explore the application of the omics as high-throughput hypotheses generation tools in the baculovirus-insect cell system, namely quantitative mass spectrometry (MS)-based proteomics. This task was complicated by the absence of genomic information on *Sf*9 cells, certainly one of the main limitations to Systems Biotechnology in general. Nevertheless, this requirement was partially overcome by cross-referencing the mass spectra obtained to a database constructed with available annotations from *S. frugiperda* and related insect species. This homology-based methodology gave the framework for extracting large-scale information from limited resources. To analyse the quantitative proteomic response to baculovirus infection and culture growth, stable isotope labeling with amino acids in cell culture (SILAC) was performed. A thorough statistical analysis of biological replicates allowed to confidently discriminate differentially expressed proteins due to each effect, including several proteins related to energy metabolism, endoplasmic reticulum stress and oxidative stress, which can be effective targets for the design of improved bioprocesses. In particular, the viral protein LEF3 was highlighted as a key determinant of a productive infection cycle and potentially related with decreased viral replication at high cell density culture. This finding suggests that the differential accumulation of other BV-encoded proteins early in infection could also play a role in determining the level of viral DNA replication and recombinant protein expression. Most probably, this is influenced by the cell physiological state at the time of infection, in particular the energetic state, therefore constituting a possible physiological mechanism for the cell density effect.

Overall, the present thesis substantially advances our understanding of the baculovirus-*Sf*9 cell system from the current state of the art, constituting a reference case-study of the application of system biology approaches to a biotechnologically relevant bioprocess. Some of the highlights of the work include i) the first comprehensive metabolic characterization of infected *Sf*9 cells and ii) the first quantitative large-scale proteomic survey of this cell line. The material result was an up to 7 fold increase of specific BV yields under unfavorable high cell density conditions. The knowledge generated in the overall work has also implications for recombinant protein expression as well as virological research of the baculovirus-insect cell molecular interaction. Future work should be directed towards deciphering the molecular interplay underlying the cell density effect; given its complexity, this will be greatly facilitated when genomic information of the *Sf*9 cell line is available.

## REFERENCES

Airenne KJ, Mahonen AJ, Laitinen OH, Yla-Herttuala S (2009) Baculovirus-mediated gene transfer: an emerging universal concept. In: Templeton NS, editor. Gene and cell therapy, therapeutic mechanisms and strategies. CRC Press

Aucoin MG, Mena JA, Kamen AA (2010) Bioprocessing of baculovirus vectors: a review. *Curr Gene Ther* **10**: 174-186

Baik JY, Lee MS, An SR, Yoon SK, Joo EJ, Kim YH, Park HW, Lee GM (2006) Initial transcriptome and proteome analyses of low culture temperature-induced expression in CHO cells producing erythropoietin. *Biotechnol Bioeng* **93**: 361-371

Balcarcel RR, Stephanopoulos G (2001) Rapamycin reduces hybridoma cell death and enhances monoclonal antibody production. *Biotechnol Bioeng* **76**: 1-10

Birch JR, Racher AJ (2006) Antibody production. *Adv Drug Deliver Rev* **58**: 671-685

Blazeck J, Alper H (2010) Systems metabolic engineering: genome-scale models and beyond. *Biotechnol J* **5**: 647-659

Boghigian BA, Seth G, Kiss R, Pfeifer BA (2010) Metabolic flux analysis and pharmaceutical production. *Metab Eng* **12**: 81-95

Butler M (2005) Animal cell cultures: recent achievements and perspectives in the production of biopharmaceuticals. *Appl Microbiol Biotechnol* **68**: 283-291

Caron AW, Archambault J, Massie B (1990) High-level recombinant protein production in bioreactors using the baculovirus-insect cell expression system. *Biotechnol Bioeng* **36**: 1133-40

Carvalhal AV, Santos SS, Calado J, Haury M, Carrondo MJT (2003) Cell growth arrest by nucleotides, nucleosides and bases as a tool for improved production of recombinant proteins. *Biotechnol Prog* **19**: 69-83

Chen K, Liu Q, Xie L, Sharp PA, Wang DIC (2001) Engineering of a mammalian cell line for reduction of lactate formation and high monoclonal antibody production. *Biotechnol Bioeng* **72**: 55-61

Covert MW, Xiao N, Chen TJ, Karr JR (2008) Integrated metabolic, transcriptional regulatory and signal transduction models in Escherichia coli. *Bioinformatics* **24**: 2044-2050

Cruz HJ, Moreira JL, Carrondo MJT (2000) metabolically optimized BHK cell fed-batch cultures. *J Biotechnol* **80**: 109-118

Dinnis DM, James DC (2005) Engineering mammalian cell factories for improved recombinant monoclonal antibody production: lessons from nature? *Biotechnol Bioeng* **91**: 180-189

Doverskog M, Ljunggren J, Ohman L, Haggstrom L (1997) Physiology of cultured animal cells. *J Biotechnol* **59**: 103-15

Duarte NC, Becker SA, Jamshidi N, Thiele I, Mo ML, Vo TD, Srivas R, Palsson BO (2007) Global reconstruction of the human metabolic network based on genomic and bibliomic data. *Proc Natl Acad Sci* **104**: 1777-1782

Ferreira TB, Ferreira AL, Carrondo MJ, Alves PM (2005) Effect of re-feed strategies and non-ammoniagenic medium on adenovirus production at high cell densities. *J Biotechnol* **119**: 272-80

Gatti MDL, Wlaschin KF, Nisson PM, Yap M, Hu W-S (2007) Comparative transcriptional analysis of mouse hybridoma and recombinant Chinese hamster ovary cells undergoing butyrate treatment. *J Biosci Bioeng* **103**: 82-91

Gòdia F, Cairó JJ (2002) Metabolic engineering of animal cells. *Bioprocess Biosyst Eng* **24**: 289-298

Griffin TJ, Seth G, Xie H, Bandhakavi S, Hu W-S (2007) Advancing mammalian cell culture engineering using genome-scale technologies. *Trends Biotechnol* **25**: 401-408

Grüning N-M, Lehrach H, Ralser M (2010) Regulatory crosstalk of the metabolic network. *Trends Biochem Sci* **35**: 220-227

Guimerà R, Amaral LAN (2005) Functional cartography of complex metabolic networks. *Nature* **433**: 895-900

Henry O, Perrier M, Kamen A (2005) Metabolic flux analysis of HEK-293 cells in perfusion cultures for the production of adenoviral vectors. *Metab Eng* **7**: 467-476

Hollister J, Grabenhorst E, Nimtz M, Conradt H, Jarvis DL (2002) Engineering the protein N-glycosylation pathway in insect cells for production of biantennary, complex N-glycans. *Biochemistry* **41**: 15093-15104

Hou JJC, Codamo J, Pilbrough W, Hughes B, Gray PP, Munro TP (2011) New frontiers in cell line development: challenges for biosimilars. *J Chem Technol Biotechnol* **86:** n/a

Hu YC (2006) Baculovirus vectors for gene therapy. *Adv Virus Res* **68**: 287-320

Ideker T, Lauffenburger D (2003) Building with a scaffold: emerging strategies for high- to low-level cellular modeling. *Trends Biotechnol* **21**: 255-262

Ikonomou L, Schneider Y-J, Agathos SN (2003) Insect cell culture for industrial production of recombinant proteins. *Appl Microbiol Biotechnol* **62**: 1-20

Irani N, Wirth M, van den Heuvel J, Wagner R (1999) Improvement of the primary metabolism of cell cultures by introducing a new cytoplasmic pyruvate carboxylase reaction. *Biotechnol Bioeng* **66**: 238-246

Jaluria P, Chu C, Betenbaugh M, Shiloach J (2008) Cells by design: a mini-review of targeting cell engineering using DNA microarrays. *Mol Biotechnol* **39**: 105-111

Jiang Z, Sharfstein ST (2008) Sodium butyrate stimulates monoclonal antibody over-expression in CHO cells by improving gene accessibility. *Biotechnol Bioeng* **100**: 189-194

Kauffman KJ, Prakash P, Edwards JS (2003) Advances in flux balance analysis. *Curr Opin Biotechnol* **14**: 491-496

Klöppinger M, Fertig G, Fraune E, Miltenburger HG (1990) Multistage production of *Autographa californica* nuclear polyhedrosis virus in insect cell cultures. *Cytotechnology* **4**: 271-8

Korke R, Gatti MDL, Lau ALY, Lim JWE, Seow TK, Chung MCM, Hu W-S (2004) Large scale gene expression profiling of metabolic shift of mammalian cells in culture. *J Biotechnol* **107**: 1-17

Kost TA, Condreay JP, Jarvis DL (2005) Baculovirus as versatile vectors for protein expression in insect and mammalian cells. *Nat Biotechnol* **23**: 567-575

Lee JM, Gianchandani EP, Eddy JA, Papin JA (2008) Dynamic analysis of integrated signalling, metabolic, and regulatory networks. *Plos Comput Biol* **4**: e1000086

Lee MS, Kim KW, Kim YH, Lee GM (2003b) Proteome analysis of antibody-expressing CHO cells in response to hyperosmotic pressure. *Biotechnol Prog* **19**: 1734-1741

Lee SY, Lee D-Y, Kim TY (2005) Systems biotechnology for strain improvement. *Trends Biotechnol* **23**: 349-358

Lee YY, Yap MGS, Hu W-S, Wong KTK (2003a) Low-glutamine fed-batch cultures of 293-HEK serum-free suspension cells for adenovirus production. *Biotechnol Prog* **19**: 501-509

Licari P, Bailey JE (1992) Modeling the population dynamics of baculovirus-infected insect cells: optimizing infection strategies for enhanced recombinant protein yields. *Biotechnol Bioeng* **39**: 432-41

Maranga L, Cruz PE, Aunins JG, Carrondo MJT (2002) Production of core and virus-like particles with baculovirus infected insect cells. Adv Biochem Eng Biotechnol 74: 183-206

Mastrangelo AJ, Hardwick JM, Bex F, betenbaugh MJ (2000) Part I. Bcl-2 and Bcl-$x_L$ limit apoptosis upon infection with alphavirus vectors. *Biotechnol Bioeng* **67**: 544-554

Mazur X, Fussenegger M, Renner WA, Bailey JE (1998) Higher productivity ofgrowth-arrested Chinese hamster ovary cells expressing the cyclin-dependent kinase inhibitor p27. *Biotechnol Prog* **14**: 705-713

Neermann J, Wagner R (1996) Comparative analysis of glucose and glutamine metabolism in transformed mammalian cell lines, insect and primary liver cells. *J Cell Physiol* **166**: 152-169

Noad R, Roy P (2003) Virus-like particles as immunogens. *Trends Microbiol* **11**: 438-444

O'Callaghan PM, James DC (2008) Systems biotechnology of mammalian cell factories. *Brief Funct Genomic Proteomic* **7**: 95-110

Oberhardt MA, Palsson BO, Papin JA (2009) Applications of genome-scale metabolic reconstructions. *Mol Syst Biol* **5**: 320

Okano K, Vanersdall AL, Mikhailov VS, Rohrmann GF (2006) Conserved molecular systems of the Baculoviridae. *Virology* **344**: 77-87

Ong S-E, Mann M (2005) Mass spectrometry-based proteomics turns quantitative. *Nat Chem Biol* **1**: 252-262

O'Reilly DR, Miller LK, Luckow VA (1994) Baculovirus expression vectors: a laboratory manual. Oxford University Press, New York

Otero JM, Nielsen J (2010) Industrial systems biology. *Biotechnol Bioeng* **105**: 439-460

Ozturk SS, Palsson BO (1991) Effect of medium osmolarity on hybridoma growth, metabolism and antibody production. *Biotechnol Bioeng* **37**: 989-993

Palomares LA, Estrada-Moncada S, Ramirez OT (2006) Principles and applications of the insect cell-baculovirus expression vector system. In: Ozturk SS, Hu W-S, editors. Cell culture technology for pharmaceutical and cell based therapies. Taylor & Francis, New York

Palomares LA, Ramirez OT (1998) Insect cell culture: Recent advances, bioengineering challenges and implications in protein production. In: Galindo E, Ramirez OT, editors. Advances in Bioprocess Engineering II. Kluwer Academic Publishers, Dordrecht

Power JF, Reid S, Radford KM, Greenfield PF, Nielsen L, K. (1994) Modeling and optimization of the baculovirus expression vector system in batch suspension culture. *Biotechnol Bioeng* **44**: 710-9

Quek L-E, Dietmair S, Krömer JO, Nielsen LK (2010) Metabolic flux analysis in mammalian cell culture. *Metab Eng* **12**: 161-171

Ramachandran A, Bashyam MD, Viswanathan P, Ghosh S, Kumar MS, Hasnain SE (2001) The bountiful and baffling baculovirus: the story of polyhedrin transcription. *Curr Sci* **81**: 998-1010

Reuveny S, Kim YC, Kemp CW, Shiloach J (1993) Production of recombinant proteins in high-density insect cell cultures. *Biotechnol Bioeng* **42**: 235-9

Rodriguez J, Spearman M, Huzel N, Butler M (2005) Enhanced production of monomeric interferon-*β* by CHO cells through the control of culture conditions. *Biotechnol Prog* **21**: 22-30

Sauer U, Heinemann M, Zamboni N (2007) Getting closer to the whole picture. *Science* **316**: 550-551

Seow TK, Korke R, Liang RCMY, Ong S-E, Ou K, Wong K, Hu W-S, Chung MCM (2001) Proteomic investigation of metabolic shift in mammalian cell culture. *Biotechnol Prog* **17**: 1137-1144

Seth G, Charaniya S, Wlaschin KF, Hu W-S (2007b) In pursuit of a super producer – alternative paths to high producing recombinant mammalian cells. *Curr Opin Biotechnol* **18**: 557-564

Seth G, Philp RJ, Lau A, Jiun KY, Yap M, Hu W-S (2007a) Molecular portrait of high productivity in recombinant NS0 cells. Biotechnol Bioeng 97: 933-951

Sheikh K, Förster J, Nielsen LK (2005) Modeling hybridoma cell metabolism using a generic genome-scale metabolic model of Mus musculus. *Biotechnol Prog* **21**: 112-121

Shen D, Sharfstein ST (2006) Genome-wide analysis of the transcriptional response of murine hybridomas to osmotic shock. *Biotechnol Bioeng* **93**: 132-145

Smith GE, Summers MD, Fraser MJ (1983) Production of human beta interferon in insect cells infected with a baculovirus expression vector. *Mol Cell Biol* **3**: 2156-2165

Sommerfeld S, Strube J (2005) Challenges in biotechnology production – generic process and process optimization for monoclonal antibodies. *Chem Eng Process* **44**: 1123-1137

Stephanopoulos G, Alper H, Moxley J (2004) Exploiting biological complexity for strain improvement through systems biology. *Nat Biotechnol* **22**: 1261-1267

Stephanopoulos G, Aristidou AA, Nielsen J (1998) Metabolic engineering. Principles and Methodologies. Academic Press, San Diego

Stockdale H, Gardiner GR (1977) The influence of the condition of cells and medium on production of polyhedra of *Autographa californica* nuclear polyhedrosis virus in vitro. *J Invertebr Pathol* **30**: 330-6

Summers MD (2006) Milestones leading to the genetic engineering of baculoviruses as expression vector systems and viral pesticides. *Adv Virus Res* **68**: 3-73

Taticek RA, Shuler ML () Effect of elevated oxygen and glutamine levels on foreign production at high cell densities using the insect cell-baculovirus expression system. *Biotechnol Bioeng* **54**: 142-152

Urabe M, Ding C, Kotin RM (2002) Insect cells as a factory to produce adeno-associated virus type 2 vectors. *Hum Gene Ther* **13**: 1935-43

Van Anken E, Romijn EP, Maggioni C, Mezghrani A, Sitia R, Braakman I, Heck AJR (2003) Sequential waves of functionally related proteins are expressed when B cells prepare for antibody secretion. *Immunity* **18**: 243-253

Van Dyk DD, Misztal DR, Wilkins MR, Mackintoch JA, Poljak A, Varnai JC, Teber E, Walsh BJ, Gray PP (2003) Identification of cellular changes associated with increased production of human growth hormone in a recombinant Chinese hamster ovary cell line. *Proteomics* **3**: 147-156

Vaughn JL, Goodwin RH, Tompkins GJ, McCawley P (1977) The establishment of two cell lines from the insect *Spodoptera frugiperda* (Lepidoptera; Noctuidae). *In vitro* **13**: 213-217

Vicente T, Peixoto C, Carrondo MJT, Alves PM (2009) Purification of recombinant baculoviruses for gene therapy using membrane processes, *Gene Ther* **16**: 766-775

Walsh G (2010) Biopharmaceutical benchmarks 2010. *Nat Biotechnol* **28**: 917-924

Wood HA, Johnston B, Burand JP (1982) Inhibition of *Autographa californica* nuclear polyhedrosis virus replication in high density *Trichoplusia ni* cell cultures. *Virology* **119**: 245-54

Wurm FM (2004) Production of recombinant protein therapeutics in cultivated mammalian cells. *Nat Biotechnol* **22**: 1393-1398

Yoon SK, Hwang SO, Lee GM (2004) Enhancing effect of low culture temperature on specific antibody productivity of recombinant Chinese hamster ovary cells: clonal variation. *Biotechnol Prog* **20**: 1683-1688

# CHAPTER I

## THE INTERPLAY BETWEEN CELL DENSITY AND MULTIPLICITY OF INFECTION ON BACULOVIRUS VECTORS PRODUCTIVITY

**ADAPTED FROM:**

Carinhas N, Bernal V, Yokomizo AY, Carrondo MJT, Oliveira R, Alves PM (2009) Baculovirus production for gene therapy: the role of cell density, multiplicity of infection and medium exchange. *Appl Microbiol Biotechnol* 81: 1041-1049.

# TABLE OF CONTENTS

## 1. SUMMARY

One significant concern when using insect cells and baculovirus expression vectors for the production of recombinant proteins is the drop in production observed when infecting cultures at high cell densities. This chapter revisits this so-called “cell density effect” in the scope of baculovirus production for gene therapy purposes. *Sf*9 cells were cultured in serum-free medium, and the patterns of production of a recombinant baculovirus were analyzed for different infection strategies. The results show viral titers and yields decrease when infections are performed at increasing cell concentrations, demonstrating a cell density effect comparable to that affecting protein expression. By infecting with a high multiplicity of infection, it is possible to “delay” the drop in baculovirus production to higher cell densities. Further, medium replacement at the time of infection considerably improves baculovirus production; volumetric titers as high as $2.6\times10^{10}$ infectious particles/mL were obtained in cultures infected at $3.5\times10^{6}$ cells/mL, while viral amplification was roughly 19 times higher than the highest value obtained without medium exchange.

## 2. INTRODUCTION

While the first gene therapy-based product has yet to be approved for commercialization, research efforts have been directed towards delivery technologies representing a safer alternative over classical mammalian viruses. During the past decade, the suitability of baculovirus vectors (BVs) to direct gene expression in mammalian cells has been explored (Kost and Condreay, 2002). The validation of this approach still lacks sufficient knowledge on the mechanisms governing tissue targeting, gene delivery, and host immunological responses. Importantly, in order to facilitate the use

of BVs for gene therapy, the development of efficient production processes to amplify the engineered vectors is needed.

In terms of process productivity, it would be desirable to infect a highly productive insect cell culture at later stages of growth, but higher cell densities often lead to lower specific product yields. Most of the studies reported on bioprocesses using the BV/insect cell system are focused on the production of recombinant proteins rather than the vector itself (Ikonomou et al., 2003). The present work focuses on assessing the interplay between cell concentration at infection (CCI) and multiplicity of infection (MOI) on the production of recombinant BVs assuming a comparative perspective with knowledge related with protein production. The questions addressed in this work are: Is there a cell density effect on the production of BVs by infection of *Sf*9 cells in serum free medium? If so, is this effect dependent on the MOI used? Finally, can this effect be repressed by restoring initial medium conditions at the time of infection? For this purpose, several indicators of system productivity were evaluated in infection experiments where different CCIs at both low and high MOIs were tested. Then, the combinations of CCIs and MOIs that yielded better production results were subject to medium replacement at the time of infection.

## 3. MATERIALS AND METHODS

### 3.1. Cell line, culture medium and maintenance

The host insect cell line *Sf*9, ECACC 89070101**,** originally isolated from the pupal ovaries of *Spodoptera frugiperda*, was provided by Dr. Otto W. Merten (Genethon, France). Cultivation was performed in 500 mL Erlenmeyer flasks (Corning, USA) with 50 mL working volume after thawing

cells from an initial passage number of 17. SF900II serum-free medium (Gibco, Invitrogen, USA), specifically designed for *Sf*9 cells, was used throughout this work. Cells for maintenance were re-inoculated every 3 days at a cell density of 4-5×$10^5$ cells/mL, and kept in a humidified incubator operated at 27ºC and 90 rpm. Cellular concentration was determined by cell count in a Fuchs-Rosenthal chamber and the viability assessed by the Trypan Blue exclusion method. To assess cellular lysis, the activity of lactate dehydrogenase (LDH; EC 1.1.1.27) released to the medium was measured by following the rate of pyruvate reduction to lactate. This reaction is coupled with the oxidation of NADH to $NAD^+$, which can be measured spectrophotometrically at 340 nm (Racher et al., 1990).

### 3.2. Virus and viral stock

The recombinant baculovirus *Ac-hisgfp*, provenient from the parental *Autographa californica* nuclear polyhedrosis virus, was provided by Dr. Monique M. van Oers (Laboratory of Virology, Wageningen University, The Netherlands), containing a *gfp* gene under the control of the polyhedrin promoter. Recombinant BVs were amplified by infecting *Sf*9 cells at 1×$10^6$ cells/mL with a MOI of 0.1 infectious particles (IP)/cell, in a 250 mL spinner flask (Wheaton, USA), and culture bulk was harvested after 5 days incubation at 27ºC and 150 rpm. After harvesting, cells were seeded by centrifuging at 1700×g for 10 minutes, and the supernatant was stored at 4ºC and protected from light for several months.

### 3.3. Experimental cultures and sampling

*A*fter several passages to ensure consistent high viabilities above 95%, *Sf*9 cells were infected with recombinant BVs for evaluation of virus production

and culture behavior. Experimental cultures were at a passage number not higher than 31. Cultures were performed in 125 mL spinner flasks (Wheaton, USA) at 27$^{o}$C, with caps partially open and with an agitation of 150 rpm. A total of six independent experiments were performed varying the CCI ($1\times10^{6}$ cells/mL (CCI 1), $2\times10^{6}$ cells/mL (CCI 2) and $3\text{-}4\times10^{6}$ cells/mL (CCI 3), corresponding to 24h, 48h and 72h of culture, respectively) for two different MOIs (0.6 IP/cell – low MOI, and 30 IP/cell – high MOI). Three additional infections with a high MOI of 6 IP/cell were carried with medium exchange at the time of infection, and the same set of CCIs was used. In these cultures, cells were centrifuged and re-suspended to the desired concentration in 10 mL of spent medium. Thereafter, recombinant BVs were inoculated, the volume was completed to 50 mL with fresh medium, and the cultures were maintained under continuous stirring to promote virus adsorption during 1 hour. Finally, the volume was completed to 125 mL with fresh medium. Every 24 h, culture samples were taken and centrifuged at 1700×g at room temperature for 10 minutes in order to separate cells from supernatant. Aliquots of the supernatant were then maintained at 4$^{o}$C for virus titration and at - 20$^{o}$C to measure glucose, lactate, ammonia and concentrations of free amino acids.

### 3.4. Analytical methods

Glucose and lactate concentrations were determined with automated enzymatic assays (YSI 7100 Multiparameter Bioanalytical System; Dayton, Ohio, USA). Ammonia was quantified enzymatically using a UV assay (No 1112732035; Boehringer Manheim, R-Biopharm AG, Darmstadt, Germany). Amino acids were quantified by high performance liquid chromatography (HPLC) analysis using a reverse phase 3.9×150 mm column (AccQ.Tag, Waters, USA). A pre-column derivatization technique was used based on

the Waters AccQ.Tag Amino Acid Analysis method. Briefly, both primary and secondary amino acid derivatives were produced by mixing with 6-aminoquinolyl N-hydroxysuccinimidyl-carbamate, allowing their separation and quantification by fluorescence detection at 395 nm. Prior to derivatization, sample proteins were precipitated by adding an equal volume of acetonitrile and discarded by centrifugation at 12400×g for 15 min, at room temperature. An internal standard (α-aminobutyric acid) was added to ensure consistent measurements between runs. Mobile phases were prepared following the manufacturer's instructions, filtered and degassed before usage.

### 3.5. Virus titration

Virus titers were determined by an end-point dilution assay. In this method, 96-well plates containing 100 µL of cellular suspension at a density of $0.5\times10^6$ cells/mL were incubated for 1 hour at 27 $^{o}$C. Dilutions of the virus samples were performed serially in SF900II medium, from $1:10^4$ to $1:10^{11}$, and 100 µL were used to infect *Sf*9 cells monolayers after medium aspiration from the plate wells. Ten replicates for each dilution were performed in the same plate, and two independent plates were infected for each viral sample. A dilution of $1:10^2$ was used as positive control. SF900II medium was used as negative control. Plates were screened after seven days for GFP signal under an inverted fluorescence microscope, using an excitation wavelength range between 450 and 490 nm. The 50% tissue-culture infectious dose ($TCID_{50}$), i. e. the dilution which is sufficient to infect half of the cells, was calculated using equations described elsewhere (King and Possee, 1992). This value was then converted to plaque-forming units (or number of IPs) by the relationship: PFU = 0.69 x $TCID_{50}$ (King and Possee, 1992).

### 3.6. Estimation of specific metabolic rates and production indicators

Specific consumption and production rates of important molecules of cell metabolism such as glucose, lactate, glutamine, serine and alanine, were estimated by dividing the slopes of concentration profiles by the average of cell density along defined time intervals (48-144 h, 72-168 h and 96-192 h). For the infection experiments, the average of cell density was calculated for the entire post-infection time, since linear concentration profiles after infection were observed for these compounds. The specific yield values presented were estimated by dividing the maximum titer (IP/mL) by the CCI used in each infection experiment. The amplification factor was calculated as the ratio between maximum titer and the inoculated value of IP/mL at the time of infection. TOH corresponds to the culture time when the maximum titer was obtained.

## 4. RESULTS

The effect of cell density on the production of recombinant BVs was assessed by infecting *Sf*9 cultures at CCIs of 1, 2 and 3-4×$10^6$ cells/mL, both at a MOI of 0.6 and 30 IP/mL, in SF900II serum-free medium. The production indicators calculated for each condition tested were the maximum titer, specific yield, amplification factor and TOH. Additionally, specific metabolic rates of glucose, lactate, glutamine, serine and alanine were assayed, and the metabolic profiles of glucose and lactate were analyzed. Three additional experiments were carried out by exchanging the medium at the time of infection with a high MOI.

### 4.1. Infections at low MOI

When *Sf*9 cells were infected with a recombinant BV (*Ac-hisgfp*) at a low MOI, a marked decrease in the growth rates upon infection was obtained, followed by a drop in viable cell density (Figure 1.1A). Cellular lysis was also monitored throughout culture time, with an increase in extracellular LDH activity consistent with loss in viability (data not shown). Figure 1.2 shows typical profiles of glucose and lactate in uninfected and infected *Sf*9 cultures. It is clear from the lower slopes in the glucose concentration profiles when compared to the uninfected culture that glucose uptake was down-regutated after infection (Figure 1.2A). Lactate accumulated in the uninfected culture up to approximately 12 mM (Figure 1.2B), with a mean specific production rate of 10.57±0.75 nmol/$10^6$ cells/h, its concentration decreasing then at the end of the culture. In the infected cultures, lactate accumulation only occurred at CCI 3, with a specific production rate of 9.59±0.57 nmol/$10^6$ cells/h. In contrast, ammonia did not accumulate significantly in the medium at any stage of cultivation in all experiments performed, remaining approximately constant in the range of 4 to 6 mM (Figure 1.3).

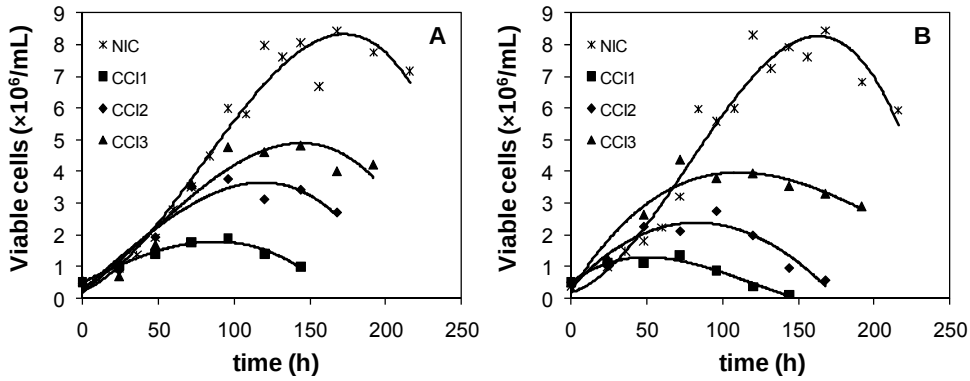


**Figure 1.1**. Uninfected (NIC) and infected *Sf*9 cultures growth in serum-free medium. Infections with a recombinant BV (*Ac-hisgfp*) were carried either with a low MOI (A) and a high MOI (B), for different CCIs, without medium exchange.

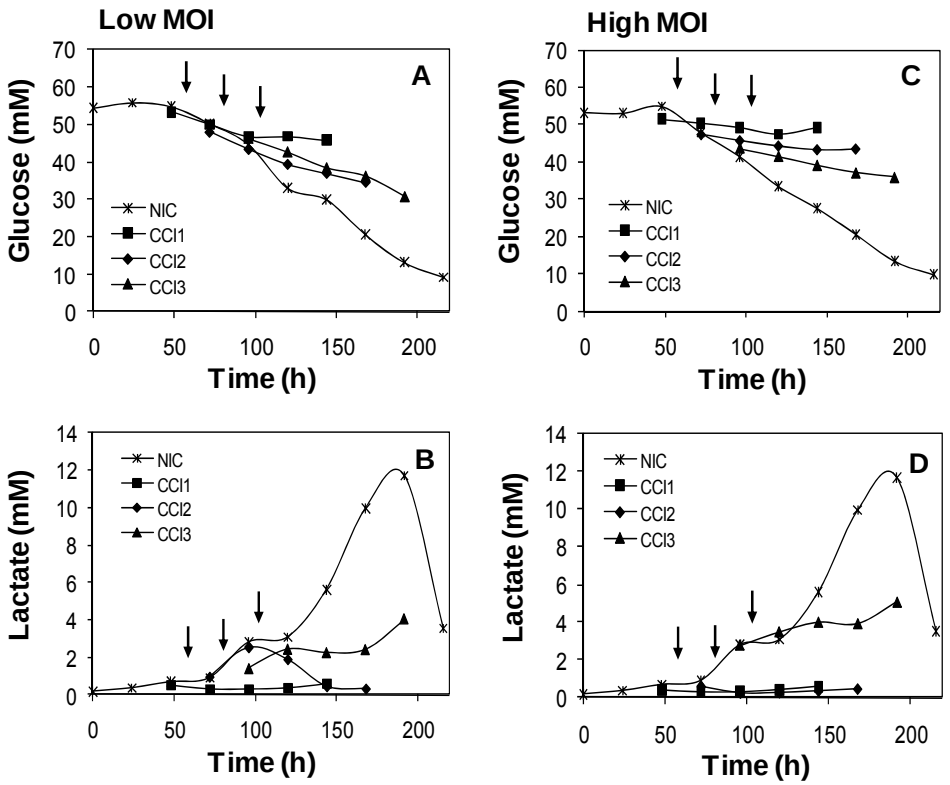


**Figure 1.2**. Metabolic profiles of glucose (A and C) and lactate (B and D) for uninfected and infected *Sf*9 cultures with a low and a high MOI, without medium exchange. Arrows indicate the time of infection for the three CCIs tested.

Figures 1.4 and 1.5 show the specific glucose and amino acid uptake rates for uninfected and infected cultures without medium exchange. It can be seen that the consumption of these nutrients clearly decreased after viral infection at low MOI. Interestingly, glucose uptake decreased both during the later stage of growth and after infection at a high CCI. The same pattern was observed for the consumption rates of serine and, more prominently, in the case of glutamine. The rates of alanine production are also represented. This was the only amino acid accumulating in the culture medium. None of the amino acids analyzed was depleted in the infected cultures, although serine was totally consumed at 170-190 h (data not shown), while cells had already stopped growing.

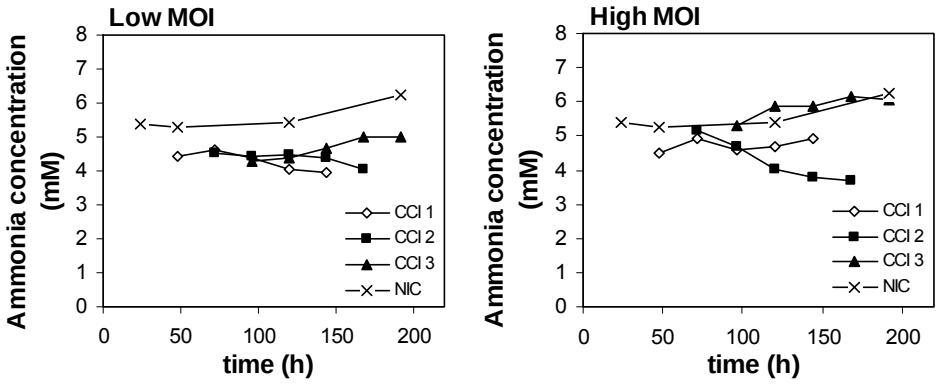


**Figure 1.3**. Concentration profiles of ammonia in the culture medium during growth and after infection with recombinant *Ac-hisgfp*. Infections were carried out either with a low or high MOI, both for three different CCIs, without medium exchange. NIC refers to uninfected cultures.

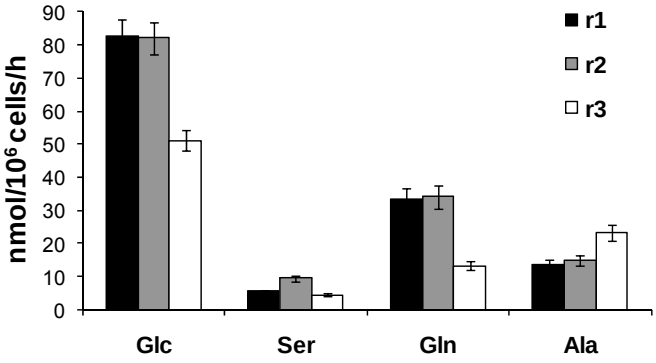


**Figure 1.4**. Specific consumption rates of glucose and selected amino acids calculated for uninfected *Sf*9 cultures. The values presented for alanine represent rates of accumulation in the culture medium. r1, r2 and r3 refer to the rates calculated for the following time spans: 48-144 h, 72-168 h and 96-192 h, respectively. The error bars presented correspond to the linear regression error of the corresponding slopes. The errors involved in the measurements of the primary variables were 5% (Glc) and 10% (Ser, Gln, Ala and cell concentration). Glc – glucose; Ser – serine; Gln – glutamine; Ala – alanine.

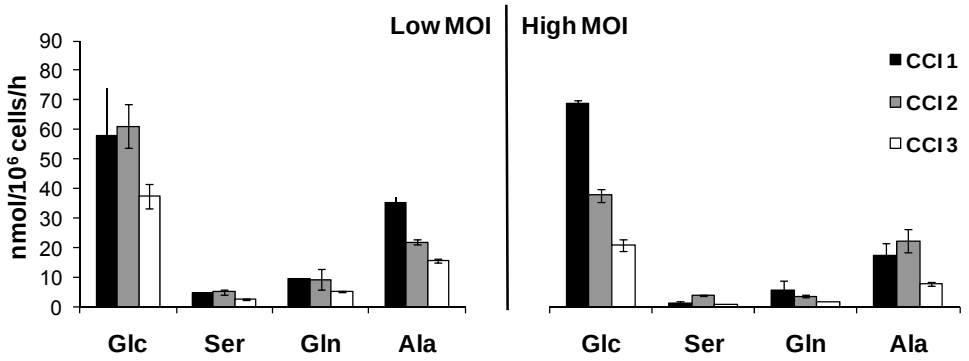


**Figure 1.5**. Specific consumption rates of glucose and selected amino acids calculated for infected *Sf*9 cultures at two MOIs and different CCIs, without medium exchange. The values presented for alanine represent rates of accumulation in the culture medium.

Regarding recombinant BV production, it can be seen in Table 1.1 that all the production indicators declined by one order of magnitude when cells were infected at progressively higher CCIs. The titer decreased from 0.18 to $0.007\times10^9$ IP/mL and the specific yield decreased from 172 to 2 IP/cell. Moreover, the amplification factor dropped from 287 to 3, and the TOH was 120 h for all CCIs tested.

### 4.2. Infections at high MOI

For the infections performed at high MOI, it is clear from the growth curves (Figure 1.1B) that cell growth was strongly inhibited after virus infection, independently of the CCI. Glucose profiles were qualitatively similar to those of the low MOI infections (Figure 1.2C), although evidencing a further down-regulation of glucose uptake which is probably associated with the synchronous infection of the cells. As in the case of the low MOI infections, lactate accumulated only at CCI 3 (Figure 1.2D) with a specific production rate of 5.90±0.28 nmol/$10^6$ cells/h. The ammonia concentration remained in the same interval of 4 to 6 mM (Figure 1.3). After calculating the specific

consumption fluxes of glucose (Figure 1.5), it was possible to confirm that these were lower than the uninfected culture and lower than the low MOI infections for CCIs 2 and 3. A decreasing trend of glucose consumption fluxes with increasing CCI was evident in these experiments. The uptake rates of serine and glutamine were lower than the uninfected and low MOI infected cultures for all CCIs. None of the amino acids analyzed was exhausted as for the previous infections.

The results of virus production at high MOI were quite contrasting with what was observed for infections at low MOI (Table 1.1). The titer increased with CCI from $0.55\times10^9$ IP/mL to $9\times10^9$ IP/mL, while the maximum specific yield was obtained at CCI 2, corresponding to a value of 2475 IP/cell. In the same way, the amplification factor for this set of infections was higher for CCI 2 (83), but lower than the highest amplification factor obtained at low MOI (287 for CCI 1).

### 4.3. Infections at high MOI with medium exchange

In order to discriminate the influence of medium condition on the cell density effect, experiments with medium exchange at the time of infection were performed using a high MOI. As explained in the Materials and Methods section, cells were centrifuged and re-suspended in fresh medium to the three CCIs tested. The main observations related to the metabolic activity of *Sf*9 cells after infection are depicted in Figure 1.6. Glucose uptake rate was lower in these experiments when compared to what was observed for uninfected and the other infected cultures (Figure 1.6). Besides, the characteristic decrease of glucose and amino acids consumption with increasing CCI appears to be reversed.

**Table 1.1.** Summary of *Ac-hisgfp* baculovirus production indicators for different cell concentrations at infection (CCIs) and multiplicities of infection (MOIs).

| | Low MOI | | | |
|---|---|---|---|---|
| | **Titer**[a] | **Specific Yield**[b] | **Amplification**[c] | **TOH**[d] |
| **CCI 1** | 0.18 | 172 | 287 | 120 |
| **CCI 2** | 0.07 | 36 | 61 | 120 |
| **CCI 3** | 0.007 | 2 | 3 | 120 |
| | **High MOI** | | | |
| | **Titer**[a] | **Specific Yield**[b] | **Amplification**[c] | **TOH**[d] |
| **CCI 1** | 0.55 | 486 | 17 | 120 |
| **CCI 2** | 5.6 | 2475 | 83 | 120 |
| **CCI 3** | 9 | 2060 | 69 | 96 |

[a]Infectious particles per mL ($10^9$ IP/mL); [b]Infectious particles per cell (IP/cell); [c]Ratio between volumetric productivity and number of viruses per mL at the time of infection (Volumetric productivity/(CCI×MOI)); [d]Time of harvest (hours).

Higher amounts of recombinant BV were obtained for this set of infections (Table 1.2). It can be seen that all the production parameters increased with CCI. At CCI 3, a specific yield of 9306 IP/cell was obtained, corresponding approximately to a 3 fold increase with respect to the higher value obtained for high MOI without medium exchange (2475 IP/cell, CCI 2). Additionally, the highest amplification factor was roughly 19 times higher than that obtained without medium exchange at CCI 2. In terms of bioprocess time, a significant decrease in TOH was observed in relation to the previous infections.

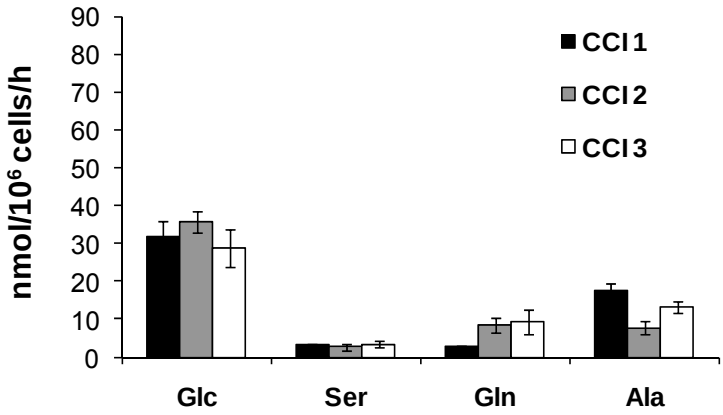


**Figure 1.6**. Specific consumption rates of glucose and selected amino acids calculated for *Sf*9 cultures infected at high MOI and different CCIs, with medium exchange at the time of infection. The values presented for alanine represent rates of accumulation in the culture medium.

## 5. DISCUSSION

The inhibition of cell division observed after virus inoculation demonstrates that viral entry into the cells has a profound impact on their physiology and metabolic state (Figure 1.1). This drop, which has been reported before in other works (Elias et al., 2000), was more pronounced for the infections at high MOI and reflects the synchronous infection of the cells.

Several authors have shown that lactate does not accumulate to high levels in *Sf*9 cultures. Therefore, the significant build up of lactate in the uninfected cultures during later stages of growth (Figure 1.2B and D), with viable cell densities above $5\times10^6$ cells/mL, suggests a possible limitation in oxygen availability in spinner flasks (Rhiel and Murhammer, 1995). On the other hand, the final drop at the end of cultivation time indicates an uptake of lactate as a result of the lower glucose concentrations (Mendonça et al.,

1999). During the infection experiments, lactate accumulation was reduced, probably due to the lower consumption of glucose. Final levels around 4-5 mM were obtained in the infections at CCI 3. The low levels of ammonia production along all uninfected and infected cultures (Figure 1.3) have already been described to be related with its detoxification through the production of alanine, which is normally released by *Sf*9 cells (Drews et al., 2000). Besides, the concentration values measured were between 4 to 6 mM, being lower than the 20 mM previously reported to be inhibitory for *Sf*9 cells (Öhman et al., 1996).

**Table 1.2.** Summary of *Ac-hisgfp* baculovirus production indicators for different cell concentrations at infection (CCIs) and a high multiplicity of infection (MOI) with medium exchange.

| | Titer[a] | Specific Yield[b] | Amplification[c] | TOH[d] |
|---|---|---|---|---|
| **CCI 1** | 0.3 | 177 | 30 | 96 |
| **CCI 2** | 13 | 5652 | 942 | 72 |
| **CCI 3** | 26 | 9306 | 1550 | 72 |

[a]$10^9$ IP/mL; [b]IP/cell; [c]Volumetric productivity/(CCI×MOI)); [d]Hours.

Comparing the metabolic rates presented in Figures 1.4 and 1.5, it can be seen that glucose uptake is lower after viral infection, hence directly correlating with its utilization for cell growth. An interesting observation was that this rate also decreased at later stages of growth in the uninfected cultures, and after infection at high CCI. Oxygen limitation could in principle play a role, as indicated by the accumulation of lactate both at later stages of growth and after high cell density infection. However, experiments in fully controlled bioreactors have shown a similar uptake pattern for glucose, despite negligible production of lactate (data not shown), thus suggesting that the effects assessed were not primarily determined by oxygen limitation.

Besides glucose, glutamine and serine were consistently consumed during all experiments. This was expected since glutamine has been demonstrated to be the major nitrogen source for *Sf*9 cells biosynthetic metabolism, being also used as a carbon and energy source (Drews et al., 2000), while serine can be directly incorporated in the central metabolism by conversion to pyruvate. Overall, lower specific consumption rates, as described for glucose, can be observed for these two amino acids after infection, especially at high MOI when infections tend to be synchronous. The decrease in serine consumption rates at higher CCI is less evident when compared with those of glucose and glutamine uptake rates; however, one should take into consideration the proportionality between rate values and associated errors that, even with low deviations, may blur the interpretation of the results.

The only amino acid to build up in the culture medium was alanine, which has been described as the major metabolic by-product in *Sf*9 cells (Drews et al., 2000). It can be estimated from the specific fluxes presented in Figures 1.4 and 1.5 that the amount of glucose diverted to alanine production ranged from 8 to 23% in uninfected cultures, and from 12 to 30% in infected cultures without medium exchange, considering glucose as the sole pyruvate source for alanine synthesis. Although concentrations up to 100 mM have not been shown to impact productivity (Bédard et al., 1993; Öhman et al., 1995), the channeling of glucose to by-product formation implies a decrease in the efficiency of its oxidation for energy production and biosynthesis. Nevertheless, these results indicate an efficiency of carbon utilization in *Sf*9 cells that is significantly higher than in cultured mammalian cell lines (Doverskog et al., 1997).

The metabolism of *Sf*9 cells after exchanging the medium at infection with a high MOI yielded relevant results (Figure 1.6). The lower consumption rates

of glucose in comparison to the values of uninfected and the other infected cultures (Figures 1.4 and 1.5) show a marked shift in cell physiology. The literature is scarce in information regarding the metabolic behavior of cells after medium restoration at infection. We suggest that exposing the cells to fresh medium induces an adaptation process somewhat resembling the lag phase present after inoculating a new culture. In *Sf*9 cells, this is characterized by extremely low consumption rates of glucose (see Figure 1.1). Thereafter, viral infection takes over preventing biomass formation and increased substrate consumption. Besides, the characteristic decrease of the consumption rates at high CCI is not as evident for glucose in this set of experiments, and even appearing to be reversed in the case of glutamine. This is probably related with the requirements for higher BV productivities seen at higher CCI.

Considering the production of BVs in the infections performed at low MOI, it is possible to see that *Sf*9 cells grown in serum-free medium exhibit the same behavior previously described for the production of recombinant proteins, clearly demonstrating a cell density effect in the system (Table 1.1). When infections were carried out at high MOI, higher productivities were obtained in cultures infected at higher CCI. Studies that have adressed the combined effects of CCI and MOI on recombinant protein titers demonstrate that for each CCI there is an optimum MOI for maximum protein production (Licari and Bailey, 1992; Power et al., 1994). More specifically, Power et al. (1994) showed that for a high MOI, the protein titer increases exponentially in proportion to the concentration of infected cells until a certain point beyond which production starts to decrease. In their particular case, this occured for a cell density of $2.4\times10^6$ cells/mL. Herein, the titers obtained increased until CCI 3 ($9\times10^9$ IP/mL), although the highest value is in the same order of magnitude than that obtained at CCI 2 ($5.6\times10^9$ IP/mL).

The cell density effect in high MOI infections can be more markedly observed when considering specific yields, where the highest value was obtained at CCI 2 (2475 IP/cell), decreasing thereafter at CCI 3 (2060 IP/cell). In this work, the values presented are based on the initial infection cell density (Wang et al., 1993). We also estimated specific yields by two other methods: 1) dividing by the highest cell density obtained after infection and 2) considering the average number of cells from infection until the maximum titer was obtained. Overall, the values show the same pattern along the CCI range for both MOIs.

There is a scarcity of data in the literature regarding the factors that affect BV vectors production by insect cells. One of the few studies that has addressed this issue also shows the same pattern of decreased productivity with increasing CCIs along a wide range of cell densities at infection, obtaining a maximum specific yield of 657 plaque forming units (pfu)/cell for a cell concentration of $4.5\times10^6$ cells/mL (Radford et al., 1997). In our work, the maximum specific yield for high MOI infections (Table 1.1) was obtained at $2\times10^6$ cells/mL, corresponding to a value of 2475 IP/cell which is approximately 4 times higher than the 657 pfu/cell reported previously. Differences can be attributed to the different MOIs, recombinant viruses and culture systems used in each case: Radford's BV had been constructed for the expression of secreted *β*-galactosidase and infections were performed at a MOI between 1 and 2 IP/cell in biorreactors, where cell densities over $20\times10^6$ cells/mL were reached without infection.

The viral amplification factor was higher for CCI 2, decreasing then at CCI 3; the fact that this higher value of 83 was still lower than the highest amplification factor obtained at low MOI (287 for CCI 1) suggests that, in terms of bioprocess performance, working at low CCI and low MOI is the

best option for virus propagation if no improvements in the culture conditions are attempted.

After exchanging the medium at the time of infection, the cell density effect was completely overcome for the range of CCIs tested, since all the production indicators were maximized at CCI 3, with maximum titer and specific yield of $2.6\times10^{10}$ IP/mL and 9306 IP/cell, respectively (Table 1.2). Furthermore, a marked decrease in the culture time for the titers to reach maximum values (TOH = 72h) was observed, which contributes to the efficiency of the bioprocess. According to the literature, the replenishment of fresh medium along with the inoculation of viruses has proved to be an efficient way of restoring the yields of different proteins in high-density *Sf*9 cultures (Caron et al., 1990; Lindsay and Betenbaugh, 1992; Tom et al., 1995). From a metabolic perspective, this increase in protein yield after medium replacement has been related with nutrient depletion rather than the accumulation of inhibitory by-products (Bédard et al., 1994; Weiss et al., 1992). This is consistent with the fact that the common by-products excreted by mammalian cell lines, ammonia and lactate, do not accumulate to toxic levels in *Sf*9 cells (Drews et al., 1995). Also, the addition of complex nutrient mixtures such as different kinds of serum substitutes and hydrolysates were reported to be beneficial to increase protein production (Ikonomou et al., 2003). However, these studies generally lacked a detailed description of cellular metabolism, failing to identify the specific components responsible for improved productivities. Exceptionally, Radford et al. (1997) have reported a complete depletion of cystine in infected cultures above $5\times10^{6}$ cells/mL, which was correlated with the decrease in recombinant protein production. In our study, we could not observe a depletion of any of the carbon sources and amino acids analyzed during infection, including cysteine. In fact, the depletion of serine in uninfcted cultures only occurred after cells had stoped growing. This fact might

indicate that the depletion of other components of the medium (eventually vitamins or trace elements) are limiting BV production.

Alternative hypothesis have been pointed as possible explanations for limited productivities in older culures without medium exchange. Some authors have shown previously the linking between oxygen uptake rate, infection and protein production in the BV-insect cell expression system (Lecina et al., 2006; Palomares et al., 2004), while others even stated that control of oxygen supply after infection is critical and determined that in order to obtain good productivities, oxygen concentration should be kept above 20% (Taticek and Shuler, 1997). As mentioned, it is not conclusive that this is the determinant factor given the metabolic depression also observed in oxygen-controlled bioreactors along culture growth (data not shown). Most of the reports that have systematically addressed the cell density effect in insect cells performed infections in shake or spinner flasks, after growing cells to the desired cell densities in bioreactor at different oxygen concentrations (Caron et al., 1990; Radford et al., 1997; Reuveny et al., 1993); therefore, oxygen was not limiting at the time of infection. From another perspective, the constitutive secretion of regulatory factors down-regulating metabolic activity could limit productivities at high cell densities (Doverskog et al., 1997), as an intrinsinc mechanism for cell density control. This hypothesis is consistent with our data, including the positive effect of ressuspending the cells in fresh medium prior infection.

In conclusion, data presented in this work provide a systematic analysis of how culture and infection parameters affect BV production. The main bottleneck appears to be the decreased productivities observed at high cell density culture, paralleling abundant information reported on recombinant protein production with the BEVS technology. One of the main strategies to overcome the cell density effect is the re-suspension of cells in fresh

medium prior to infection. However, total medium replacement, though feasible for small scale cultures, is not suitable for higher production scales, increasing the cost of the bioprocess due to the need for separation devices and extra medium costs. On the other hand, the simple addition of complex nutrient mixtures hinders the identification of the individual components that may be limiting production, besides involving higher operation costs and inducing variability in process performance. Considering this, we believe that future improvement of the insect cell-baculovirus system is highly dependent on a detailed characterization of insect cells metabolism along culture time and after infection. The growing application of recombinant BVs for gene therapy represents an opportunity to deepen the knowledge around this system.

## ACKNOWLEDGEMENTS

This work was supported by the European Project BACULOGENES, contract FP6-037541. Nuno Carinhas is grateful to Dr. John Aunins (Merck, USA) for fruitful discussions and acknowledges Fundação para a Ciência e a Tecnologia (FCT) for his Ph.D. grant (SFRH/BD/36676/2007). This work was also partially financed by FCT project POCTI/BIO/55975/2004. Vicente Bernal and Adriana Y. Yokomizo hold post-doctoral fellowships of Fundación Séneca (Murcia, Spain) and Conselho Nacional de Desenvolvimento Científico e Tecnológico (Brazil), respectively.

## REFERENCES

Bédard C, Kamen A, Tom R, Massie B (1994) Maximization of recombinant protein yield in the insect cell/baculovirus system by one-time addition of nutrients to high-density batch cultures. *Cytotechnology* **15**: 129-38

Bédard C, Tom R, Kamen A (1993) Growth, nutrient consumption, and end-product accumulation in Sf-9 and BTI-EAA insect cell cultures: insights into growth limitation and metabolism. *Biotechnol Prog* **9**: 615-24

Caron AW, Archambault J, Massie B (1990) High-level recombinant protein production in bioreactors using the baculovirus-insect cell expression system. *Biotechnol Bioeng* **36**: 1133-40

Doverskog M, Ljunggren J, Ohman L, Haggstrom L (1997) Physiology of cultured animal cells. *J Biotechnol* **59**: 103-15

Drews M, Doverskog M, Ohman L, Chapman BE, Jacobsson U, Kuchel PW, Haggstrom L (2000) Pathways of glutamine metabolism in *Spodoptera frugiperda* (Sf9) insect cells: evidence for the presence of the nitrogen assimilation system, and a metabolic switch by 1H/15N NMR. *J Biotechnol* **78**: 23-37

Drews M, Paalme T, Vilu R (1995) The growth and nutrient utilization of the insect cell line *Spodoptera frugiperda* Sf9 in batch and continuous culture. *J Biotechnol* **40**: 187-98

Elias CB, Zeiser A, Bedard C, Kamen AA (2000) Enhanced growth of Sf-9 cells to a maximum density of 5.2 x 107 cells per mL and production of *β*-galactosidase at high cell density by fed batch culture. *Biotechnol Bioeng* **68**: 381-8

Ikonomou L, Schneider YJ, Agathos SN (2003) Insect cell culture for industrial production of recombinant proteins. *Appl Microbiol Biotechnol* **62**: 1-20

King LA, Possee RD (1992) The baculovirus expression vector system: a laboratory guide. Chapman & Hall, London

Kost TA, Condreay JP (2002) Recombinant baculoviruses as mammalian cell gene-delivery vectors. *Trends Biotechnol* **20**: 173-80

Lecina M, Soley A, Gracia J, Espunya E, Lazaro B, Cairo JJ, Godia F (2006) Application of on-line OUR measurements to detect actions points to improve baculovirus-insect cell cultures in bioreactors. *J Biotechnol* **125**: 385-94

Licari P, Bailey JE (1992) Modeling the population dynamics of baculovirus-infected insect cells: optimizing infection strategies for enhanced recombinant protein yields. *Biotechnol Bioeng* **39**: 432-41

Lindsay DA, Betenbaugh MJ (1992) Quantification of cell culture factors affecting recombinant protein yields in baculovirus-infected insect cells. *Biotechnol Bioeng* **39**: 614 - 8

Mendonça RZ, Palomares LA, Ramiréz OT (1999) An insight into insect cell metabolism through selective nutrient manipulation. *J Biotechnol* **72**: 61-75

Öhman L, Alarcon M, Ljunggren J, Ramqvist A-K, Häggström L (1996) Glutamine is not an essential amino acid for Sf-9 insect cells. *Biotechnol Lett* **18**: 765-70

Öhman L, Ljunggren J, Häggström L (1995) Induction of a metabolic switch in insect cells by substrate-limited fed-batch cultures. *Appl Microbiol Biotechnol* **43**: 1006-13

Palomares LA, López S, Ramírez OT (2004) Utilization of oxygen uptake rate to assess the role of glucose and glutamine in the metabolism of infected insect cell cultures. *Biochem Eng J* **19**: 87-93

Power JF, Reid S, Radford KM, Greenfield PF, Nielsen L, K. (1994) Modeling and optimization of the baculovirus expression vector system in batch suspension culture. *Biotechnol Bioeng* **44**: 710-9

Racher AJ, Looby D, Griffiths JB (1990) Use of LDH release to assess changes in culture viability. *Cytotechnology* **3**: 301-7

Radford KM, Reid S, Greenfield PF (1997) Substrate limitation in the baculovirus expression vector system. *Biotechnol Bioeng* **56**: 32-44

Reuveny S, Kim YJ, Kemp CW, Shiloach J (1993) Production of recombinant proteins in high-density insect cell cultures. *Biotechnol Bioeng* **42**: 235-239

Rhiel M, Murhammer DW (1995) The effect of oscillating dissolved oxygen concentrations on the metabolism of a *Spodoptera frugiperda* IPLB-Sf21-AE clonal isolate. *Biotechnol Bioeng* **47**: 640–50

Taticek RA, Schuler, ML (1997) Effect of elevated oxygen and glutamine levels on foreign protein production at high cell densities using the insect cell-baculovirus expression system. *Biotechnol Bioeng* **54**: 142-52

Tom RL, Debanne MT, Bédard C, Caron AW, Massie B, Kamen AA (1995) Improved yields of the extracellular domain of the epidermal growth factor receptor produced using the baculovirus expression system by medium replacement following infection. *Appl Microbiol Biotechnol* **44**: 53–8

Wang M-Y, Kwong S, Bentley WE (1993) Effects of oygen/gucose/gutamine feeding on insect cell baculovirus protein expression: a study on epoxide hydrolase production. *Biotechnol Prog* **9**: 355-61

Weiss SA, Whitford WG, Godwin GP, Reid S (1992) Media design: optimizing of recombinant proteins in serum free culture. In: Vlak JM, Schlaeger E-J, Bernard AR, editors. Workshop on Baculovirus and Recombinant Protein Production Processes, March 29-April 1, Interlaken, Switzerland.

# CHAPTER II

## METABOLIC CHARACTERIZATION OF GROWTH AND BACULOVIRUS INFECTION OF *SF*9 CELLS

**ADAPTED FROM:**

Bernal V/Carinhas N, Yokomizo AY, Carrondo MJT, Alves PM (2009) Cell density effect in the Baculovirus-Insect Cells system: a quantitative analysis of energetic metabolism. *Biotechnol Bioeng* **104**: 162-180.

# TABLE OF CONTENTS

## 1. SUMMARY

In this chapter, a model for the central metabolism of serum-free suspension cultures of *Sf*9 cells is proposed and used to investigate the metabolic basis for the so-called cell density effect. The main metabolic pathways (glycolysis, pentose-phosphate pathway, tricarboxylic acids cycle, glutaminolysis and amino acids metabolism), cellular growth and energetics were considered. The analysis of the stoichiometric model allowed further understanding of the interplay of the consumption of carbon and nitrogen sources in insect cells. Moreover, metabolic flux analysis revealed that *Sf*9 cells undergo a progressive inhibition of central metabolism when grown to high cell densities, for which the lower incorporation of amino acids carbon backbones into the tricarboxylic acids cycle (mainly glutamine) and the down-regulation of glycolysis are partially responsible. Following infection by baculovirus and cellular division arrest, central energy metabolism depended on the infection strategy chosen (cell concentration at the moment of infection and multiplicity of infection), an inhibition being observed at high cell densities. Interestingly, the energetic status of the cells correlated with the decrease in production of baculovirus vectors, meaning that there is room for process optimization through the application of metabolic engineering techniques.

## 2. INTRODUCTION

Metabolic Flux Analysis (MFA) is a well established technique for the assessment of metabolic adaptations undergone by any type of cell in culture (Stephanopoulos et al., 1998). Since the early 90's, metabolic models have been developed for the study of cellular physiology and for the optimization of bioproduction systems in many organisms. Because of their higher simplicity and the wealth of data existing on the metabolism and

physiology of yeast and bacteria, most of the initial applications of MFA were developed for microorganisms. However, the increasing interest gained by animal cell-based bioprocesses for high added value products has encouraged the application of these techniques to the more complex eukaryotic cells. Improvement of cell metabolism would yield increased growth, viability, productivity, substrate spectrum, energy yield and/or bioprocess robustness, thus reducing process costs.

Although some authors have highlighted the need for an in depth analysis of the main metabolic constraints limiting productivity in the baculovirus-insect cells system, to date very few works have dealt with this issue (Bhatia et al., 1997; Ferrance et al., 1993; Ikonomou et al., 2003). In particular, a fundamental understanding of the well documented loss in specific productivity when insect cells are infected at high densities would be valuable to design optimized bioprocesses (Bhatia et al., 1997; Ikonomou et al., 2003; Palomares et al., 2006; Taticek and Shuler, 1997). As current practice, infection is normally performed at a low cell concentration at infection (CCI) to obtain higher protein yields (Maranga et al., 2003). Moreover, depending on the infection strategy, cell culture system and medium used, a wide range of cell concentrations have been considered to be either low or high densities (for example, compare Chapter I with Radford et al., 1997).

Reports on the metabolism and physiology of insect cells, and on *Spodoptera frugiperda Sf*9 cells in particular, are scarce. Nutrient depletion has been proposed as the main cause for reduced recombinant protein yields in cultures of intermediate cell densities rather than inhibition by waste products (Drews et al., 1995). In fact, unlike most mammalian cell lines, alanine and ammonia are not related to growth inhibition (Doverskog et al., 1997). Glucose is the preferred carbon source, while there are contradictory reports concerning the consumption of disaccharides such as

maltose and sucrose (Ikonomou et al., 2003; Rhiel et al., 1997; Sugiura and Amann, 1996). Lactate and pyruvate cannot support *Sf*9 cell growth, which led some to propose that gluconeogenesis does not operate efficiently in insect cells (Bhatia et a., 1997). An important difference with respect to mammalian cell lines is that some insect cell lines, including *Sf*9 cells, do not significantly accumulate lactate, which has been attributed to a more active tricarboxylic acids (TCA) cycle (Neermann and Wagner, 1996). Finally, regarding nitrogen metabolism, there is a preference for the uptake of amino acids over their synthesis (Bhatia et al., 1997; Doverskog et al., 1997; Ferrance et al., 1993).

Remarkably, even fewer works have dealt with the metabolism of *Sf*9 cells after baculovirus infection. There are reports on the increase in oxygen uptake after infection (Cruz et al., 1998; Palomares et al., 2004) and on the effect of supplementation of growth media with glucose and glutamine, yeastolate or total/partial medium exchange at infection, which may increase protein production (Bhatia et al., 1997; Chapter I; Ikonomou et al., 2003; Palomares et al., 2004). Recently, RNA interference has been demonstrated as a useful strategy for the improvement of bioprocess performance using *Sf*9 cells (Kim et al., 2007). Nevertheless, there is still a lack of knowledge on the correlation of metabolic shifts occurring with cellular productivity. Moreover, model derived information would be crucial for the development of rational feeding strategies in order to increase the production of proteins or BVs by insect cells.

In this work, Metabolic Flux Analysis has been applied to assess the metabolic shifts in *Sf*9 insect cells as a consequence of cell density and baculovirus infection.

## 3. METABOLIC NETWORK

A metabolic model considering the central pathways of *Sf*9 cells was herein constructed. For that purpose, available information from previous models developed for other animal cell lines, basic biochemistry text books and public access databases were considered (Altamirano et al., 2006; Berg et al., 2002; Bonarius et al., 1996; Caspi et al., 2008; Henry et al., 2005; Nadeau et al., 2000; Wahl et al., 2008). Moreover, specific information available for *Sf*9 cells metabolism was also included (Doverskog et al., 2000b; Doverskog et al., 1997; Drews et al., 2000; Drews et al., 1995; Ferrance et al., 1993; Ikonomou et al., 2003; Öhman et al., 1995). The model considers the main reactions of central metabolism of cultured animal cells, namely glycolysis, pentose-phosphate pathway (PPP), anaerobic fermentation, TCA cycle, respiratory pathways, amino acids metabolism (including glutaminolysis) and biomass formation. The complete set of reactions, along with an index of metabolite/cell component abbreviations, is provided in Appendix 1; Figure 2.1 shows a simplified scheme of the metabolic network. The energy dependence of membrane transport was also taken into account (Doverskog et al., 1998; Wahl et al., 2008). The 26 transmembrane transport systems considered are also listed in Appendix 1.

### 3.1. Glycolysis and pentose-phosphate pathway

Carbohydrates are assumed to be the main carbon source of *Sf*9 cells. Consumption of three carbohydrates was considered (glucose, maltose and sucrose), in accordance with previous reports (Ikonomou et al., 2003). Carbohydrates are taken up by facilitated transport and metabolized through glycolysis (Bhatia et al., 1997). The pentose-phosphate pathway serves as a source of building blocks for nucleic acids and reducing power

for biosynthetic purposes. In our model, the PPP diverges from glycolysis to yield R5P and NADPH, and it does not reconnect back to glycolysis, being directly determined by the demand of R5P for nucleic acids biosynthesis. This is a reasonable simplification since it is not possible to distinguish between parallel pathways using solely metabolite balances. Nevertheless, the underestimation of the PPP flux due to a higher demand of NADPH than that of R5P would amount to only 27%, based on the stoichiometry of the biomass synthesis reactions. The gluconeogenesis pathway was not included since it is not active in insect cells (Bhatia et a., 1997; Ferrance et al., 1993).

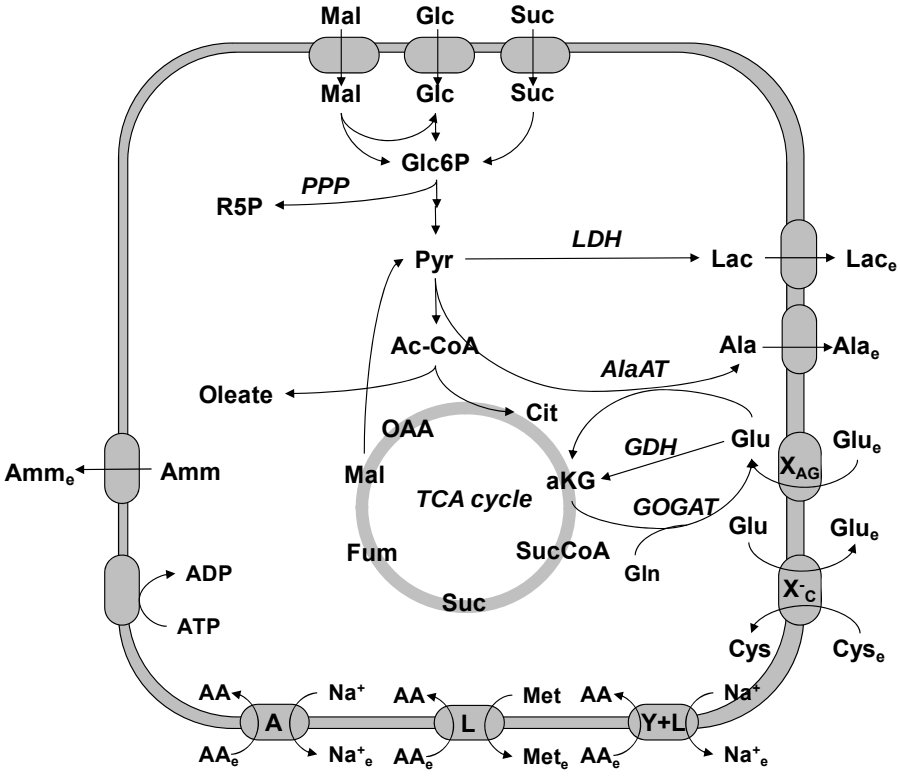


**Figure 2.1.** Main metabolic pathways considered in the central metabolism of *Sf*9 cells. See the text for details and Appendix 1 for the complete list of reactions and abbreviations index.

### 3.2. TCA cycle and malate-pyruvate shunt

The TCA cycle has been reported to be fully functional in cultured *Sf*9 cells, in contrast to what has been observed in cultured mammalian cell lines (Neermann and Wagner, 1996) and also in some other insect cell lines (Bhatia et a., 1997). For simplicity, reactions linking the TCA cycle with biosynthetic pathways were lumped into the malate-pyruvate shunt (malic enzyme, ME).

### 3.3. Pyruvate and α-ketoglutarate metabolic nodes

The role of pyruvate and α-ketoglutarate nodes is key in redirecting intracellular metabolic fluxes. Pyruvate participates in various reactions as an intermediary in the metabolism of a few amino acids, recipient of the ammonia group for detoxification, as an electron sink in fermentative pathways and, specially, as the link between glycolysis and the TCA cycle. Pyruvate formed by glycolysis can either be used as metabolic fuel in the TCA cycle to obtain reducing power or to be used for the formation of alanine or lactate by means of alanine aminotransferase (AlaAT) or lactate dehydrogenase (LDH) activities, respectively (Figure 2.1). On the other hand, α-ketoglutarate has a pivotal role connecting the metabolism of amino acids with the TCA cycle, also being connected with the pyruvate pool through AlaAT (Figure 2.1).

### 3.4. Amino acids transport

The requirements of amino acids by *Sf*9 cells have been reported to be higher than those strictly necessary for the synthesis of cellular proteins. Amino acids such as glutamine, glutamate, aspartate, serine, arginine and

methionine are used for energy production (Drews et al., 1995; Ferrance et al., 1993). The uptake of amino acids from the growth medium is energy-dependent, while outflow can be assumed to occur by diffusion (Caspi et al., 2008; Doverskog et al., 1997; Wahl et al., 2008). For our modelling purposes, amino acids outflow was relevant only in the case of alanine, which is the only amino acid with a net positive production rate.

Importantly, the thermodynamics of amino acids transport is highly dependent on their chemical nature (Wahl et al., 2008). Negatively charged glutamate and aspartate use the System $X^-_{AG}$ Transporters, consuming 1 molecule of ATP for each molecule transported, in order to overcome electrochemical gradients. Neutral amino acids are transported through two main systems: short chained neutral amino acids (methionine, threonine, serine, proline, glycine, asparagine and alanine) are taken up by System A Transporters, while large hydrophobic amino acids (tryptophan, phenylanine, valine, leucine, isoleucine, glutamine, histidine and tyrosine) use System L Transporters. These two systems consume 0.33 molecules of ATP *per* molecule taken inside the cell. Positively charged amino acids can be transported through various mechanisms, but System y+L Transporters are assumed in this work for the transport of lysine and arginine. This system also consumes 0.33 ATP molecules per transported amino acid. Cysteine uptake occurs through the $X_C^-$ Transporter, an antiport system that exchanges glutamate for cysteine and is driven by the concentration gradients of these amino acids (Doverskog et al., 1998).

The regulation of amino acids uptake by cell cycle and growth arrest has been already demonstrated. In fact, System A Transporters are closely related to the position in the cell cycle and in mammalian cells they are regulated by growth factors (such as insulin), also causing, indirectly, the cessation of System L Transporters (Doverskog et al., 1997).

### 3.5. Nitrogen metabolism and ammonia detoxification

Amino acids can face various metabolic fates, either being used for protein production or degraded to be used as carbon and nitrogen sources. In a rich medium such as SF900II, biosynthesis of amino acids can be neglected. The reactions for amino acids degradation were taken from the literature (Berg et al., 2002; Caspi et al., 2008; Voet and Voet, 1995). For simplicity, non-ramified reactions in these pathways were lumped into simpler reactions, as indicated in Appendix 1.

Some peculiarities of the nitrogen metabolism of insect cells have already been reported. A NADH-dependent glutamate synthase (GOGAT) activity has been detected in cell free extracts of *Sf*9 cells and other Lepidopteran species (Doverskog et al., 2000b). This activity catalyzes the reductive transfer of the amido group of glutamine to α-ketoglutarate, forming glutamate and by-passing the production of ammonia. Moreover, in glutamine-free medium, ammonium ions can be incorporated into amino acids such as alanine and glutamine (Drews et al., 2000). In fact, NADH-dependent glutamate dehydrogenase (GDH) and glutaminase activities were also detected using $^{1}H,^{15}N$-NMR-based methods, although activities were about 55% and 11% of that of GOGAT, respectively (Doverskog et al., 2000b). Additionally, the fact that these activities are dependent on NADH and not on NADPH further supports a catabolic rather than anabolic role.

Cultured *Sf*9 cells do not accumulate ammonia in the presence of excess of glucose and glutamine, alanine being the main by-product (Drews et al., 2000). Pyruvate functions as a recipient of the ammonia group from glutamate in a reaction catalyzed by the alanine aminotransferase (AlaAT) activity. This activity allows coupling the entrance of glutamate (formed

from other amino acids) to the TCA cycle as α-ketoglutarate without the concomitant production of free ammonia.

### 3.6. Energy production

Reduced cofactors generated by the central metabolism (NADH and $FADH_2$) are oxidized in the mitochondrial electron transport chain with oxygen as a final acceptor. A transhydrogenase reaction was included to account for the interconversion of NADH and NADPH. The balance of ATP was not closed, since not all the phenomena leading to energy consumption (cellular maintenance, futile cycles) can be incorporated. A unidirectional flux was set to represent the expense of ATP molecules associated with other metabolic events, including waste through futile cycles.

### 3.7. Cellular growth

In order to account for cellular growth, *Sf*9 cells biomass was considered to be formed mostly of proteins, lipids and nucleic acids. The cellular dry weight of *Sf*9 cells and macromolecular composition was estimated from previously published data for insect cells (Ferrance et al., 1993); these were similar to data published for other cell lines (Gambhir et al., 2003; Nadeau et al., 2000; Xie and Wang, 1994; Zupke and Stephanopoulos, 1995).

To account for protein synthesis, the amino acids composition was taken from the literature (Ferrance et al. 1993; Xie and Wang 1994). Consumption of ATP for protein synthesis was also considered.

The total lipidic bulk of *Sf*9 cells was assumed to be composed of oleic acid, which accounts for almost half of the total fatty acids, being the most prevalent component of the most abundant phospholipids in this cell line (Marheineke et al., 1998). A lumped equation for oleic acid synthesis from acetyl-CoA was derived, calculating the extra ATP necessary for the transport of acetyl-CoA from the mitochondria to the cytosol as citrate (1 ATP per acetyl-CoA molecule) and for the transfer of reducing equivalents from mitochondria to the cytosol (Berg et al., 2002).

The GC content of lepidopteran DNA is about 35-40% (The international Lepidopteran Genome Project). The lumped equation for DNA synthesis was determined considering a G/C content of 40%. The size of the haploid genome of *S. frugiperda* is $8 \cdot 10^8$ bp; from this data, 1.4% of the cellular weight is computed to correspond to DNA. However, polyploidy and chromosome instability have previously been reported for this insect cell line (Jarman-Smith et al., 2002), and the value of 4.8% previously determined experimentally by Ferrance et al. (1993) was considered to obtain the biomass production equation shown in Appendix 1.

### 3.8. Mitochondrial compartmentalization

Mitochondrial compartmentalization is not explicitly considered in the model since mitochondrial shuttle mechanisms have not been characterized in insect cell lines. Moreover, mitochondrial and cytosolic pools of redox nucleotides can be considered to be in equilibrium since lactate production is much lower than in mammalian cells. However, the energetic requirements for certain mitochondrial transmembrane transport phenomena were taken into account, as already underlined in the case of the lumped equation for the synthesis of lipids.

# 4. MATERIALS AND METHODS

Detailed materials and methods on cell maintenance, baculovirus amplification and titration, experimental cultures and infections, glucose, lactate, ammonia and amino acids analyses can be found in Chapter I. In addition to these metabolites, the concentrations of maltose and sucrose were measured in the culture medium. These were enzymatically hydrolyzed using α-glucosidase and baker's yeast invertase from Sigma-Aldrich (St. Louis, MO, USA), respectively. Glucose resulting from these reactions was measured using the YSI 7100 system as before.

## 4.1. Metabolic Flux Analysis

A system of mathematical equations was formulated on the basis of material balances for the metabolic network, according to general MFA theory (Stephanopoulos et al., 1998):

$$r(t) = Av(t) \quad , \qquad \text{(Eq. 1)}$$

where r(t) is the vector for the accumulation rates of each compound considered in the network, A is the stoichiometric matrix of the metabolic network and v(t) is the vector of the fluxes through the various biochemical reactions listed in Appendix 1.

The pseudo-steady-state hypothesis for intracellular metabolites, considering their accumulation inside the cells as negligible, is generally accepted as reasonable (Altamirano et al., 2006; Nadeau et al., 2000). In a typical biochemical network, the number of reaction rates is higher than the number of metabolites, resulting in an underdetermined system with a

variable number of degrees of freedom (meaning that not all the rates can be uniquely computed). In order to solve the system of equations, some fluxes have to be experimentally determined. The most common case is to determine transmembrane rates of metabolites consumed and/or secreted by the cells. Together with the irreversibility of some reactions, these are the modelling constraints that cannot be violated when solving metabolic network.

In the model hereby considered, the total number of reactions was 73, with 52 internal (balanced) intracellular metabolites/cell components. The balances of urea, mevalonate and ADP could not be closed, as these metabolites intervene in reactions not considered in the network. As stated above, an unidirectional flux was used to represent the expense of ATP molecules associated with cellular maintenance and waste through futile cycles. The rank of the resulting stoichiometric matrix was 49, meaning that there are 3 (52 less 49) conservation relations (corresponding to the balances of redox cofactors: $NAD^+$/NADH, $NADP^+$/NADPH and FAD/$FADH_2$). The resulting number of degrees of freedom of the system is thus 24 (73 reactions less 49 independent balances). From the profiles of extracellular concentrations, 24 metabolite consumption/production rates were experimentally determined. Additionally, the specific growth rate was measured, and some intracellular reaction rates (namely the intracellular hydrolysis of maltose and sucrose and the synthesis of lactate from pyruvate), were set equal to the respective extracellular measured fluxes. In total, 28 known rates were considered.

The vector of fluxes in Eq. (1) was then partitioned into known flux and unknown flux vectors, $v_b$ and $v_n$, respectively. Similarly, the stoichiometric matrix A was partitioned into $A_b$ and $A_n$. Eq. (1) was rewritten as:

$$0 = Av = A_b v_b + A_n v_n \quad . \qquad \text{(Eq. 2)}$$

The analysis of the matrices showed that the system is determined (meaning that it is possible to uniquely compute all rates of $v_n$) and also redundant, according to the classification proposed by Klamt et al. (2002). The redundant system at hand was solved by the weighted least squares method using the Penrose pseudo-inverse matrix. The balanceable rates, which arise from system redundancy, were used to calculate the consistency index, *h*, according to Wang and Stephanopoulos (1983). Comparison of *h* with the $\chi^2$-test function was done in order to evaluate the consistency of the experimental values along with the assumed biochemistry and the pseudo-steady-state assumption within the error dictated by measurement uncertainties. From our analysis, errors for disaccharides and amino acid uptake rates stood below 12%, while for glucose consumption was below 6%. All the calculations were performed using the CellNetAnalyzer software (Klamt et al., 2007). In addition, material balances were performed to confirm that all key components of the system were covered and, on average, fit within 100% ± 15% for all phases (100% ± 10% for more than half of the phases analyzed). This shows that the experimental data are consistent with the assumed biochemistry and the pseudo-steady state assumption, and that there were no systematic or gross measurement errors.

# 5. RESULTS

## 5.1. Effect of cell density on the central metabolism of *Sf*9 insect cells

In order to determine the effect that the different phases of cellular growth have on the energetic metabolism of *S. frugiperda*, *Sf*9 cells were cultured in SF900II serum free medium as explained in Chapter I. For the analysis

of metabolic adaptations undergone, seven phases were defined by considering the growth and metabolic profiles (see Figure 1.1 in Chapter I). The pseudo-steady state hypothesis for intracellular metabolites was assumed to be valid within each phase, and consumption and production rates (extracellular fluxes) were determined from bulk concentrations of carbon sources, amino acids and the main by-products (alanine, lactate and ammonia). Main extracellular fluxes of sugars, amino acids and by-products are shown in Table 2.1, expressed in nmol/$10^6$ cells/h. Preliminary analysis showed that the application of MFA to the lag and cell death phases did not yield any interpretable result, since the consistency index condition ($h < \chi^2$) was not fulfilled, probably due to the high experimental error associated to the determination of low consumption/production rates and/or to the liberation of intracellular compounds to the growth medium as a consequence of cell lysis, respectively. Consequently, only five phases were ultimately considered: initial, medium and late exponential growth (cell densities: 1-2×$10^6$ cells/mL, 24-48 h; 2-3.5×$10^6$ cells/mL, 48-72 h; 3.5-8×$10^6$ cells/mL, 72-96 h, respectively), and early and late stationary phases (8-9×$10^6$ cells/mL, 96-120 and 120-168 h, respectively).

As previously described, growth of *Sf*9 cells was linked to sugar consumption. Three carbon sources are used by *Sf*9 cells for growth in SF900II medium. The major carbon source is glucose (which is present at high concentration, around 55 mM), while consumption of alternative sugar sources (maltose and sucrose, present at lower concentrations) was detected, although at much lower rates than glucose (Table 2.1). Lactate production was only detected when high cell densities were attained, while ammonia levels remained in the range of 4-6 mM throughout the culture, with little or no accumulation. As already described, alanine was the most important by-product (Bédard et al., 1993; Kamen et al., 1991), its

production spanning the whole culture. *Sf*9 cells consumed the amino acids present in the growth medium, especially asparagine, arginine, aspartate, glutamine and glutamate, which are known to be processed through the TCA cycle for energy generation and biosynthesis, and are also those existing at the higher concentrations (around 10 mM). Serine was the only amino acid to be totally consumed at 170-190 h (as pointed out in Chapter I), while cells had stopped growing by that time and the specific growth rate significantly decreased much before (Table 2.1). At end of the culture, the rest of the amino acids and sugar sources were still available in the growth medium.

The extracellular rates determined were used to estimate intracellular metabolic fluxes using the model described. The main intracellular fluxes for uninfected *Sf*9 cells are shown in Figure 2.2.

*Glycolysis and pentose-phosphate pathway.* The three sugars taken up (glucose, maltose and sucrose) were mainly channelled to pyruvate through the glycolytic pathway (Figure 2.2A). Fluxes of glucose-6-phosphate through the pentose-phosphate pathway (PPP) were directly proportional to cellular growth rate, reaching a maximum during the early exponential growth phase (2.5-3.5 nmol/$10^6$cells/h). This flux was positive along all the phases considered and evolved from 3.3% of the flux through the glycolytic pathway during the early exponential growth phase to 0.6% at the stationary phase, thus representing a lower proportion of glucose consumed than the 10-14% previously reported for animal cells (Benslimane et al., 2005; Neermann and Wagner, 1996).

**Table 2.1.** Specific consumption/production rates of the main metabolites of *Sf*9 cells during culture growth. Cultures were performed as described in Chapter I. Five phases (I-V) are considered (initial, medium and late exponential phases and early and late stationary phases). Rates are expressed as nmol/$10^6$cells/h.

**Extracellular fluxes for uninfected *Sf*9 cells**

| Phase | I | II | III | IV | V |
|---|---|---|---|---|---|
| **Time span (h)** | 24-48 | 48-72 | 72-96 | 96-120 | 120-168 |
| **Cell density (cells/mL)** | $1.4\times10^6$ | $2.7\times10^6$ | $4.7\times10^6$ | $6.6\times10^6$ | $7.7\times10^6$ |
| **Glc** | -82.74 | -82.13 | -51.11 | -43.51 | -45.23 |
| **Lac** | 9.43 | 3.36 | 17.05 | 7.62 | 12.44 |
| **Sucr** | -1.54 | -7.01 | -4.12 | -2.91 | -0.46 |
| **Malt** | -13.61 | -5.47 | -8.24 | -2.99 | -3.07 |
| **Amm** | -2.84 | -2.92 | 0.41 | 1.79 | 1.52 |
| **Asp** | -14.25 | -8.10 | -3.97 | -2.81 | -2.81 |
| **Glu** | -19.64 | -14.86 | -4.25 | -7.16 | -4.48 |
| **Ser** | -5.32 | -9.42 | -4.33 | -3.60 | -3.32 |
| **Asn** | -7.80 | -4.02 | -2.36 | -1.43 | -0.93 |
| **Gly** | -6.81 | -4.12 | -1.24 | -0.55 | -0.39 |
| **Gln** | -33.11 | -34.06 | -13.21 | -7.28 | -5.70 |
| **Thr** | -5.10 | -4.74 | -1.61 | -1.18 | -0.93 |
| **Ala** | 13.54 | 14.78 | 23.12 | 15.74 | 9.42 |
| **Pro** | -14.40 | -5.22 | -0.69 | -0.71 | -0.57 |
| **Tyr** | -5.32 | -4.12 | -0.32 | -0.64 | -0.44 |
| **Val** | -7.44 | -8.98 | -1.46 | -0.80 | -0.97 |
| **Met** | -9.22 | -6.90 | -0.43 | -0.47 | -0.67 |
| **Ile** | -7.09 | -8.32 | -0.94 | -0.88 | -0.61 |
| **Leu** | -4.68 | -6.72 | -2.45 | -1.44 | -1.06 |
| **Phe** | -7.66 | -8.87 | -2.06 | -0.77 | -0.50 |
| **His** | -5.74 | -2.45 | -0.86 | -0.68 | -0.23 |
| **Arg** | -10.99 | -8.76 | -1.89 | -2.64 | -1.65 |
| **Lys** | -10.78 | -7.70 | -1.82 | -0.67 | -0.35 |
| **Growth rate (/h)** | 0.029 | 0.025 | 0.022 | 0.011 | 0.004 |

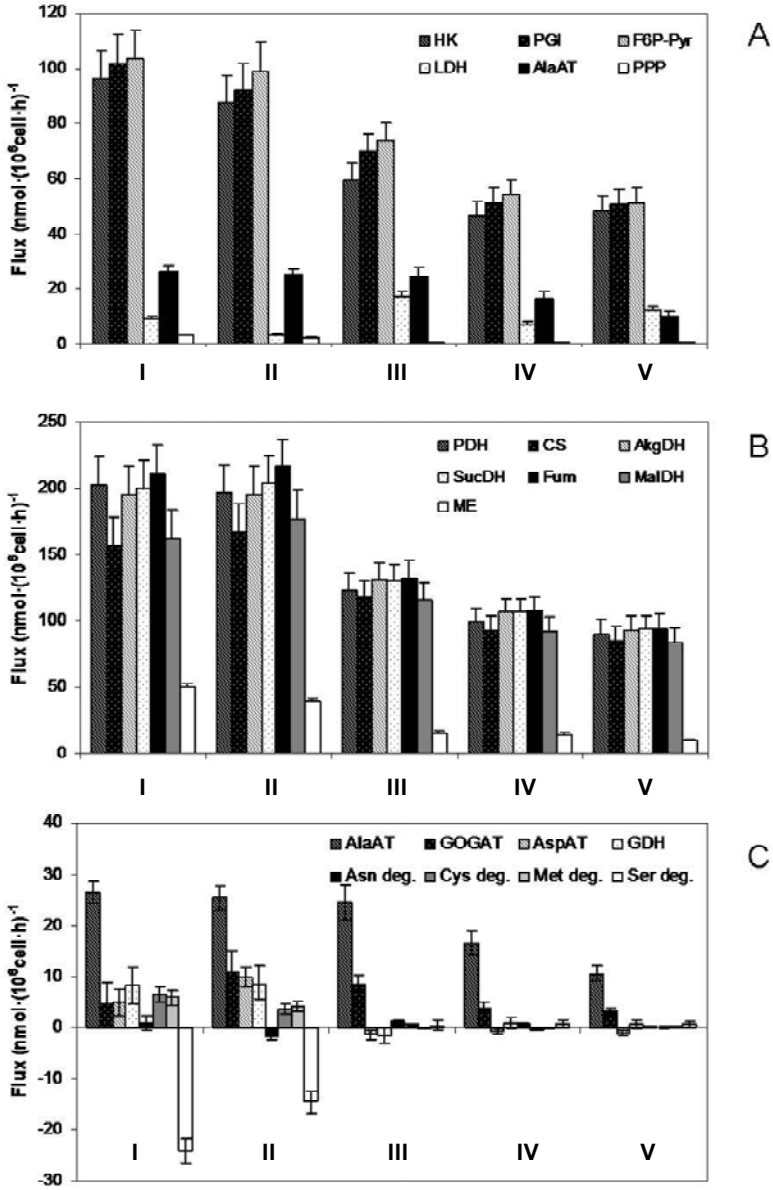


**Figure 2.2.** Main metabolic fluxes for uninfected *Sf*9 cells. (A) Glycolysis and related fluxes; (B) TCA cycle and malate-pyruvate shunt, (C) nitrogen metabolism fluxes and (D) macromolecules synthesis. Error bars correspond to standard deviations computed with the CellNetAnalyzer software. *Deg.* stands for degradation.

*TCA cycle.* The TCA cycle was fully active in *Sf*9 cells (Figure 2.2B), the ratio between the fluxes of citrate synthase (first step of the TCA cycle) and glycolysis ranging from 0.76 to 0.86, meaning that carbon oxidation was high during all phases of culture considered, even increasing at the stationary phase paring a lower use of acetyl-CoA for the synthesis of lipids under non-growing conditions (Figure 2.2B). The parallel decreasing trend observed in the fluxes of glycolysis and the TCA cycle along culture time did not correlate with the exhaustion of any medium component. The fluxes through the TCA cycle at the early and late stationary phases were around 50% of those of exponentially growing cells, revealing a high activity of maintenance metabolism and high energy needs (Figure 2.2B). Moreover, the high metabolic activity of TCA cycle was also due to amino acids consumption, since a high incorporation of carbon backbones was assessed at the α-ketoglutarate node (Figures 2.2B and 2.3C). This was especially relevant during the initial growth phases, when the highest amino acid consumption rates were observed and most of the amino acids were transformed into glutamate to enter the TCA cycle as α-ketoglutarate (Table 2.1).

*Malate-pyruvate shunt.* To allow for the complete oxidation of the carbon backbones of amino acids in the TCA cycle or diversion to biosynthesis, the functioning of the malate-pyruvate shunt is compulsory (lumped as the ME flux). The oxidation of amino acid carbon backbones further led to increased production of reduced equivalents ($FADH_2$ and NADH). An important metabolic switch was observed at cell densities of around $3\times10^6$ cell/mL, with a drastic reduction in the uptake of amino acids and in their incorporation into the TCA cycle; this led to a subsequent decrease in the flux of ME (Figures 2.2B and 2.2C). At the higher cell density phases, the decrease in these fluxes was much steeper than that of the TCA cycle, as a consequence of this cyle being fuelled mostly by glucose.

*Nitrogen metabolism.* Continued alanine production constrained ammonia cell excretion. All other amino acids were consumed although at very different rates (Table 2.1). The highest uptake rates were observed for both glutamine and glutamate during all the experimentation time, although their assimilation was highly reduced at cell densities above $3\times10^6$ cells/mL. Glutamine consumption was preferential, since glutamate uptake only increased once glutamine levels in the bulk media decreased. The most relevant amino acid fluxes are shown in Figure 2.2C. As shown, the glutamate synthase (GOGAT) pathway was more active during the initial phases of growth. A similar trend was observed for aspartate aminotransferase and glutamate dehydrogenase pathways, both of which were active in the synthesis of α-ketoglutarate from glutamate.

Interestingly, metabolic flux analysis revealed net fluxes for the synthesis of serine from pyruvate during the initial phases of growth. This active pathway supports the idea that alanine aminotransferase is not the only pathway used for *Sf*9 cells for ammonia detoxification. The existence of various active pathways collaborating in this task are likely to provide the physiological robustness to ammonia described for this cell line.

*Cellular redox and energetic state.* Oxidative phosphorylation allowed for the regeneration of the reduced cofactors produced (Figure 2.4A). The consumption and production of NADPH and NADH was balanced through a transhydrogenase reaction, although this flux revealed to be very low for all phases modelled (data not shown). The oxygen uptake rate (OUR) of *Sf*9 cells was estimated for each phase of growth from the MFA calculations, reaching a maximum for exponentially growing cells (around 560 nmol/$10^6$cells/h), these values decreasing to approximately half (260-290 nmol/$10^6$cells/h) during the stationary phase.

The net rate of energy generation was estimated from the computed fluxes as already described by other authors (Henry et al., 2005; Nadeau et al., 2002; Wahl et al., 2008). It should be underlined that consumption of ATP for transport and protein synthesis was taken into account. The energetic state of the cell suffered a steep decrease at cell densities higher than $3\times10^6$ cells/mL, coinciding with all aforementioned effects (Figure 2.5A). However, despite the net fall in the ATP production rate (more than 40%) at the stationary phase, this remained quite high, underlining the high necessity of ATP for cell maintenance.

*Synthesis of macromolecules.* As expected, the rates of synthesis of biomass components (proteins, DNA, RNA and lipids) decreased with the specific cellular growth rate (data not shown).

### 5.2. Effect of baculovirus infection on the central metabolism of Sf9 cells

*Sf*9 cells were infected with a recombinant baculovirus at different times of culture (cell concentrations at infection, CCI, around 1, 2 and $3.5\times10^6$ cells/mL) and at two MOIs, in order to analyze the interplay of these two factors on the physiology of infected cells. High MOI ensures synchronous infection and the arrest of cell division, thus allowing separating the effects of growth and infection; on the other hand, in an asynchronous infection at low MOI, cells keep on dividing and the interplay of both factors has to be considered (see Figure 1.1 in Chapter I).

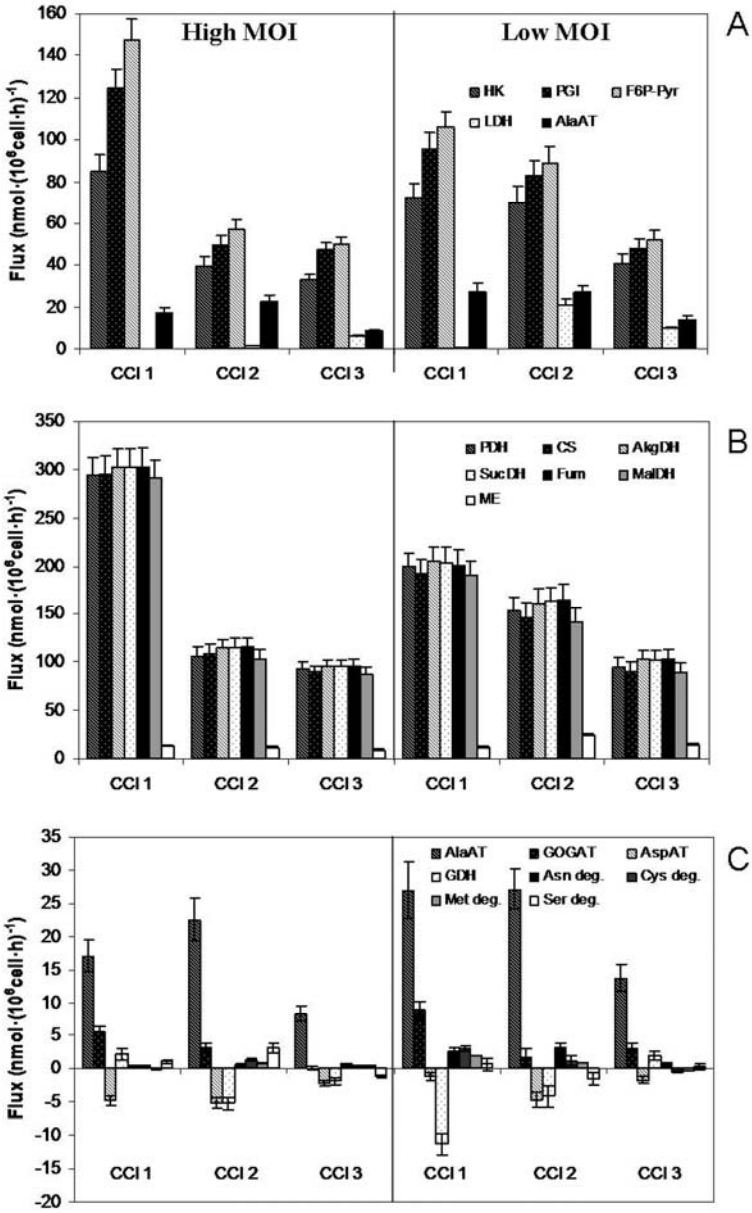


**Figure 2.3.** Main metabolic fluxes of baculovirus-infected *Sf*9 cells at high (left) and low (right) MOI. Infections were performed at three different CCIs (1, 2 and $3.5\times10^6$ cells/mL). (A) Glycolysis and related pathways, (B) TCA cycle and malate-pyruvate shunt, (C) nitrogen metabolism fluxes and (D) macromolecules synthesis. Error bars correspond to standard deviations computed with the CellNetAnalyzer software. *Deg.* stands for degradation.

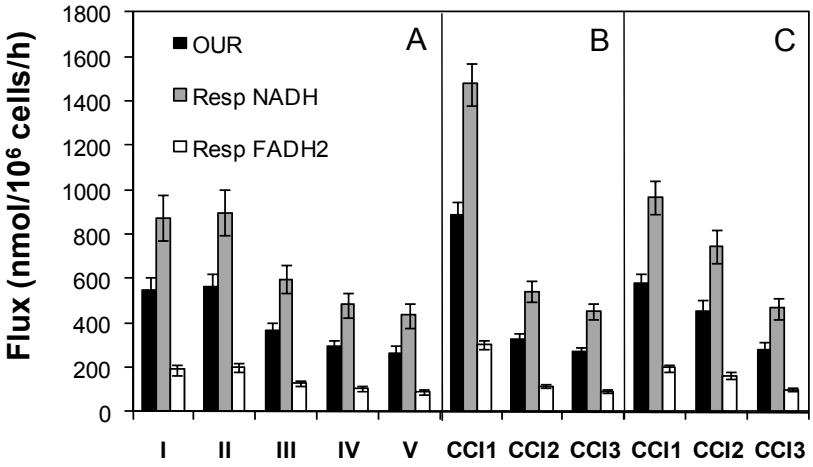


**Figure 2.4.** Respiratory fluxes of *Sf*9 cells at (A) different phases of culture growth and (B) infection at high and (C) low MOI. Error bars correspond to standard deviations computed with the CellNetAnalyzer software. *Resp.* stands for respiration.

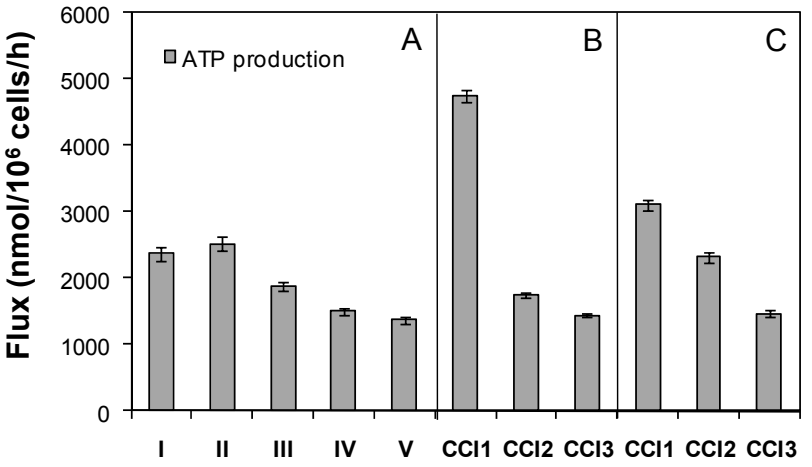


**Figure 2.5.** Estimation of net specific ATP production by *Sf*9 cells from computed metabolic fluxes. Net ATP production was represented by a unidirectional sink towards cell maintenance and futile cycles, after deducting all known expenditures explicit in the model. (A) Different phases of culture growth, (B) cells infected at different CCIs at a high and (C) at a low MOI. Error bars are standard deviations computed with the CellNetAnalyzer software.

For the determination of metabolic fluxes, a single phase post-infection was considered. To ensure the applicability of the steady-state hypothesis, experimental data were only considered such that (i) biomass levels varied only slightly and (ii) metabolite rates were almost linear. Data from the end of the experimental infections (72 hpi onwards) were not taken into account since metabolite profiles were then largely altered as a consequence of cell lysis. Additionally, the time window for baculovirus production at the MOIs used has been shown to be shorter.

The correlation between the time of infection and the metabolic pattern of infected cells was obvious, a cell density effect being observed. In general, post-infection metabolic rates decreased with CCI.

*Glycolysis and pentose-phosphate pathway.* The fluxes through glycolysis, AlaAT and LDH were in good agreement with extracellular consumption/production rates (Figure 2.3A and Table 2.2). Most of the sugars consumed were transformed into pyruvate, since the fluxes determined for the PP pathway were conditioned by the growth arrest after infection, especially in the case of high MOI. In fact, the percentage of glucose consumed that was metabolized through the PPP was always below 1%. Interestingly, the rate of glycolysis in cells infected at CCI 1 was higher than for uninfected cells at the same cell density (Figure 2.2A and 2.3A). This was due to an increase in the consumption rate of disaccharides (maltose and sucrose), together with high consumption rates of glucose (Table 2.1 and 2.2). An increase in the glycolytic fluxes in the case of low MOI infection of around 5% was detected, which for high MOIs increased to 45%. For high CCIs, glucose consumption and glycolytic rates decreased substantially, being lower than in uninfected cells at comparable cell densities. This was more pronounced for high MOI infections, directly correlating with lower carbon utilization for cell growth.

*Malate-pyruvate shunt.* The incorporation of amino acids to the TCA cycle was quantitatively reduced following infection, especially at high MOI, correlating with reduced biosynthetic needs. Consequently, the fluxes through ME of *Sf*9 cells infected at low MOI almost doubled those of cells infected at high MOI (Figure 2.3B).

*TCA cycle.* Similarly to what was observed for uninfected cells, a decreasing trend with CCI was observed for the fluxes through the TCA cycle at both MOIs. Interestingly, fluxes through the TCA cycle of *Sf*9 cells infected at $1 \cdot 10^6$ cells/mL were higher than those determined for uninfected cells at the same cell density, the differences being higher in the case of high MOI infection experiments (Figure 2.3B). At higher CCIs, the rates through the TCA cycle were sensibly lower, and closer to those observed in stationary phase *Sf*9 cells (Figure 2.3B).

*Nitrogen metabolism.* As previously stated, the metabolism of amino acids suffered deep alterations and the effects were highly dependent on the strategy of infection. In general, the fluxes for amino acid metabolism observed for baculovirus-infected *Sf*9 cells were in the range observed for non/slow-dividing cells (Table 2.2). Alanine was produced along the whole time post-infection under all the infection strategies analyzed. Specific alanine production was higher after infection at low MOI (Table 2.2), confirming that amino acids consumed were not used primarily for viral protein synthesis. The effect on alanine production seems to be dependent on the cell density; indeed, for the high MOI infections, at a cell density of $1 \times 10^6$ cells/mL, alanine specific production was higher for infected cells, at $2 \times 10^6$ cells/mL was similar to uninfected cells, while at a CCI of $3 \times 10^6$ cells/mL, alanine production after infection was lower than for uninfected cells.

**Table 2.2.** Specific consumption/production rates of the main metabolites of *Sf*9 cells infected with *Ac-hisgfp*. Cells were cultured in batch and infected at low and high MOI, as stated in the Materials and Methods section. A single phase post infection was considered. Rates are expressed as nmol/$10^6$cells/h.

**Extracellular fluxes for infected *Sf*9 cells**

| | High MOI | | | Low MOI | | |
|---|---|---|---|---|---|---|
| | **CCI 1** | **CCI 2** | **CCI 3** | **CCI 1** | **CCI 2** | **CCI 3** |
| **Glc** | -68.89 | -37.68 | -20.66 | -58.10 | -61.03 | -37.31 |
| **Lac** | -1.41 | 1.32 | 5.90 | 0.59 | 21.40 | 9.59 |
| **Sucr** | -23.24 | -7.85 | -2.66 | -10.02 | -6.10 | -4.41 |
| **Malt** | -16.55 | -1.96 | -12.20 | -14.09 | -9.01 | -3.50 |
| **Amm** | -4.01 | 0.81 | -1.01 | -6.71 | -1.46 | 2.26 |
| **Asp** | -4.48 | -4.71 | -2.63 | 0.26 | -6.31 | -2.84 |
| **Glu** | 0.08 | 0.33 | -6.10 | 4.60 | -14.31 | -8.33 |
| **Ser** | -0.99 | -3.77 | -0.82 | -4.47 | -4.91 | -2.23 |
| **Asn** | -0.33 | -0.61 | -1.02 | 2.96 | -5.01 | -1.22 |
| **Gly** | 0.00 | 0.47 | -0.02 | 0.79 | -1.30 | -0.43 |
| **Gln** | -5.64 | -3.44 | -1.64 | -9.21 | -9.11 | -5.06 |
| **Thr** | -0.08 | -0.38 | -0.22 | -0.20 | -1.53 | -0.61 |
| **Ala** | 17.08 | 22.28 | 7.52 | 35.32 | 21.76 | 15.53 |
| **Pro** | -0.25 | 0.42 | 0.22 | -0.66 | 0.00 | -0.25 |
| **Tyr** | -0.33 | -0.09 | 0.10 | -0.39 | -0.98 | -0.36 |
| **Val** | 0 | -0.33 | -0.35 | 0 | -3.09 | -0.68 |
| **Met** | 0 | -0.85 | -0.64 | 0 | -1.62 | -0.05 |
| **Ile** | -0.50 | -0.14 | -0.27 | 0 | -2.18 | -0.65 |
| **Leu** | -0.02 | -0.66 | -0.22 | -1.71 | -2.96 | -0.90 |
| **Phe** | -0.41 | -0.24 | -0.47 | 0 | -1.95 | -0.54 |
| **His** | 0 | -0.04 | -0.02 | 0 | -0.55 | -0.20 |
| **Arg** | -0.91 | -2.12 | -0.35 | -0.59 | -2.73 | -0.72 |
| **Lys** | -0.06 | -0.42 | -0.20 | 0 | -2.18 | -0.72 |
| **Cys** | -0.50 | -0.57 | -0.22 | -1.38 | -1.46 | -0.20 |
| **Growth rate (/h)** | 0.004 | 0.004 | 0.000 | 0.004 | 0.006 | 0.004 |

Moreover, glutamine uptake rates and intracellular related fluxes decreased with CCI, while the contrary effect was assessed for glutamate (Table 2.2 and Figure 2.3C). Interestingly, flux through the GOGAT pathway followed a parallel trend to alanine production (Figure 2.3C), which were the most active pathways in nitrogen metabolism at both MOIs. Considering the rest of the amino acids, lower utilization rates and intracellular metabolic fluxes were assessed as a consequence of lower biomass synthesis after cell growth arrest and despite none of them being limiting in the medium (Figure 2.3C). All fluxes determined occurred in the direction of glutamate formation, while this was channelled to alanine formation by transamination with pyruvate (AlaAT) and α-ketoglutarate (Figure 2.1).

*Cellular redox and energetic state.* As expected, the alteration of the TCA cycle activity was followed by a corresponding modification of mitochondrial respiration and ATP synthesis (Figure 2.4B,C and 2.5B,C). For low and high MOI infections at a CCI of $1\times10^6$ cells/mL, OUR reached 580 and 890 nmol/$10^6$cells/h, respectively, representing an increment of 6 and 63% with respect to uninfected conditions. This increase is in accordance with previously published data for baculovirus infected insect cells (Gotoh et al., 2004; Kamen et al., 1996; Lecina et al., 2006; Palomares et al., 2004). At higher CCIs, the specific OURs were lower than those determined for uninfected cells (around 60-80% of values obtained at equivalent cell densities).

In the case of baculovirus infected insect cells, the fluxes determined through the transhydrogenase reaction were also very low for all conditions modelled, thus pointing to a balanced redox metabolism after infection (data not shown).

*Synthesis of macromolecules.* The rates of synthesis of biomass components decreased 5 to 20-fold following infection as a consequence of

the cell division arrest. This effect was dependent on the MOI of infection and, therefore, more important at high MOI (data not shown).

## 6. DISCUSSION

Despite the wide spreading of the applications of the BEVS for the production of proteins, virus-like particles and viruses, the metabolic behaviour of *Sf*9 cells has not been fully characterized to date. In a first attempt to quantify metabolic fluxes of uninfected *Sf*9 cells, Ferrance et al. (1993) used carbon balances and a simple metabolic network. In the present paper, a comprehensive network describing carbon and nitrogen metabolism brings together, for the first time, data from published literature for insect cells and models previously developed for mammalian cell lines. To our knowledge, this is the first report on the effect of baculovirus infection on metabolic fluxes of *Sf*9 cells. The application of this methodology sheds light on the interplay of cell density and baculovirus infection on the cellular metabolic state.

The results presented herein are in accordance with the most prevalent metabolic features previously stated for the *Sf*9 insect cell line. Undoubtedly, the most striking characteristic is its active TCA cycle, which has been considered to be responsible for the low lactate production rates. For mammalian cell lines, the high lactate to glucose ratio is used as an indication of the low efficiency of glucose oxidation, while in *Sf*9 cells 70-80% of glucose is oxidized in the TCA cycle (Neerman and Wagner, 1996). In our work, relevant lactate formation was only detected at very high cell densities (Table 2.1 and 2.2). Meanwhile, an important proportion of glucose-derived pyruvate is channelled to alanine formation through AlaAT activity, being the main reaction reducing the efficiency of glucose

utilization. Refining our estimations of metabolic efficiency provided in Chapter I, the metabolic model developed herein calculates that the proportion of pyruvate diverted for alanine and lactate production ranged from 6 to 18% and 0 to 11%, respectively. In addition, the ME flux was less active at high cell densities and after infection (Figure 2.2B and 2.3B), indicating that under non or slow growth conditions, anaplerotic TCA intermediaries are not being addressed for biosynthesis.

Discrepancy is observed with the results shown by Benslimane et al. (2005), who reported a quite low experimental flux for the TCA cycle (only 3% of metabolized glucose), despite the fact that lactate and alanine production could only explain around 30% of the total glucose consumed, the fate of the remainder not being justified. However, different growth media (serum supplemented IPL-41 medium vs. serum-free SF900II), glucose concentration (14 vs. 55 mM) and culture systems (erlenmeyer vs. spinner flask) were used in this work and data needs to be carefully compared. Moreover, Maier et al. (2008) have recently described important differences in flux distributions determined based on extracellular rates and fluxes calculated from transient $^{13}$C-labelling patterns of intracellular metabolites; the differences affected especially the TCA cycle and the PP pathway. More conclusively, Neermann and Wagner (1996) determined an 80% of glucose entrance to the TCA in *Sf*21 cells cultured in serum-free Ex-cell-401 medium, with 35 mM glucose, which is in accordance with our studies.

In contrast to what has been described for mammalian cells, the amino acid consumption pattern of insect cells is conditional, depending on the nutritional and proliferative status and cell line specific properties (Doverskog et al., 1997). In our experiments, no sugar limitation was observed throughout batch cultures of infected and uninfected cells due to

the high concentration of sugars in SF900II medium. Despite this fact, amino acid consumption was observed to be higher than the strictly necessary for protein synthesis, suggesting that anaplerotic fluxes were quantitatively important, especially at low cell densities (Tables 2.1 and 2.2, Figures 2.2C and 2.3C). This results in the generation of intracellular nitrogen in the form of glutamate and ammonia. The ammonia moiety from glutamate, primarily derived from glutamine through GOGAT activity but also from other amino acids, is transferred to pyruvate, forming alanine through AlaAT and resulting in a net generation of α-ketoglutarate. Alanine is the main carbon compound secreted by insect cells under glucose excess, and even consumed after glucose depletion (Bédard et al., 1993; Kamen et al., 1991; Öhman et al., 1995). On the other hand, our results indicate that the high efficiency of free ammonia recycling depends on the net production of serine from pyruvate, which was observed in uninfected fast growing cells at low densities (Figure 2.2C). Amino acids consumption and consequent alanine production decreased at higher cell densities (beyond 3-4×$10^6$ cells/mL), when glucose levels were not yet limiting. It should be noted that although the use of amino acids to fuel the central metabolism of *Sf*9 cells leads to a decreased efficiency of carbohydrate utilization for nitrogen detoxification, this is still much more efficient than what has been reported for mammalian cell lines (Neerman and Wagner, 1996).

In this work, the general down-regulation of the central metabolism of *Sf*9 cells with cell density has been quantified for the first time by means of MFA. Namely, the fluxes through glycolysis and TCA cycle were down regulated with increasing cell concentrations, while ME fluxes dropped to half from their initial values (Figures 2.2A and 2.2B). The major impact of the down-regulation of the TCA cycle was the sharp decrease in the production of metabolic energy, in agreement with the fact that maximum

energy production is linked to rapid cellular growth, which, however, kept being produced for cell maintenance at high cell densities (Figure 2.5). The observed effects occurred before any major component of medium reached limiting concentrations, the metabolism of *Sf*9 cells being more active at low cell densities. However, minor components of the SF900II medium (namely those supplied by hydrolysates) were not considered for this work. In fact, although these components are known to have a major impact on insect cell growth and final infection yield (Ikonomou et al., 2003), their concentrations are low and can not be considered in the material balances of the model. It cannot thus be ruled out that the limitations assessed at high cell densities could be due in part to their exhaustion, since vitamins and oligoelements act as cofactors for key metabolic enzymes. Further work should be done in order to determine the role of these limitations in the BEVS.

While lactate, alanine or ammonia have already been shown not to exert any inhibitory effect on the physiology of insect cells (Doverskog et al., 1997; Ikonomou et al., 2003; Öhman et al., 1995), it could be hypothesized that this effect could be due to the accumulation of inhibitory levels of compounds not yet identified. The relationship of cellular growth in serum-free media with the production and secretion of autocrine/paracrine growth factors by the *Sf*9 cell line has already been described. The accumulation of a human insulin-like growth factor I (IGF-I) was described and correlated with the decline and cessation of growth, occurring when the medium was still nutritionally sufficient (Doverskog et al., 1997). Moreover, the same authors showed that the cysteine biosynthetic pathway was down regulated in cells at late exponential growth (Doverskog et al., 1998) and cell cycle regulation by conditioned medium components has also been described and related to protein productivity (Doverskog et al., 2000a). The results presented herein corroborate these assumptions and the discussion

provided in Chapter I, suggesting the existence of a regulatory mechanism triggered by cell density, exerting an inhibitory effect on metabolism. This mechanism, probably operating at the level of gene regulation and/or silencing, could be seen as a cell density control and protection mechanism, avoiding the total exhaustion of the nutrients in the growth medium which would lead to a steep loss of viability. Sensing mechanisms for cell density regulation in prokaryotes and eukaryotes alike have been reported before (Brazill et al., 1998; You et al., 2004).

Results presented herein underline that alteration of cellular metabolism is also exerted by baculovirus infection, since the metabolic machinery of infected cells is fully devoted to virus replication. Early after infection, as BVs start controlling cellular machinery, cell cycle is arrested in the G2/M phase (Braunagel et al., 1998) and the expression of the host genes ceases (Palomares et al., 2006). Calculations allowed us to determine that the diversion of building blocks for the synthesis of macromolecular components of BVs alone does not explain the metabolic effects/limitations assessed; thus, equations for BV synthesis were not considered herein. The alteration in the metabolism of sugars, in particular the enhanced consumption of disaccharides (maltose and sucrose) after infection at low CCI (Table 2.2) led to higher glycolytic fluxes in infected cells (Figure 2.3A). This resulted in a higher pyruvate flux towards acetyl-CoA which, together with the arrest of cellular growth (and consequently the decrease in the synthesis of lipids) further contributed to the observed enhancement in the carbon flux through the TCA cycle (Figure 2.3B) and on the energetic state. In fact, the energetic state of infected *Sf*9 cells was highly dependent on the CCI, as shown by the net specific ATP production rate (Figure 2.5).

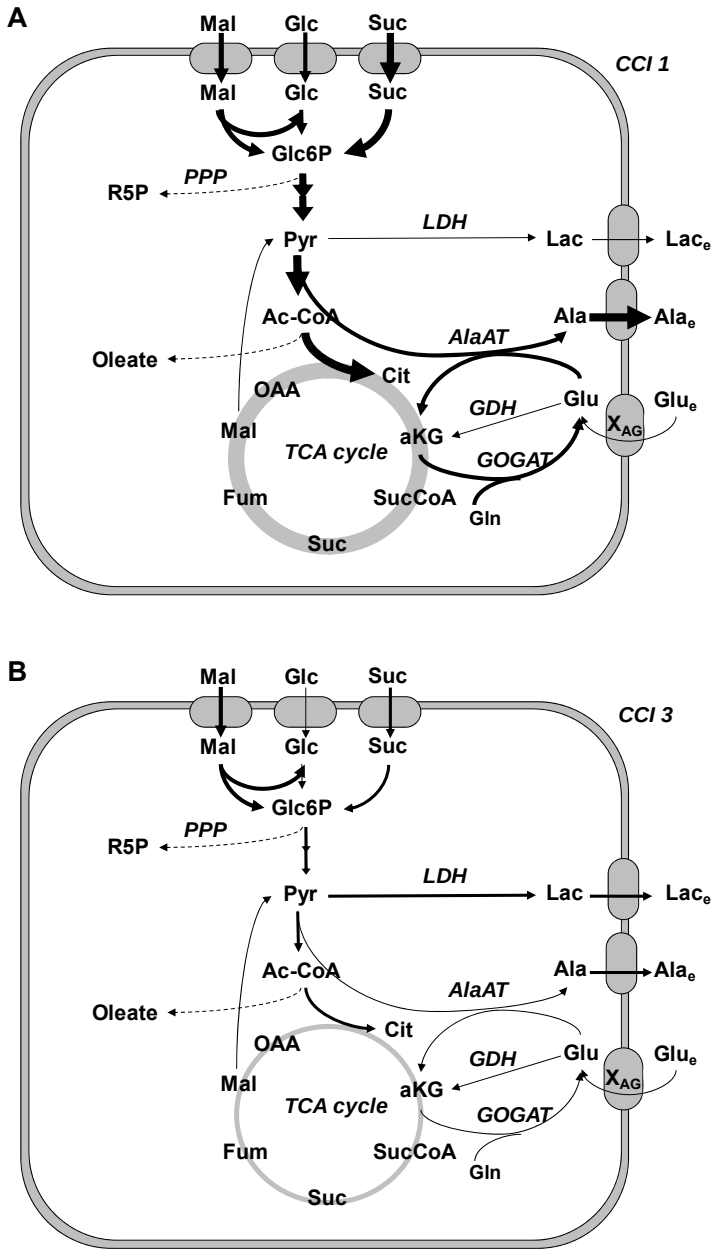


**Figure 2.6.** Overview of the metabolic effects of baculovirus infection on the metabolism of *Sf*9 insect cells infected at (A) CCI 1 and (B) CCI 3. The size of the arrows is proportional to the alteration observed on the fluxes in cells infected with a high MOI when compared to uninfected cells, under each condition.

In light of our results, the cellular energetic state seems more likely to be the main limitation to BV assembly and/or protein synthesis, thus establishing the link between metabolic state and the cell density effect (see Chapter I for BV production results). It has been previously described that intracellular ATP levels greatly increase following infection in High-Five™ cells (Olejnik et al., 2004), while total cellular ATP content determines virus replication in Vero cell cultures (Burgener et al., 2006). In this work, the cellular energetic state was drastically altered following infection, this alteration depending on the interplay of CCI and MOI and reflected by the cellular OUR (Figures 2.4 and 2.5). From our calculations, an increase of around 60% in specific OUR of *Sf*9 cells infected at a high MOI and a CCI of $1\times10^6$ cells/mL was determined, which is in accordance with the literature (Gotoh et al., 2004; Kamen et al., 1991, 1996; Lecina et al., 2006; Palomares et al., 2004). The extent of the increase was dependent on the MOI used, thus further supporting the fact that it was related to the infection mechanism. Some authors have previously shown the link between OUR, infection and protein production in the BVES (Lecina et al., 2006; Palomares et al., 2004; Kamen et al., 1991, 1996); in order to obtain good productivities, other authors have stated that oxygen concentration should be above 20% of air saturation (Taticek and Shuler, 1997). However, the oxygen uptake rates estimated for infections in this work did not suggest a limitation at high cell densities, since these were still lower than for uninfected cells. In addition, as pointed out in Chapter I, a similar metabolic pattern was also observed in *Sf*9 cultures performed in oxygen-controlled bioreactors.

Finally, the cell density at the time of infection drastically affected the post-infection behaviour of the cell line. Data presented in Chapter I supports the occurrence of a cell density effect on the replication of BV in *Sf*9 cells. In fact, specific yields were lower at the highest cell densities

assayed, an effect that was especially obvious when infection was performed at low MOI. If productivities are analyzed in view of the metabolic analysis herein presented, a clear correlation between a highly productive metabolic state and the enhancement of oxidative metabolism/energetic state of the cells can be drawn. The enhancement of the cellular energetic state following infection assessed at CCI 1 (Figure 2.5) is a consequence of various alterations as schematically shown in Figure 2.6), leading together to increased fluxes in the central carbon pathways and augmented ATP synthesis. This shift in metabolism failed to occur at CCI 3, which explains the observed effect on BV replication.

In conclusion, the results presented hereby demonstrate the linking of cell density and baculovirus infection with metabolic dynamics in insect cells. Many authors have pointed out medium exchange at the moment of infection as a suitable strategy to delay the onset of the cell density effect (Chapter I; Ikonomou et al., 2003; Palomares et al., 2006). Nutrient consumption and end-product accumulation in *Sf*9 cultures have already been analyzed and amino acids levels do not seem to be limiting. Moreover, glutamine limitation was shown to increase the consumption of other amino acids, mainly aspartate, glutamate and asparagine, reflecting metabolic flexibility (Bhatia et al., 1997; Ferrance et al., 1993; Öhman et al., 1995), while some authors detected consumption of central metabolism organic acids (α-ketoglutarate, malate, pyruvate, citrate and succinate), especially at the stationary phase (Bédard et al., 1993). Therefore, the connection of intracellular pools of amino acids and TCA cycle intermediaries seems to have a central role in the metabolic dynamics of insect cells. Despite the potency of MFA for determining intracellular fluxes, it can not be ascertained whether the metabolic alterations described herein are due to alteration of gene expression, inefficient channelling or partitioning of substrates/metabolites between cytosol and mitochondria. To

this respect, further characterization of *Sf*9 metabolism and physiology is needed. Moreover, the development of tailored strategies for improved metabolic performance is a promising challenge in order to optimize insect cells bioprocesses.

## ACKNOWLEDGEMENTS

This work was supported by E.C. contract Baculogenes (FP6-037541). Dr. M. van Oers (University of Wageningen, Holland) is gratefully acknowledged for providing the recombinant baculovirus. Dr. A.L. Simplício (IBET, Portugal) is acknowledged for her help with HPLC analysis of amino acids. Dr. S. Klamt (Max Planck Institute, Magdeburg, Germany) is acknowledged for providing the CellNetAnalyzer software. V. Bernal and A.Y. Yokomizo hold post-doctoral fellowships of Fundación Séneca (Murcia, Spain) and Conselho Nacional de Desenvolvimento Científico e Tecnológico (Brazil), respectively. N. Carinhas holds a PhD fellowship from Fundação para a Ciência e a Tecnologia (SFRH/BD/36676/2007, FCT, Portugal). Dr. A.P. Teixeira is gratefully acknowledged for fruitful discussions.

## REFERENCES

Altamirano C, Illanes A, Becerra S, Cairo JJ, Godia F (2006) Considerations on the lactate consumption by CHO cells in the presence of galactose. *J Biotechnol* **125**: 547-56

Bédard C, Tom R, Kamen A (1993) Growth, nutrient consumption, and end-product accumulation in Sf9 and BTI-EAA insect cell cultures: insights into growth limitation and metabolism. *Biotechnol Prog* **9**: 615-24

Benslimane C, Elias CB, Hawari J, Kamen A (2005) Insights into the central metabolism of *Spodoptera frugiperda* (Sf9) and *Trichoplusia ni* BTI-Tn-5B1-4 (Tn-5) insect cells by radiolabeling studies. *Biotechnol Prog* **21**: 78-86

Berg JM, Tymoczko JL, Stryer L (2002) Biochemistry. W.H. Freeman and Co., New York

Bhatia R, Jesionowski G, Ferrance J, Ataai MM (1997) Insect cell physiology. *Cytotechnology* **24**: 1-9

Bonarius HP, Hatzimanikatis V, Meesters KP, de Gooijer CD, Schmid G, Tramper J (1996) Metabolic flux analysis of hybridoma cells in different culture media using mass balances. *Biotechnol Bioeng* **50**: 299-318

Braunagel SC, Parr R, Belyavskyi M, Summers MD (1998) *Autographa californica* nucleopolyhedrovirus infection results in Sf9 cell cycle arrest at G2/M phase. *Virology* **244**: 195-211

Burgener A, Coombs K, Butler M (2006) Intracellular ATP and total adenylate concentrations are critical predictors of reovirus productivity from Vero cells. *Biotechnol Bioeng* **94**: 667-79

Caspi R, Foerster H, Fulcher CA, Kaipa P, Krummenacker M, Latendresse M, Paley S, Rhee SY, Shearer AG, Tissier C and others (2008) The MetaCyc Database of metabolic pathways and enzymes and the BioCyc collection of Pathway/Genome Databases. *Nucleic Acids Res* **36**: D623-31

Cruz PE, Cunha A, Peixoto CC, Clemente J, Moreira JL, Carrondo MJ (1998) Optimization of the production of virus-like particles in insect cells. *Biotechnol Bioeng* **60**: 408-18

Doverskog M, Bertram E, Ljunggren J, Öhman L, Sennerstam R, Haggstrom L (2000a) Cell cycle progression in serum-free cultures of Sf9 insect cells: modulation by conditioned medium factors and implications for proliferation and productivity. *Biotechnol Prog* **16**: 837-46

Doverskog M, Han L, Haggstrom L (1998) Cystine/cysteine metabolism in cultured Sf9 cells: influence of cell physiology on biosynthesis, amino acid uptake and growth. *Cytotechnology* **26**: 91-102

Doverskog M, Jacobsson U, Chapman BE, Kuchel PW, Haggstrom L (2000b) Determination of NADH-dependent glutamate synthase (GOGAT) in *Spodoptera frugiperda* (Sf9) insect cells by a selective $^{1}H/^{15}N$ NMR in vitro assay. *J Biotechnol* **79**: 87-97

Doverskog M, Ljunggren J, Öhman L, Haggstrom L (1997) Physiology of cultured animal cells. *J Biotechnol* **59**: 103-115

Drews M, Doverskog M, Öhman L, Chapman BE, Jacobsson U, Kuchel PW, Haggstrom L (2000) Pathways of glutamine metabolism in *Spodoptera frugiperda* (Sf9) insect cells: evidence for the presence of the nitrogen assimilation system, and a metabolic switch by $^{1}H/^{15}N$ NMR. *J Biotechnol* **78**: 23-37

Drews M, Paalme T, Vilu R (1995) The Growth and Nutrient Utilization of the Insect-Cell Line *Spodoptera frugiperda* Sf9 in Batch and Continuous-Culture. *J Biotechnol* **40**: 187-198

Ferrance JP, Goel A, Ataai MM (1993) Utilization of glucose and amino acids in insect cell cultures: Quantifying the metabolic flows within the primary pathways and medium development. *Biotechnol Bioeng* **42**: 697-707

Gambhir A, Korke R, Lee J, Fu PC, Europa A, Hu WS (2003) Analysis of cellular metabolism of hybridoma cells at distinct physiological states. *J Biosci Bioeng* **95**: 317-27

Gotoh T, Chiba K, Kikuchi K (2004) Oxygen consumption profiles of Sf9 insect cells and their culture at low temperature to circumvent oxygen starvation. *Biochem Eng J* **17**: 71-78

Henry O, Perrier M, Kamen A (2005) Metabolic flux analysis of HEK-293 cells in perfusion cultures for the production of adenoviral vectors. *Metab Eng* **7**: 467-76

Ikonomou L, Schneider YJ, Agathos SN. 2003. Insect cell culture for industrial production of recombinant proteins. *Appl Microbiol Biotechnol* **62**: 1-20

Jarman-Smith RF, Armstrong SJ, Mannix CJ, Al-Rubeai M (2002) Chromosome instability in *Spodoptera frugiperda* Sf9 cell line. *Biotechnol Prog* **18**: 623-628

Kamen AA, Bédard C, Tom R, Perret S, Jardin B (1996) On-line monitoring of respiration in recombinant-baculovirus infected and uninfected insect cell bioreactor cultures. *Biotechnol Bioeng* **50**: 36-48

Kamen AA, Tom RL, Caron AW, Chavarie C, Massie B, Archambault J (1991) Culture of insect cells in helical ribbon impeller bioreactor. *Biotechnol Bioeng* **38**: 619-28

Kim EJ, Kramer SF, Hebert CG, Valdes JJ, Bentley WE (2007) Metabolic engineering of the baculovirus-expression system via inverse "Shotgun" genomic analysis and RNA interference (dsRNA) increases product yield and cell longevity. *Biotechnol Bioeng* **98**: 645-654

Klamt S, Saez-Rodriguez J, Gilles ED (2007) Structural and functional analysis of cellular networks with CellNetAnalyzer. *BMC Syst Biol* **1**: 2

Klamt S, Schuster S, Gilles ED (2002) Calculability analysis in underdetermined metabolic networks illustrated by a model of the central metabolism in purple nonsulfur bacteria. *Biotechnol Bioeng* **77**: 734-751

Lecina M, Soley A, Gracia J, Espunya E, Lazaro B, Cairo JJ, Godia F (2006) Application of on-line OUR measurements to detect actions points to improve baculovirus-insect cell cultures in bioreactors. *J Biotechnol* **125**: 385-394

Maier K, Hofmann U, Reuss M, Mauch K (2008) Identification of metabolic fluxes in hepatic cells from transient 13C-labeling experiments: Part II. Flux estimation. *Biotechnol Bioeng* **100**: 355-370

Maranga L, Brazão TF, Carrondo MJ (2003) Virus-like particle production at low multiplicities of infection with the baculovirus insect cell system. *Biotechnol Bioeng* **84**: 245-253

Marheineke K, Grunewald S, Christie W, Reilander H (1998) Lipid composition of *Spodoptera frugiperda* (Sf9) and *Trichoplusia ni* (Tn) insect cells used for baculovirus infection. *FEBS Lett* **441**: 49-52

Nadeau I, Gilbert PA, Jacob D, Perrier M, Kamen A (2002) Low-protein medium affects the 293SF central metabolism during growth and infection with adenovirus. *Biotechnol Bioeng* **77**: 91-104

Nadeau I, Jacob D, Perrier M, Kamen A (2000) 293SF metabolic flux analysis during cell growth and infection with an adenoviral vector. *Biotechnol Prog* **16**: 872-884

Neermann J, Wagner R (1996) Comparative analysis of glucose and glutamine metabolism in transformed mammalian cell lines, insect and primary liver cells. *J Cell Physiol* **166**: 152-169

Öhman L, Ljunggren J, Haggstrom L (1995) Induction of a Metabolic Switch in Insect Cells by Substrate Limited Fed-Batch Cultures. *Appl Microbiol Biotechnol* **43**: 1006-1013

Olejnik AM, Czaczyk K, Marecik R, Grajek W, Jankowski T (2004) Monitoring the progress of infection and recombinant protein production in insect cell cultures using intracellular ATP measurement. *Appl Microbiol Biotechnol* **65**: 18-24

Palomares LA, Estrada-Moncada S, Ramirez OT (2006) Principles and applications of the insect cell-baculovirus expression vector system. In: Ozturk SS, Hu WS, editors. Cell culture technology for pharmaceutical and cell based therapies. Taylor & Francis, New York

Palomares LA, Lopez S, Ramirez OT (2004) Utilization of oxygen uptake rate to assess the role of glucose and glutamine in the metabolism of infected insect cell cultures. *Biochem Eng J* **19**: 87-93

Radford KM, Reid S, Greenfield PF (1997) Substrate limitation in the baculovirus expression vector system. *Biotechnol Bioeng* **56**: 32-44

Rhiel M, MitchellLogean CM, Murhammer DW (1997) Comparison of *Trichoplusia ni* BTI-Tn-5B1-4 (High FiveTM) and *Spodoptera frugiperda* Sf9 insect cell line metabolism in suspension cultures. *Biotechnol Bioeng* **55**: 909-920

Stephanopoulos G, Aristidou AA, Nielsen J (1998) Metabolic engineering. Principles and Methodologies. Academic Press, San Diego

Sugiura T, Amann E (1996) Properties of two insect cell lines useful for the Baculovirus expression system in serum-free culture. *Biotechnol Bioeng* **51**: 494-499

Taticek RA, Shuler ML (1997) Effect of elevated oxygen and glutamine levels on foreign protein production at high cell densities using the insect cell-baculovirus expression system. *Biotechnol Bioeng* **54**: 142-152

Voet, D. and Voet, J.G., 1995. Biochemistry. John Wiley & Sons, New York.

Wahl A, Sidorenko Y, Dauner M, Genzel Y, Reichl U (2008) Metabolic flux model for an anchorage-dependent MDCK cell line: Characteristic growth phases and minimum substrate consumption flux distribution. *Biotechnol Bioeng* **101**: 135-152

Wang NS, Stephanopoulos G (1983) Application of macroscopic balances to the identification of gross measurement errors. *Biotechnol Bioeng* **25**: 2177-2208

Xie LZ, Wang DIC (1994) Applications of improved stoichiometric model in medium design and fed-batch cultivation of animal-cells in bioreactor. *Cytotechnology* **15**: 17-29

Zupke C, Stephanopoulos G (1995) Intracellular flux analysis in hybridomas using mass balances and in-vitro $^{13}$C-NMR. *Biotechnol Bioeng* **45**: 292-303

# CHAPTER III

## IMPROVING BACULOVIRUS VECTORS PRODUCTION THROUGH MANIPULATION OF ENERGETIC METABOLISM

**ADAPTED FROM:**

Carinhas N, Bernal V, Monteiro F, Carrondo MJT, Oliveira R, Alves PM (2010) Improving baculovirus production at high cell density through manipulation of energy metabolism. *Metab Eng* **12**: 39-52.

# TABLE OF CONTENTS

## 1. SUMMARY

The baculovirus-insect cells system has been recognized as a potentially safe and suitable technology to produce gene therapy vectors. Efficient and robust production processes, able to deliver higher product concentrations, are however still needed to cope with increased requirements for manufacture. The work presented in this chapter describes a combined experimental and modeling effort to quantify and environmentally manipulate the metabolism of *Spodoptera frugiperda* cells, targeting high cell density production of baculovirus vectors. Culture medium supplementation with energetic metabolites pyruvate or α-ketoglutarate at the time of infection resulted in 6-7 fold higher specific baculovirus yields at high cell density when compared to control cultures. This pushed volumetric titers to levels higher than classical low cell density infections. A quantitative description of intracellular pathways is provided using metabolic flux analysis; a direct stimulation of carbon flow through the tricarboxylic acids cycle was observed. Analysis of flux partitioning coefficients at the pyruvate and α-ketoglutarate branch-points further revealed a metabolic transition to a more energetically active state, which was confirmed by increased intracellular adenosine triphosphate generation rates. These results represent a cost-efficient strategy for high cell density production of recombinant baculovirus vectors.

## 2. INTRODUCTION

A bottleneck which has been recognized for several years is the loss in productivity after infection above $1\times10^6$cells/mL, resulting not only in poor specific product yields, but also considerably lower volumetric titers (Caron et al., 1990; Chapter I). Efforts have been directed at optimizing upstream

processing of baculovirus-insect cells system so as to meet product demands in industrially attractive processes (Ikonomou et al., 2003). However, most attempts to overcome this cell density effect in insect cells yielded only modest improvements, often requiring cumbersome protocols of medium exchange, impractical for large-scale manufacture.

An efficient strategy to optimize the output in a relevant cellular process is to manipulate the carbon and nitrogen pathways of host cells (Stephanopoulos, 1999). Given the complexity of such biological systems, the rapid expansion of metabolic engineering approaches to attain these objectives has been associated with the development of modelling tools aiming to simulate and analyze the outcome of such manipulations. Stoichiometric analysis based on metabolite balancing is an established framework for the quantification of intracellular fluxes and their distribution within a network representative of the main cellular metabolic events. In particular, Metabolic Flux Analysis (MFA) is an enabling tool to estimate a metabolic state constrained by exchange fluxes of nutrients between cells and the environment (Stephanopoulos et al., 1998). It has been also successfully exploited to identify principal nodes in the primary metabolism which are characterized by significant changes in flux partitioning under different conditions, and thus can be regarded as potential control points for manipulation (van Gulik et al., 2000).

The application of MFA to BV-infected insect cells was previously carried out in Chapter II to address the post-infection adaptations of insect cells metabolism. The identification of the energetic state as a reliable sensor of system productivity seems conclusive from these results, making possible the design of rational strategies for bioprocess optimization. In the present work, we hold to the same hypothesis and go a step further by manipulating the metabolic pathways of *Spodoptera frugiperda Sf*9 cells through medium

supplementation in order to boost recombinant BV production at high cell density. After testing key compounds as culture supplements, the stimulatory effects on the host energetic metabolism are quantified, confirming the potential of the strategy herein presented.

## 3. MATERIALS AND METHODS

Cell maintenance was performed as in the previous chapters. In the present Chapter, a different recombinant baculovirus, *Ac-vp39egfp*, kindly provided by Dr. K. Airenne (University of Kuopio, Finland) and coding for the baculovirus major structural capsid protein, vp39, fused N-terminally to a EGFP reporter (Kukkonen et al., 2003), was used. Viral amplification and titration were performed as previously described (Chapter I).

### 3.1. Effect of medium supplementation on baculovirus production

All cultures were inoculated at a cell density of $0.5\times10^6$ cells/mL in 125 mL spinner flasks (Wheaton, USA), operated as previously described. Infections with *Ac-vp39egfp* were carried out at a cell density of $3\text{-}4\times10^6$ cells/mL, using a multiplicity of infection (MOI) of 0.1 IP/mL. A series of exploratory experiments was carried out with supplementation at the time of infection. All supplements and compounds fed to the cultures were chemically defined (Sigma-Aldrich, USA). Stock solutions of sodium pyruvate (Catalogue no.: P-5280), disodium α-ketoglutarate (Catalogue no.: K-3752) and L-glutamine (Catalogue no.: G-8540) were prepared in PBS, followed by sterile-filtration (0.22 μm). Concentrations were chosen so as to minimize culture medium dilution upon addition of Pyr, αKG and Gln to a final concentration of 12 mM, or combined addition of 12 mM Pyr plus 12

mM αKG. Lipids (Catalogue no.: L-0288) and amino acids (Catalogue no.: R-7131) mixtures were diluted 1:100 and 1:50, respectively, following indications of the manufacturer. A low-protein Insect Medium Supplement (Catalogue no.: I-7267), developed as a serum replacement for cell growth and containing a proprietary mixture of amino acids, lipids, vitamins, growth factors and trace elements, was diluted 1:10.

In order to optimize pyruvate feeding, cultures were performed varying the time of supplementation (24 h before infection) and the concentration (24 mM). Furthermore, cultures with the addition of small amounts of pyruvate at defined time intervals were performed in order to simulate fed-batch conditions: 1) starting with 2 mM at the time of infection followed by the addition of 1.5 and 1 mM after 14 and 10 h intervals, respectively; 2) applying the same supplementation schedule but starting with 13 mM Pyr.

Samples were collected at given time points and centrifuged at 1700×g for 10 minutes, at room temperature. Cell-free sterile supernatants were stored at 4$^{o}$C for later virus titration, or at - 20$^{o}$C to measure the concentration of sugars, lactate, ammonia, amino acids and organic acids.

### 3.2. Analytical procedures

Quantification of medium glucose, lactate, ammonia, maltose, sucrose and amino acids was done as described in the previous chapters. For the analysis of the organic acids α-ketoglutarate and pyruvate, a HPLC method based on ion-exclusion was developed, using a 8×300 mm sugar SH1011 column (Shodex, USA). Operating conditions included isocratic elution using 5 mM sulfuric acid, with a flow rate of 1 mL/min at room temperature. Column regeneration prior to and after analysis was accomplished overnight with 25 mM sulfuric acid at 0.5 mL/min. Both compounds were

detected by reading absorbance at 200 nm. Standards were prepared in SF900II medium and, along with samples, were filtered before injection.

### 3.3. Statistical analysis

Hypothesis testing on the comparison between volumetric titers from different infection strategies was performed using single-factor analysis of variance (ANOVA). The least significant difference (LSD) method was chosen for multiple contrasts. A 95 % confidence level was considered to be statistically significant.

### 3.4. Metabolic flux analysis

The model considers the main reactions of the central metabolism of *Sf*9 cells as described in Chapter II. The alterations to the previous model are the inclusion of uptake fluxes of pyruvate and α-ketoglutarate, which were not considered before since these compounds are not found in the culture medium. The complete list of reactions is presented in Appendix 1.

The updated model here considered totalizes 75 reactions (instead of the previous 73), with 52 internal (balanced) metabolites/cell components, defined by a 75×52 stoichiometric matrix. The resulting number of degrees of freedom is now 26, as computed by the number of total reactions (75) minus the rank of the stoichiometric matrix (49). 27 exchange fluxes were experimentally determined, including the uptake/production rates of Pyr and αKG, as well as the formation of biomass. For the cultures where Pyr or αKG were not supplemented, the corresponding uptake rates were set to 0. As before, three intracellular reaction rates, namely the intracellular hydrolysis of maltose and sucrose, and the synthesis of lactate from

pyruvate, were set equal to the respective extracellular measured rates. The resultant system of equations is overdetermined, with 4 redundant measurements. The weighted least squares method was used to calculate the model solution (Stephanopoulos et al., 1998). Overall, the carbon and nitrogen balances closed to an average 88% and 67%, respectively, for the different cultures presented in this chapter.

Balanceable rates, which arise from system redundancy, were used to calculate model consistency as previously described (Wang and Stephanopoulos, 1983). Furthermore, the propagated impact of experimental errors on any individual unknown reaction rate was assessed by analyzing how much it varies with respect to small (infinitesimal) changes in the measured fluxes. Sensitivity equations are based only on the stoichiomtry of the metabolic network and can be found in Daae and Ison (1999). All computational tasks were performed using the FluxAnalyzer software (Klamt et al., 2003).

## 4. RESULTS

### 4.1. Uptake of pyruvate and α-ketoglutarate

The rational followed in this work arises from the possibility to enhance energy production through purposeful alteration of the cellular environment, attempting to sustain consistently high ATP generation rates even after infection at high cell densities. Pyruvate, a central metabolite connecting glycolysis with the TCA cycle, and *α-ketoglutarate*, a TCA cycle intermediate bridging this pathway with glutamine utilization and nitrogen metabolism, were selected to directly enhance TCA cycle fluxes and boost energy generation in the cell. *Sf*9 cells were supplemented at the time of infection, according to the description in Materials and Methods. To our

knowledge, this is the first time either Pyr or *α*KG are added to insect cell cultures, although other media formulations exist that already contain low amounts of these and other carboxylic acids (Bédard et al., 1993). HPLC results show that SF900II medium does not contain detectable amounts of Pyr or *α*KG.

The consumption of both Pyr and *α*KG by *Sf*9 cells is demonstrated by the analysis of culture supernatants (Figure 3.1). It takes approximately 96 h and 72 h to deplete 12 mM of Pyr or *α*KG added at the infection point, respectively, specific uptake rates being comparable to those of Glc (Table 3.1). Interestingly, rather distinct profiles were observed for both compounds, possibly reflecting differences in the kinetics of associated transport systems. In agreement, combined addition of 12 mM Pyr plus 12 mM *α*KG did not affect the uptake of each compound, since similar profiles were obtained in relation to their individual supplementation (data not shown; see Table 3.1 for specific uptake rates). The specific Pyr consumption rate increased by over two-fold during the initial phase post-infection when 24 mM were added instead of 12 mM (see Table 3.1), indicating that, in this concentration range, Pyr transporters and assimilation pathways are not saturated.

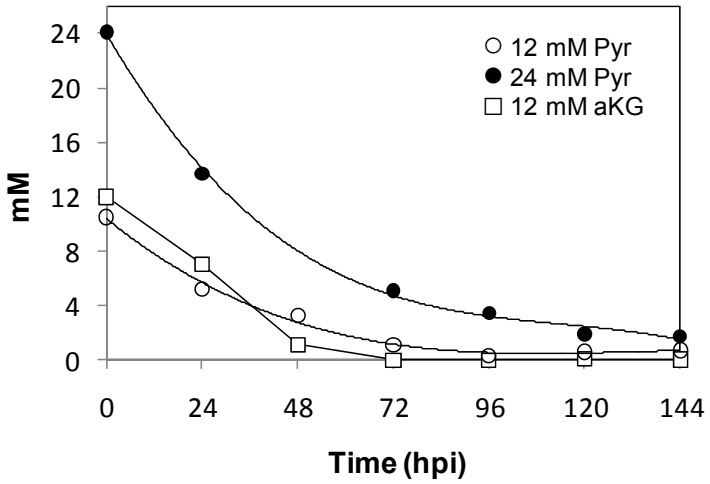


**Figure 3.1.** Time profiles of pyruvate and α-ketoglutarate concentrations after supplementation of the culture medium at the time of infection (hpi – hours post-infection). Cultures were infected at a CCI of 3-4×$10^6$ cells/mL with a MOI of 0.1 IP/cell (see Materials and Methods for details). Results were obtained using ion exclusion chromatography as explained in Materials and Methods.

### 4.2. Effect of metabolic supplements on baculovirus production

Supplementation schemes based on carboxylic acids and glutamine were tested in order to steer TCA cycle activity and positively impact baculovirus productivity. It should be highlighted that all cultures were infected and supplemented at high cell densities of 3-4×$10^6$ cells/mL. Therefore, in order to rule-out possible nutrient limitations, lipids and amino acid cocktails, as well as a complete Insect Medium Supplement (see Materials and Methods for details), were also tested in separate cultures.

**Table 3.1.** Specific consumption/production rates of the main nutrients of *Sf*9 cells metabolism, expressed as nmol/$10^6$cells/h, after infection at 3-4×$10^6$cells/mL and culture supplementation as described in Materials and Methods. Shown are average rates for the initial 48-72 h post-infection (phase I). Standard deviations are omitted for simplicity.

| | Control | 12mM Pyr | 12mM αKG | 12mM Gln | Pyr + αKG | 24mM Pyr |
|---|---|---|---|---|---|---|
| **Glc** | -45.297 | -47.938 | -54.824 | -40.805 | -28.403 | -14.861 |
| **Lac** | 3.719 | 3.532 | 7.146 | 4.766 | 11.882 | 11.696 |
| **Sucr** | 0 | -6.573 | 0 | 0 | -1.335 | -5.562 |
| **Malt** | -4.115 | -6.974 | 0 | -2.559 | -5.099 | -6.166 |
| **Pyr** | n.a. | -30.806 | n.a. | n.a. | -44.944 | -66.108 |
| **αKG** | n.a. | n.a. | -60.501 | n.a. | -50.352 | n.a. |
| **Amm** | 1.441 | -1.946 | -5.066 | 0.574 | -5.916 | -0.519 |
| **Asp** | -2.811 | -2.112 | -11.936 | -2.938 | -8.991 | -3.408 |
| **Glu** | -4.500 | 0.471 | 0.636 | -3.812 | 11.179 | 0.465 |
| **Ser** | -3.788 | -3.060 | -4.320 | -4.537 | -4.823 | -2.854 |
| **Asn** | -0.903 | -1.598 | -4.015 | -3.585 | -1.795 | -3.627 |
| **Gly** | -0.544 | 0.869 | -0.894 | -2.880 | -0.676 | 0.041 |
| **Gln** | -7.842 | -4.143 | -15.846 | -12.104 | -12.108 | -12.614 |
| **Thr** | -1.104 | -0.904 | -1.700 | -1.922 | -1.770 | -1.007 |
| **Ala** | 19.365 | 21.366 | 20.886 | 24.219 | 20.925 | 22.921 |
| **Pro** | -1.454 | -0.192 | -1.311 | -1.291 | -1.334 | -1.106 |
| **Tyr** | -1.185 | -0.027 | -1.021 | -1.093 | -0.806 | -0.862 |
| **Val** | -1.601 | -0.842 | -2.291 | -3.264 | -2.893 | -0.695 |
| **Met** | -1.662 | -0.616 | -2.005 | -3.553 | -2.491 | -2.065 |
| **Ile** | -1.528 | -0.558 | -1.888 | -3.504 | -3.026 | -0.897 |
| **Leu** | -2.208 | -1.047 | -2.446 | -2.820 | -2.808 | -1.300 |
| **Phe** | -1.294 | -0.306 | -2.150 | -0.495 | -2.173 | -3.063 |
| **His** | -0.503 | -0.028 | -0.563 | -1.098 | -0.141 | -0.713 |
| **Arg** | -1.467 | -0.250 | -2.576 | -1.838 | -1.903 | -2.300 |
| **Lys** | -0.571 | -2.453 | -2.473 | -0.509 | -3.270 | -0.090 |
| **Cys** | -0.229 | -0.108 | -1.676 | -0.518 | -1.888 | -0.835 |
| **Growth rate (/h)** | 0.006 | 0.004 | 0.008 | 0.004 | 0.002 | 0.002 |

Figure 3.2A summarizes the results of BV production obtained from these exploratory experiments. Individual addition of 12 mM Pyr or 12 mM *α*KG resulted in significantly higher volumetric titers in comparison to the non-supplemented control ($p<0.001$), even reaching levels higher than the ones obtained from classical low cell density cultures ($6.64\pm2.76\times10^7$ IP/mL; $p<0.01$). Accordingly, specific yields increased on average 6-7 fold by individually adding Pyr or *α*KG, respectively (Figure 3.2B). A less pronounced but still significant improvement was obtained when these components were supplemented in conjunction ($p<0.01$), while neither the addition of 12 mM Gln, Gln plus Pyr (12 mM each), amino acids, lipids or complete Insect Medium Supplement resulted in significant production improvements. These results indicate that nutrient exhaustion is not the primary cause of decreased production levels at high cell density, while the uptake of energy-generating metabolic intermediates positively impacted cellular productivity.

### 4.3. Quantification of metabolic fluxes to evaluate baculovirus production

Metabolic flux analysis was used to assess the effects of infection and medium supplementation on cellular metabolism. The criterion for performing MFA was based on the highest baculovirus titers/specific yields obtained (12 mM Pyr, *α*KG, Pyr+*α*KG, 24 mM Pyr), including a control and a non-effective supplementation (12 mM Gln) for comparison. For the calculation of metabolic fluxes, culture time was divided in two post-infection phases: phase I extends from the time of infection until 48-72 hpi, when the viable cells reach the maximum concentration, while phase II encompasses the remaining culture time until harvest (Figure 3.4). The following sub-sections provide a comprehensive analysis of the metabolic events undergone by cells in each supplementation setting.

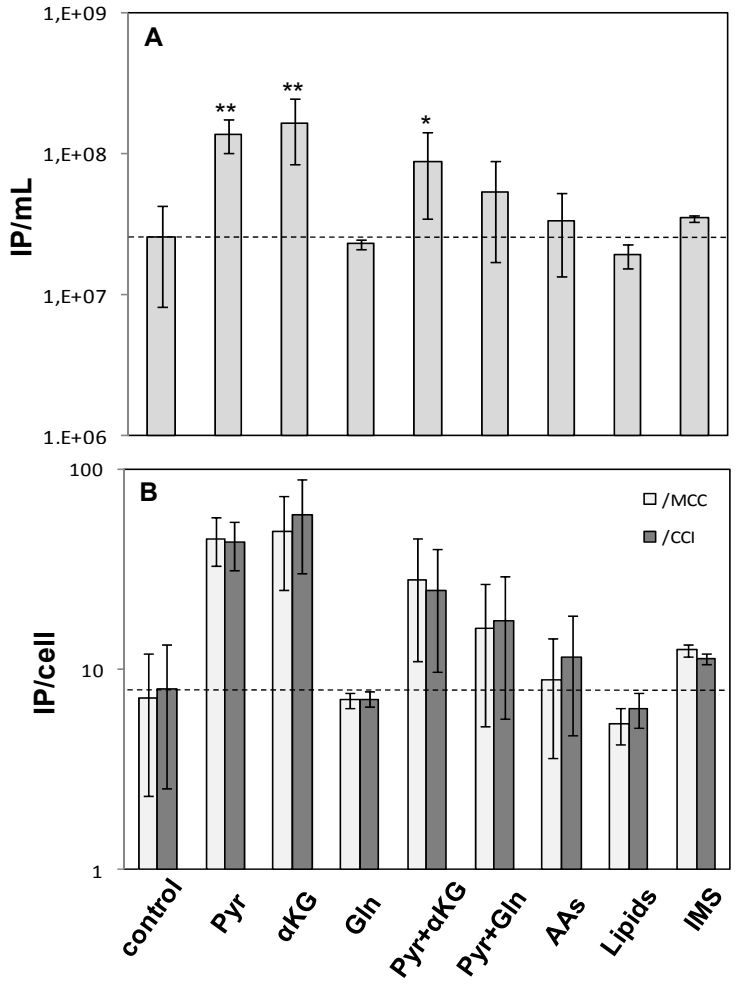


**Figure 3.2.** Effect of medium supplementation on *Ac-vp39egfp* production. All supplements were added at infection time. Cultures were infected at a CCI of 3-4×$10^6$ cells/mL with a MOI of 0.1 IP/cell. IMS refers to Insect Medium Supplement, described in Materials and Methods. (A) Average volumetric titers obtained at the end of the culture. Statistical significance against the control was assessed using at least 2 titration replicates (* $p<0.01$, ** $p<0.001$). (B) - Virus specific yields calculated as the final titer divided by either the mean cell concentration after infection (/MCC) or the cell concentration at infection (/CCI).

*A priori*, selecting between Pyr or *α*KG as medium additives is not straightforward since considerable differences in virus production are not apparent. In terms of metabolism, both compounds can be inter-converted in mitochondria through the TCA cycle. Because the feeding time, feeding regimen and total quantity supplied could result in further improvement of productivity, Pyr was chosen as a model compound for further optimization studies (Figure 3.3). Supplementing the culture before infection attempted to stimulate metabolic activity and thus cellular responsiveness to virus replication. On the other hand, high and low Pyr concentration fed-batches could lead to a more efficient allocation of nutrient sources and diminished overflow metabolism. However, neither of these approaches allowed surpassing the BV yields obtained with one-time addition of 12 mM Pyr, while doubling this concentration yielded very similar results. A cost-effective production process at high cell density based on one-time supplementation of Pyr or *α*KG can therefore be perceived.

*Network consistency and sensitivity analyses.* In all scenarios, the consistency index *h* was below the $\chi^2$ value within a 95% confidence interval. This condition indicates that the model is well-posed and that no gross measurement errors are being propagated in the measured fluxes.

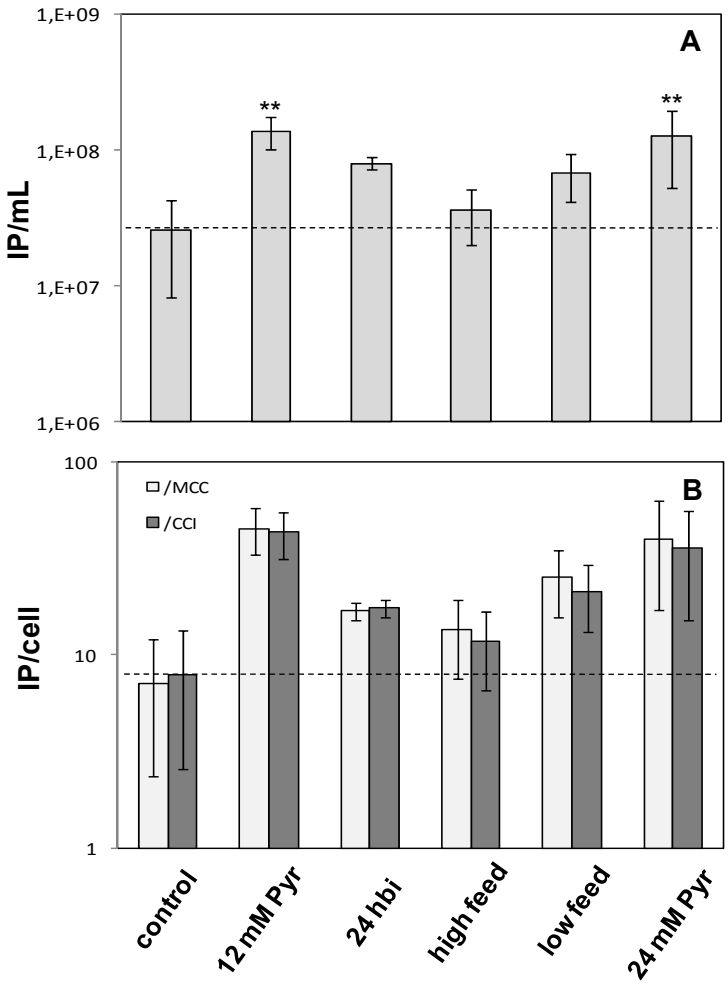


**Figure 3.3.** Baculovirus volumetric titers (A) and specific yields (B) for experiments with different schemes of pyruvate supplementation. All cultures were infected at 3-4×$10^6$ cells/mL using a MOI of 0.1 IP/cell. See Materials and Methods for experimental details. Statistical significance against the control was established using at least 2 titration replicates (** $p<0.001$).

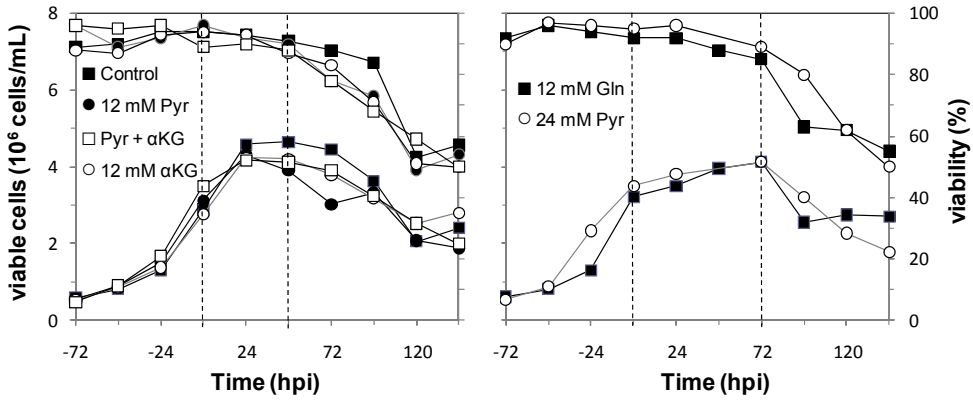


**Figure 3.4.** Time profiles of viable *Sf*9 cells. All cultures were infected at 3-4×$10^6$ cells/mL using a MOI of 0.1 IP/cell. Supplementations were performed as described in Materials and Methods. Dashed lines indicate phases used for flux analysis. See the text for details.

The sensitivities of all 45 unknown reactions (excluding intracellular defined rates) were calculated with respect to each of the 27 measured fluxes. It is shown that fluxes through the central carbon metabolism and energetic reactions are less affected by noise in experimental data (Figure 3.5). Maximum relative variations do not go beyond 2-3% for glycolysis, the TCA cycle, NADH/$FADH_2$ respiration and ATP generation rates, attesting the robustness of these pathways. The most affected fluxes, namely catabolic reactions of most essential and non-essential amino acids, are characterized by having low absolute rates and the metabolites involved have a lower participation in other cellular pathways. However, important reactions associated with nitrogen metabolism are among the least sensitive to measurement uncertainty, owing to the dampening effect caused by a higher connectivity to other pathways of the associated metabolites (Gln, Glu, Ala, αKG, Amm) and considerably higher fluxes. These reactions include the activities of GOGAT, AspAT, GDH and AlaAT, whose relative sensitivities do not go beyond 19%. Overall, the cellular

energetic state seems fairly robust and resilient to small changes in the extracellular environment, in conjunction with the overall carbon and nitrogen flows.

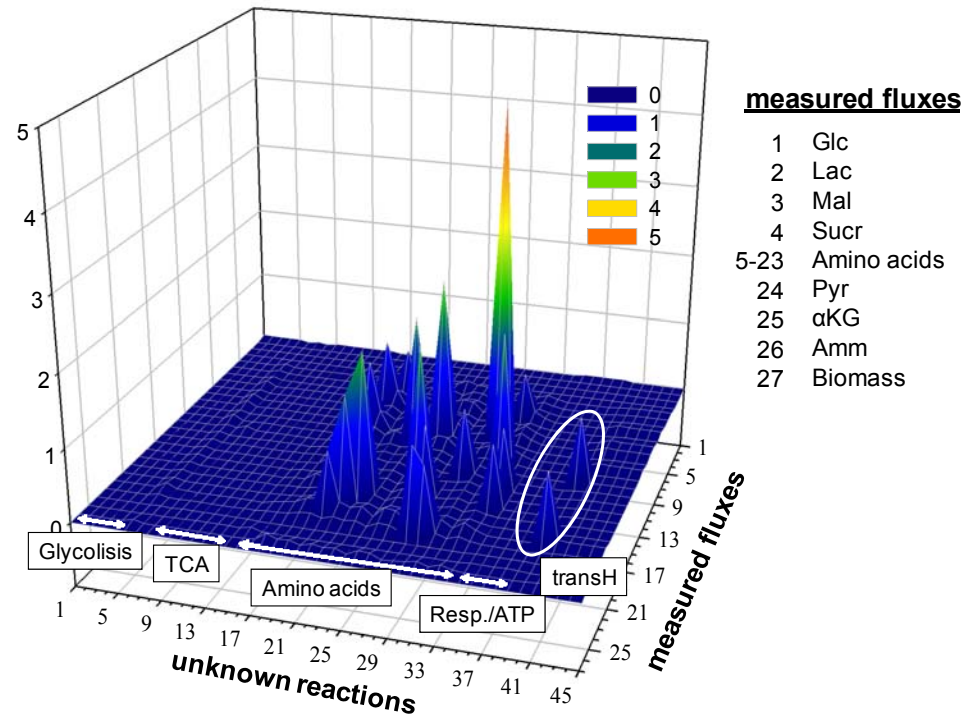


**Figure 3.5.** Sensitivity analysis of the intracellular unknown reactions with respect to uncertainty in experimentally determined fluxes (0-5 – relative variation of unknown flux with respect to unit variation in known flux). Equations used are described in Materials and Methods, and were computed using FluxAnalyzer (Klamt et al., 2003).

*Central carbon pathways: glycolysis and TCA cycle.* In this section, the central carbon pathways of *Sf*9 cells subjected to infection and selected supplementation strategies are analyzed. Enhancing the activity of these pathways was one of the main purposes of the present study, as this would influence the cellular energetic state.

Figure 3.6A shows the main adaptations in the glycolytic fluxes to the different infection strategies. An obvious observation are the lower fluxes during the second phase (from 48-72 hpi until harvest), when cellular division no longer compensates for accentuated death rates, as the main viral replication events have already taken place (Roldão et al., 2008). This phase is characterized by a markedly lower consumption rate of glucose, while maltose and sucrose uptake rates are only slightly enhanced (Table 3.2). Focusing on the initial phase after infection, considerable differences are obvious between different cultures, with the overall activity of the glycolytic pathway peaking after supplementation with 12 mM Pyr. In all other situations, activities were comparable to or smaller than in control cultures, specifically after supplementation with Pyr+αKG (12 mM each) or 24 mM Pyr. These results are highly correlated with the decreased Glc uptake rates observed (Table 3.1), and has also been previously observed in mammalian cell lines upon supplementation with Pyr or αKG (Genzel et al., 2005; Hassell and Butler, 1990), possibly reflecting a feed-back controlling effect on the activity of glycolytic enzymes. On the other hand, the higher glycolytic flux after adding only 12mM Pyr resulted from a net uptake of sucrose, which was not observed in the control. Whilst glucose is considered as the preferred carbon source in insect cells, the consumption of disaccharides such as maltose and sucrose has been already reported (Bhatia et al., 1997; Chapter II). Interestingly, in our work sucrose consumption coincided with Pyr supplementation, individually or in combination.

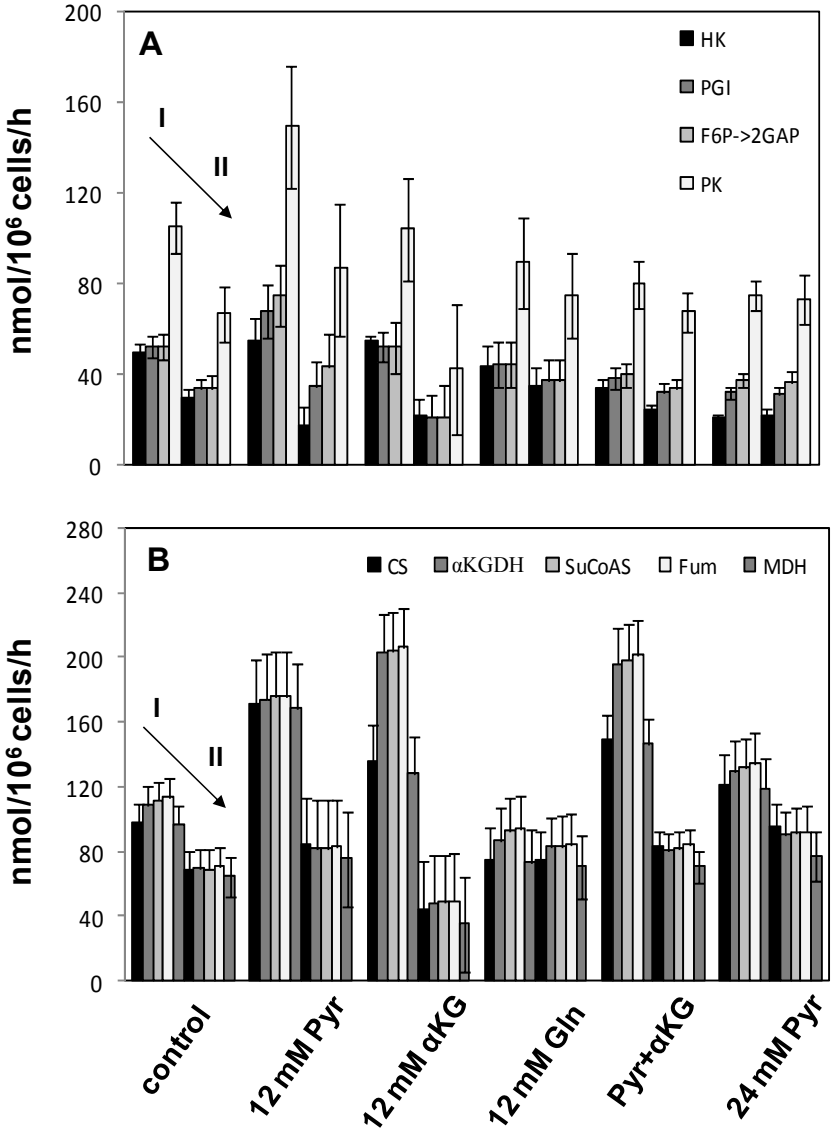


**Figure 3.6.** Fluxes through the main carbon pathways of *Sf*9 cells after infection at high cell density, subjected to different supplementation strategies: (A) Glycolytic fluxes and (B) TCA cycle reactions. I, II represent the initial (from infection until 48-72 hpi) and late (from 48-72 hpi until harvest) metabolic phases, respectively. Error bars correspond to standard deviations computed with the FluxAnalyzer software.

**Table 3.2.** Specific consumption/production rates of the main nutrients of *Sf*9 cells metabolism (nmol/$10^6$cells/h), for phase II post-infection (48-72 h until harvest). Supplementation strategies are described in Materials and Methods.

| | Control | 12mM Pyr | 12mM αKG | 12mM Gln | Pyr + αKG | 24mM Pyr |
|---|---|---|---|---|---|---|
| **Glc** | -24.461 | -8.222 | -21.478 | -32.000 | -18.181 | -19.930 |
| **Lac** | -3.445 | -4.994 | -6.238 | -5.372 | -7.431 | -19.900 |
| **Sucr** | 0 | -8.746 | 0 | 0 | -1.671 | -7.459 |
| **Malt** | -4.832 | -9.280 | 0 | -3.122 | -6.475 | -8.269 |
| **Pyr** | n.a. | -0.543 | n.a. | n.a. | -13.992 | -17.015 |
| **αKG** | n.a. | n.a. | -2.230 | n.a. | -0.535 | n.a. |
| **Amm** | 0.481 | -4.494 | -2.797 | 0.700 | -6.371 | -14.495 |
| **Asp** | -3.866 | -9.752 | -8.210 | -3.585 | -12.027 | -18.212 |
| **Glu** | -1.735 | 0.596 | 0.720 | -4.650 | 1.429 | 0.554 |
| **Ser** | -2.607 | -2.752 | -2.885 | -2.084 | -1.604 | -3.584 |
| **Asn** | -1.977 | -2.021 | -1.801 | -2.551 | -2.258 | -4.928 |
| **Gly** | -0.613 | -0.082 | 0.667 | -0.338 | 0.043 | 0.049 |
| **Gln** | -1.732 | -2.908 | -3.682 | -6.213 | -1.258 | -0.475 |
| **Thr** | -0.524 | -0.308 | -0.401 | -0.303 | -0.094 | -0.679 |
| **Ala** | 6.852 | 5.743 | 19.317 | 13.955 | 14.604 | 16.205 |
| **Pro** | 0.286 | -0.262 | 0.315 | -1.494 | -0.876 | -0.249 |
| **Tyr** | -0.111 | -0.356 | -0.203 | -0.601 | -0.438 | -0.115 |
| **Val** | -0.293 | -0.472 | -0.194 | -0.379 | -0.363 | -0.828 |
| **Met** | -0.005 | -0.781 | -0.727 | -1.416 | -1.490 | -1.855 |
| **Ile** | -0.092 | -0.674 | -0.313 | -0.558 | -0.628 | -1.756 |
| **Leu** | -0.593 | -0.677 | -0.676 | -0.708 | -0.367 | -0.625 |
| **Phe** | -1.467 | -0.400 | -0.528 | -0.604 | -1.757 | -1.044 |
| **His** | -0.118 | -0.039 | -0.012 | -0.328 | -0.176 | -0.356 |
| **Arg** | -0.603 | -0.286 | -0.230 | -0.164 | 0.449 | -0.382 |
| **Lys** | -0.546 | 0.000 | 0 | -0.621 | 0 | -0.107 |
| **Cys** | -0.207 | -0.124 | -0.634 | -0.632 | 0.123 | -0.078 |
| **Growth rate (/h)** | 0 | 0 | 0 | 0 | 0 | 0 |

As for the TCA cycle activity, an obvious up-shift can be seen after feeding cells with either Pyr, αKG or Pyr and αKG in combination, during the first phase post-infection (Figure 3.6B). Reaction rates increased to levels ranging between 173 and 177 nmol/$10^6$cells/h, approaching those obtained after infections performed at a low cell density of $1\times10^6$ cells/mL (Chapter II). This increment was lower for the cultures supplemented with 24 mM Pyr, owing to the strong inhibition of Glc consumption (Table 3.1). Interestingly, a bi-partitioning of TCA cycle rates can be seen, especially after the addition of αKG, with a higher flux through metabolites downstream the αKG node, due to an enhancement in carbon entrance. The incorporation of carbon backbones derived from amino acids at αKG also contributed to the overall activity of the TCA cycle. It has been previously observed that insect cells have a preference for the uptake of amino acids over their synthesis, even for the case of non-essential amino acids (Chapter I and II, Ferrance et al., 1993). Gln and Ser had the highest contribution in control cultures, whereas the supplementation of organic acids and Gln also elicited the uptake of other essential and non-essential amino acids (Table 3.1). As in the case of glycolysis, TCA cycle activities decreased considerably after the initial 48-72 hpi, owing not only to decreased consumption rates of sugars and organic acids, but also to a significant inhibition of amino acids consumption, particularly Gln (Table 3.2), reinforcing the metabolic contraction previously mentioned. On the whole, these observations indicate that the uptake of either 12 mM Pyr or 12 mM αKG efficiently boosted TCA cycle fluxes after high cell density infection, building on the carbon flow and energy generation in the cell, without repressing glucose consumption.

*Glutaminolysis and nitrogen metabolism.* The contribution of amino acids integration into the TCA cycle was already addressed in the previous sub-section; a more in-depth analysis can be found in Chapter II. Here,

attention will be given to selected reactions related with nitrogen metabolism during phase I post-infection, as the main metabolic adaptations to the supplementation strategies employed are more evident during this time period. It should be noted that the following analysis in not compromised by the fact that the nitrogen balance closed to an average 63%; this balance is mostly affected by unavoidable experimental errors in the biomass formation measurements, as well as uncertainty in its elementary composition (for details, see Chapter II).

Glutamine consumption was preferential among all the amino acids, largely driving nitrogen inflow to the cells (Table 3.1). As shown in Figure 3.7, GOGAT activity closely followed the uptake rates of Gln. Through the concerted activity of GOGAT and AlaAT, Gln-derived ammonia could be efficiently transferred to Pyr for the production of Ala, the main by-product released to the culture medium. While *Sf*9 insect cells do not secrete significant amounts of Amm (Drews et al., 2000), Ala production was not significantly affected by the supplementation of Pyr and/or αKG, whereby added carboxylic acids were not primarily directed to an increment in AlaAT activity. Conversely, Gln addition resulted in a slightly higher Ala production rate, evidenced by increased fluxes through AlaAT and GOGAT. Interestingly, Amm was consumed in every case when organic acids were added to the cultures, correlating with the production of Glu through GDH. Negative GDH activities driving glutamate formation from ammonia and α-ketoglutarate condensation have been observed in Chapter II. In fact, this reaction is responsible for the ability of *S. frugiperda* cell lines to synthesize Glu and Gln from Amm supplied to the culture medium (Öhman et al., 1996). This can be seen more markedly in the case of supplementation with Pyr plus αKG, owing to the accretion effect on the pool of αKG (Figure 3.7).

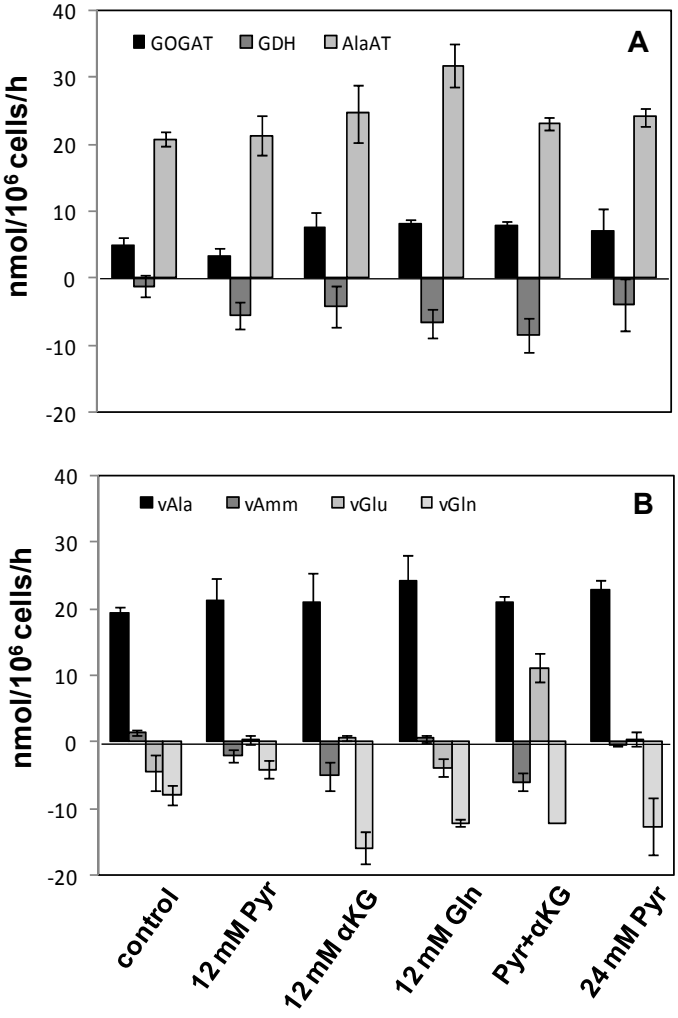


**Figure 3.7.** (A) Consumption (negative) and production (positive) fluxes of amino acids involved in nitrogen metabolism after infection. (B) Reaction rates of the main nitrogen pathways in *Sf*9 cells metabolism calculated as model outputs in FluxAnalyzer. A negative rate indicates that a reversible reaction proceeds in the opposite direction, as defined in Appendix 1.

From this analysis, it is evident how *Sf*9 cells can efficiently handle excess nitrogen intake through the flexible and combined activity of different reactions cooperating in this task. Importantly, the strategies that

contributed mostly to improve cellular productivity coped with an efficient control of nitrogen homeostasis, without a significant increment in alanine excretion.

*Analysis of pyruvate and α-ketoglutarate metabolic nodes.* Taking a closer look at key nodes of cellular metabolism offers valuable information on the fine-tuning of flux distributions in response to perturbations. Previous studies on various metabolic adaptations of microorganisms attest the importance of this evaluation (Vallino and Stephanopoulos, 1993; Zhu and Shimizu, 2005). This is even more critical when the manipulations attempted in the present work targeted the two main crossroads within the central carbon and nitrogen pathways, i. e., the Pyr and αKG branch-points.

Figure 3.8 schematizes the metabolic partitioning at the Pyr node occurring during the initial 48-72 hpi with the different supplementation schemes. Besides the partitioning coefficients associated with inflow and outflow reactions, significant increments or decreases in net reaction rates are highlighted. It is clear from the control that *Sf*9 cells have a rather efficient metabolism, with 80% of the Pyr formed being channelled into the TCA cycle. These results match our previous observations in Chapter II, also fitting with determinations by others (Neermann and Wagner, 1996). While the addition of Gln did not significantly affect the ratio between glycolytic (Pyr coming from PEP) and malic enzyme (Pyr coming from Mal) inflow reactions, Ala production was strongly enhanced (see Figure 3.7), resulting in a lower efficiency in the generation of ACoA. Noteworthy are the alterations observed after feeding cells with Pyr, namely a higher net flux towards the formation of ACoA, slightly increasing its partitioning coefficient in comparison to the control. As a result of higher Pyr consumption, the inflow contribution from malate decreased considerably. In contrast, the generation of Pyr molecules from Mal increased substantially when the

supplement was αKG, significantly rising the coefficient partitioning of this reaction. This observation supports what has already been mentioned on the characteristic behaviour of the TCA cycle after αKG supplementation (Figure 3.6B). In fact, the build up of the αKG pool leads to higher fluxes towards the formation of Mal, which needed to be apportioned into the formation of both OAA and Pyr, ensuring TCA cycle functionality and avoiding the accumulation of metabolic intermediates. Consequently, an indirect plumping of the Pyr pool after αKG supplementation resulted also in increased fluxes towards Lac production (see Table 3.1), although the outflow partitioning coefficients remained essentially unaltered (Figure 3.8).

In a similar way, metabolic partitioning at the αKG node shows that the addition of Pyr or αKG resulted in a similar inflow and outflow flux partitioning when compared to the control (Figure 3.9). The main alterations in net fluxes were somewhat expected from the build up of the intracellular Pyr and αKG pools. Interestingly, addition of αKG resulted in an enhanced GOGAT activity, coping with the higher Gln uptake rate observed in this case (Table 3.1, Figure 3.7). On the other hand, a completely different scenario can be recognized when Gln was the supplement chosen, with partitioning coefficients of AlaAT and GOGAT/GDH catalyzed reactions increasing in relation to the TCA cycle reactions.

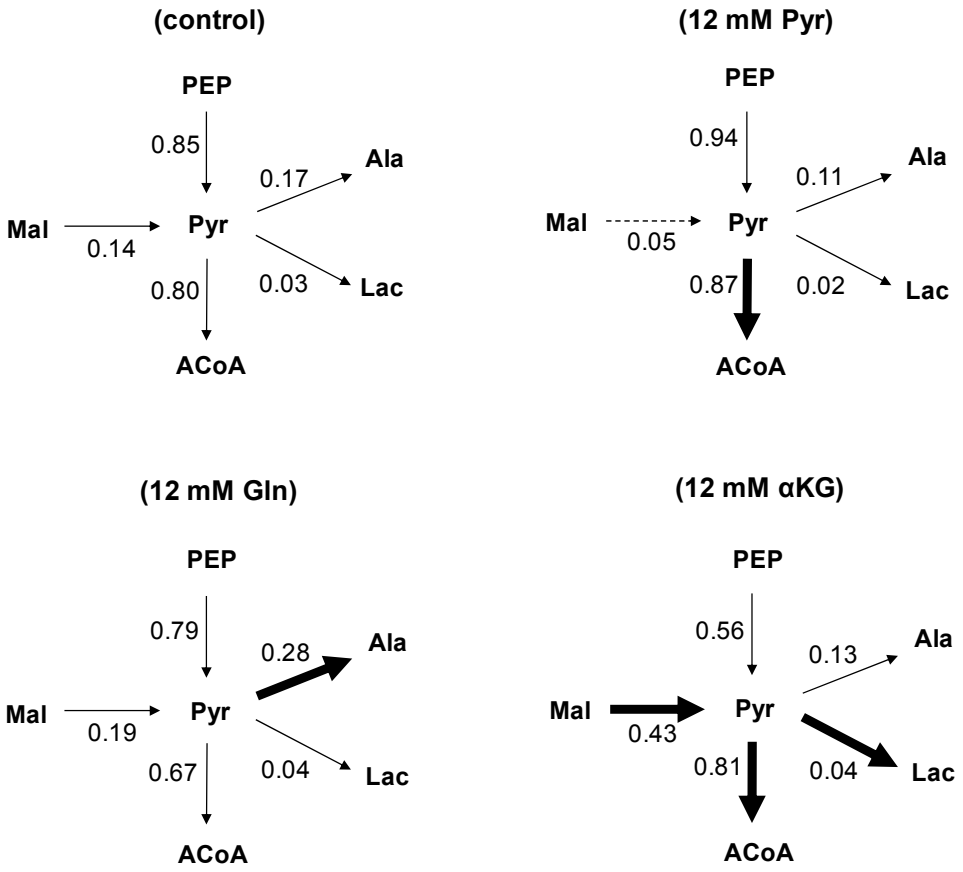


**Figure 3.8.** Metabolic partitioning coefficients at the pyruvate node of infected *Sf*9 cells. A bold arrow indicates a net flux increase by at least 50% in relation to the control. A dashed arrow represents a 50% decrease or more. Coefficients were calculated based on all reaction rates leading to the formation or depletion of pyruvate in each case (see Appendix 2). Only the most representative pathways are pictured: Inflow reactions - ME (Mal), PK (PEP); Outflow reactions - PDH (ACoA), AlaAT (Ala), LDH (Lac).

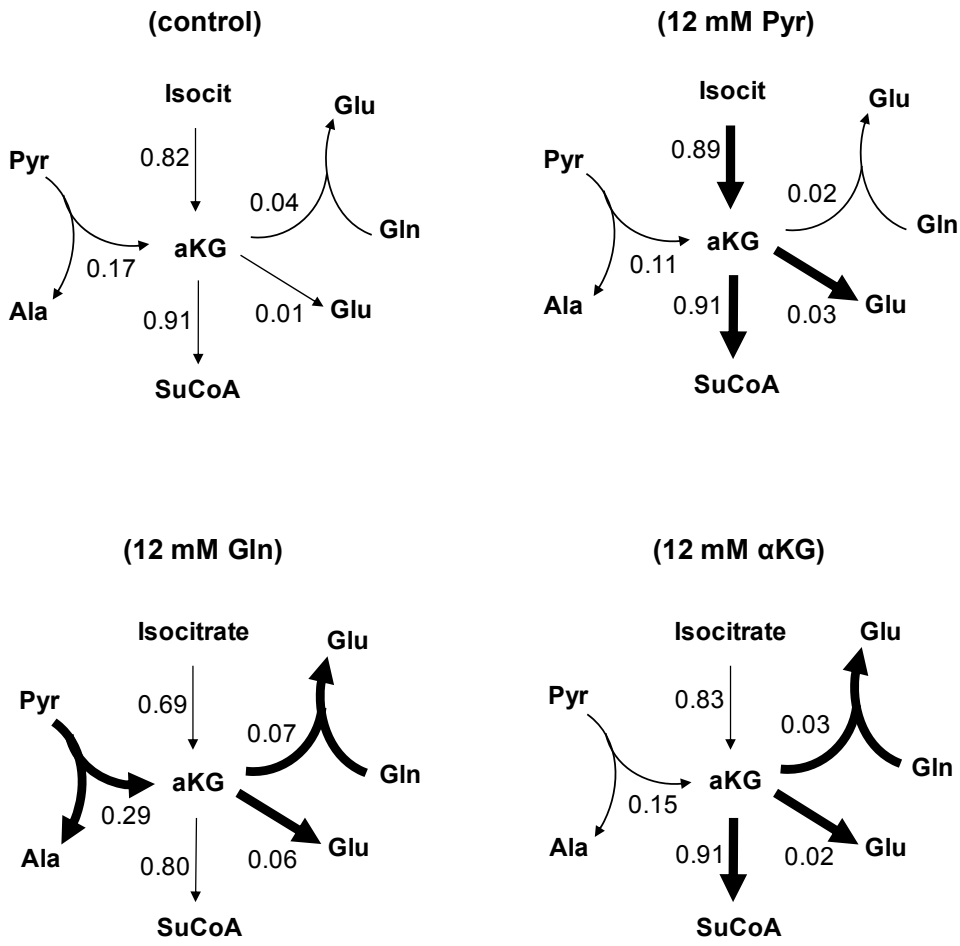


**Figure 3.9.** Metabolic partitioning coefficients at the α-ketoglutarate node of infected *Sf*9 cells. A bold arrow indicates a net flux increase by at least 50% in relation to the control. A dashed arrow represents a 50% decrease or more. Coefficients were calculated based on all reaction rates leading to the formation or depletion of pyruvate in each case (see Appendix 2). The most representative pathways include: Inflow reactions – ICDH (Isocitrate), AlaAT (Pyr->Ala); Outflow reactions – αKGDH (SuCoA), GOGAT (Gln->Glu), GDH (Glu). The reaction catalyzed by ICDH is part of a lumped route in the model (see Appendix 2).

The results above show that both Pyr and αKG additions resulted in an enhancement of fluxes through the TCA cycle, maintaining the already

efficient outflow flux partitioning at both metabolic nodes. Additionally, Pyr addition did not increase overflow metabolism, while the addition of αKG considerably increased the formation of Lac. In striking contrast, the addition of Gln clearly shows that nitrogen metabolism gained ground against the central carbon pathways, with potential negative implications for the cellular energetic state.

*Energetic metabolism: respiration and ATP synthesis.* Most of the metabolic adaptations here reported have as a corollary the capacity of cells to generate energy in the form of ATP. Figure 3.10 shows the output model estimations for the main respiratory events and ATP synthesis occurring during phase I post-infection. It is clear how the net rate of ATP formation closely follows that of NADH respiration, which is known to have the largest contribution for the proton gradient across the inner mitochondrial membrane (Voet and Voet, 1995). In this work, a direct link between the energetic state of cells and the flow through the TCA cycle, where the majority of NADH equivalents are generated, can be established. Successful supplementation with key TCA cycle intermediates resulted in an anaplerotic effect causing the flow through the TCA cycle to increase, which in turn led to superior ATP synthesis rates. These were as high as 2642 and 2170 nmol/$10^6$cells/h during the initial 48-72 hpi after supplementation with 12 mM Pyr or 12 mM αKG, respectively, corresponding to a mean 54% increase with respect to the control. This confirms MFA estimations by Sidorenko et al. (2008) performed in Madin-Darby canine kidney (MDCK) cells, yielding much higher net ATP synthesis rates for pyruvate-containing than for glutamine-containing media used as control. Importantly, a parallel up-shift in the estimated specific oxygen uptake rate (OUR) was observed, corroborating our previous observations that limitations in oxygen availability are not likely the main

cause for poor virus replication. A direct correlation can then be envisaged between target product specific yields and cellular energetic capacity.

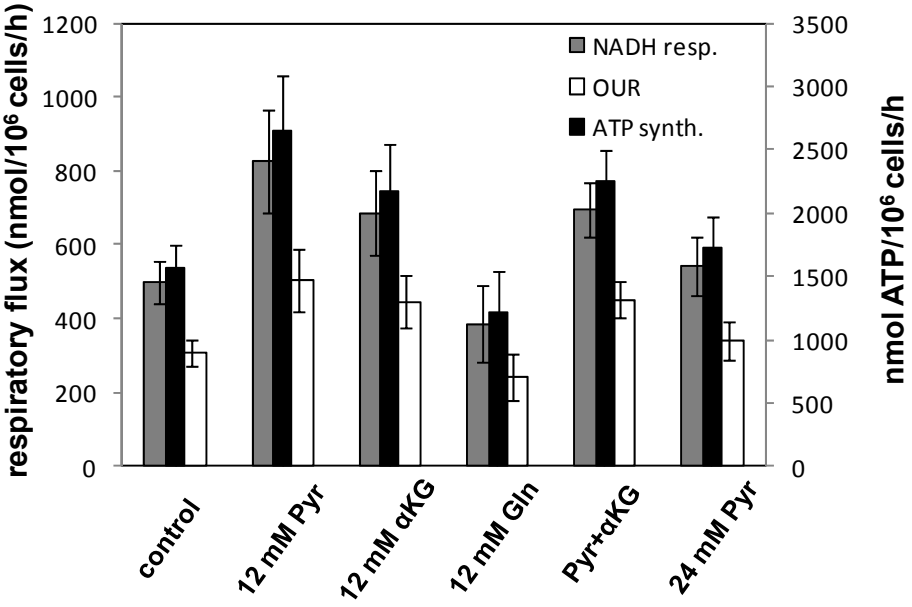


**Figure 3.10.** Estimation of respiratory fluxes (left vertical axis) and net specific ATP synthesis rates in *Sf*9 cells during phase I post-infection. Reactions listed in Appendix 1 were considered as the only sources/sinks for ATP. Error bars are standard deviations computed with the FluxAnalyzer software.

## 5. DISCUSSION

The importance of the high-energy molecule ATP in industrial production processes has received much attention during the past decades, extending the border line of metabolic engineering (Zhou et al., 2009). Both mitochondrial respiration and ATP synthesis play a fundamental role in metabolism, largely determining the throughput and ability of cells to thrive in different environments. In fact, a central aspect determining cellular

responsiveness to virus replication seems to be the capacity to maintain an active metabolic state. Measurements of intracellular ATP content have been used to monitor infection and recombinant protein production in insect cell cultures (Olejnik et al., 2004), while total cellular ATP content has been shown to determine virus replication in Vero cell cultures (Burgener et al., 2006).

Both the TCA cycle and glycolysis provide most of the redox equivalents for cellular respiration, also contributing to ATP synthesis through substrate-level phosphorylation (Voet and Voet, 1995). Transfecting cells to express key enzymes bridging glucose utilization and oxidation through the TCA cycle has been previously attempted in some mammalian cell lines for enhanced recombinant protein production and decreased lactate accumulation (Irani et al., 1999; Kim and Lee, 2007). However, this is a frail strategy to be carried in *S. frugiperda*-derived cells, since they were shown to already possess a fully functional TCA cycle and accumulate low levels of lactate (Neermann and Wagner, 1996), suggesting that TCA cycle enzymatic activities are not limiting. Alternatively, feeding ATP directly to the cells holds relevant drawbacks, mainly due to higher costs involved and to the inhibitory effect upon glycolytic rates demonstrated in eukaryotic hosts, which could compromise cellular productivity (Larsson et al., 2000). For these reasons, supplementation schemes composed by intermediates involved in central metabolic pathways, such as pyruvate and α-ketoglutarate, were attempted to directly enhance TCA cycle fluxes and boost energy generation in the cell. To the best of our knowledge, the supplementation of these compounds to insect cells cultures has not been reported before.

The use of organic acids as medium additives in previous studies of mammalian cell culture attempted at reducing ammonia production by

substituting glutamine in the culture medium (Genzel et al., 2005; Hassell and Butler, 1990). Feeding hybridoma cell lines with αKG has also been exploited as a strategy to increase monoclonal antibody production (Nilsang et al., 2008). Although Pyr and αKG transporters have not been specifically described in insect cells, a $H^+$-monocarboxylate co-transporter is well described in mammalian plasma membranes, facilitating the diffusion of Pyr along with L-lactate and a wide range of other aliphatic monocarboxylates (Poole and Halestrap, 1993). αKG transporters are poorly described in the literature, though some mechanisms have been reported in mammals, including a $Na^+$-dependent carrier in perfused rat liver with competition by different dicarboxylic acids (Stoll and Haussinger, 1991), and a carrier-independent diffusion process in fibroblasts (Aussel et al., 1996). In the present work, we could accurately measure concentration profiles of Pyr and αKG in culture supernatants, and demonstrate that *Sf*9 cells readily uptake these metabolites in a non-competitive manner (Figure 3.1).

The interpretation of baculovirus production results is not straightforward in the light of previous theories relating lower productivities at high cell density with nutrient depletion (Bédard et al., 1994; Bhatia et al., 1997). In fact, neither glucose nor any amino acid reached limiting concentrations before harvest time (data not shown), whereas supplementation of amino acids or lipids did not have an effect on productivity (see Figure 3.2). Interestingly, the addition of the Insect Medium Supplement, a complete nutritious and low-protein formulation developed as a serum replacement for insect cell growth, also did not impact significantly baculovirus production. These discrepancies could be explained by the different culture media used: the medium used in this work, SF900 II serum-free, has an exceptionally rich formulation, designed to support the high cell densities currently attained in insect cell cultures. Furthermore, the significant up-shift in the estimated

OUR observed after culture supplementation with Pyr and/or αKG further suggests that limitations in oxidative metabolism are not primarily responsible for decreased productivities at high cell densities. In face of these observations, we further reinforce the hypothesis carried along the previous chapters that the extracellular accumulation of conditioned medium factors down-regulating overall metabolic activity constitutes the main restraint to nutrient utilization at high cell densities, probably a protection mechanism avoiding medium exhaustion under stress conditions (Doverskog et al., 1997; Doverskog et al., 2000). The direct stimulation of central carbon pathways by supplemented Pyr or αKG seems to have by-passed most of these repressing mechanisms, with an overall positive effect on the cellular energetic and productive states.

## ACKNOWLEDGEMENTS

This work was partially supported by the European Projects BACULOGENES (FP6 LHSB-CT-2006-037541) and CLINIGENE-NoE (FP6 LSHB-CT-2004-018933). Nuno Carinhas acknowledges Fundação para a Ciência e a Tecnologia (FCT) for his Ph.D. grant (SFRH/BD/36676/2007). Vicente Bernal holds a post-doctoral fellowship from Fundación Séneca (Murcia, Spain). The authors are thankful to Ana Luísa Simplício for her advice during the implementation of the HPLC protocol for amino acids analysis.

## REFERENCES

Aussel, C., Coudray-Lucas, C., Lasnier, E., Cynober, L. and Ekindjian, O.G., 1996. alpha-Ketoglutarate uptake in human fibroblasts. Cell Biol Int 20, 359-63

Bédard, C., Kamen, A., Tom, R. and Massie, B., 1994. Maximization of recombinant protein yield in the insect cell/baculovirus system by one-time addition of nutrients to high-density batch cultures. Cytotechnology 15, 129-138

Bédard, C., Tom, R. and Kamen, A., 1993. Growth, nutrient consumption, and end-product accumulation in Sf-9 and BTI-EAA insect cell cultures: insights into growth limitation and metabolism. Biotechnol Prog 9, 615-24

Bhatia, R., Jesionowski, G., Ferrance, J.P. and Ataai, M.M., 1997. Insect cell physiology. Cytotechnology 24, 1-9

Burgener, A., Coombs, K. and Butler, M., 2006. Intracellular ATP and total adenylate concentrations are critical predictors of reovirus productivity from Vero cells. Biotechnol Bioeng 94, 667-79

Caron, A.W., Archambault, J. and Massie, B., 1990. High-level recombinant protein production in bioreactors using the baculovirus-insect cell expression system. Biotechnol Bioeng 36, 1133-1140

Daae, E.B. and Ison, A.P., 1999. Classification and sensitivity analysis of a proposed primary metabolic reaction network for Streptomyces lividans. Metab Eng 1, 153-65

Doverskog, M., Bertram, E., Ljunggren, J., Ohman, L., Sennerstam, R. and Haggstrom, L., 2000. Cell cycle progression in serum-free cultures of Sf9 insect cells: modulation by conditioned medium factors and implications for proliferation and productivity. Biotechnol Prog 16, 837-46

Doverskog, M., Ljunggren, J., Ohman, L. and Haggstrom, L., 1997. Physiology of cultured animal cells. J Biotechnol 59, 103-15

Drews, M., Doverskog, M., Ohman, L., Chapman, B.E., Jacobsson, U., Kuchel, P.W. and Haggstrom, L., 2000. Pathways of glutamine metabolism in Spodoptera frugiperda (Sf9) insect cells: evidence for the presence of the nitrogen assimilation system, and a metabolic switch by 1H/15N NMR. J Biotechnol 78, 23-37

Drews, M., Paalme, T. and Vilu, R., 1995. The growth and nutrient utilization of the insect cell line Spodoptera frugiperda Sf9 in batch and continuous culture. J Biotechnol 40, 187-198

Ferrance, J.P., Goel, A. and Ataai, M.M., 1993. Utilization of glucose and amino acids in insect cell cultures: Quantifying the metabolic flows within the primary pathways and medium development. Biotechnol Bioeng 42, 697-707

Ferreira, T.B., Ferreira, A.L., Carrondo, M.J. and Alves, P.M., 2005. Effect of re-feed strategies and non-ammoniagenic medium on adenovirus production at high cell densities. J Biotechnol 119, 272-80

Genzel, Y., Ritter, J.B., Konig, S., Alt, R. and Reichl, U., 2005. Substitution of glutamine by pyruvate to reduce ammonia formation and growth inhibition of mammalian cells. Biotechnol Prog 21, 58-69

Hassell, T. and Butler, M., 1990. Adaptation to non-ammoniagenic medium and selective substrate feeding lead to enhanced yields in animal cell cultures. J Cell Sci 96 ( Pt 3), 501-8

Henry, O., Perrier, M., Kamen, A., 2005. Metabolic flux analysis of HEK-293 cells in perfusion cultures for the production of adenoviral vectors. Metab Eng 7, 467-476

Ikonomou, L., Schneider, Y.J. and Agathos, S.N., 2003. Insect cell culture for industrial production of recombinant proteins. Appl Microbiol Biotechnol 62, 1-20

Irani, N., Wirth, M., van Den Heuvel, J. and Wagner, R., 1999. Improvement of the primary metabolism of cell cultures by introducing a new cytoplasmic pyruvate carboxylase reaction. Biotechnol Bioeng 66, 238-46

Kim, S.H. and Lee, G.M., 2007. Functional expression of human pyruvate carboxylase for reduced lactic acid formation of Chinese hamster ovary cells (DG44). Appl Microbiol Biotechnol 76, 659-65

Klamt, S., Stelling, J., Ginkel, M. and Gilles, E.D., 2003. FluxAnalyzer: exploring structure, pathways, and flux distributions in metabolic networks on interactive flux maps. Bioinformatics 19, 261-9

Kukkonen, S.P., Airenne, K.J., Marjomaki, V., Laitinen, O.H., Lehtolainen, P., Kankaanpaa, P., Mahonen, A.J., Raty, J.K., Nordlund, H.R., Oker-Blom, C., Kulomaa, M.S. and

Yla-Herttuala, S., 2003. Baculovirus capsid display: a novel tool for transduction imaging. Mol Ther 8, 853-62

Larsson, C., Pahlman, I.L. and Gustafsson, L., 2000. The importance of ATP as a regulator of glycolytic flux in Saccharomyces cerevisiae. Yeast 16, 797-809

Neermann, J. and Wagner, R., 1996. Comparative analysis of glucose and glutamine metabolism in transformed mammalian cell lines, insect and primary liver cells. J Cell Physiol 166, 152-69

Nilsang, S., Kumar, A. and Rakshit, S.K., 2008. Effect of alpha-ketoglutarate on monoclonal antibody production of hybridoma cell lines in serum-free and serum-containing medium. Appl Biochem Biotechnol 151, 489-501

Öhman, L., Alarcon, M., Ljunggren, J., Ramqvist, A.-K. and Häggström, L., 1996. Glutamine is not an essential amino acid for Sf-9 insect cells. Biotechnol Lett 18, 765-770

Olejnik, A.M., Czaczyk, K., Marecik, R., Grajek, W. and Jankowski, T., 2004. Monitoring the progress of infection and recombinant protein production in insect cell cultures using intracellular ATP measurement. Appl Microbiol Biotechnol 65, 18-24

Poole, R.C. and Halestrap, A.P., 1993. Transport of lactate and other monocarboxylates across mammalian plasma membranes. Am J Physiol Cell Physiol 264, 761-782

Roldão, A., Carrondo, M.J.T., Alves, P.M. and Oliveira, R., 2008. Stochastic simulation of protein expression in the baculovirus/insect cells system. Comput Chem Eng 32, 68-77

Sidorenko, Y., Wahl, A., Dauner, M., Genzel, Y. and Reichl, U., 2008. Comparison of metabolic flux distributions for MDCK cell growth in glutamine- and pyruvate-containing media. Biotechnol Prog 24, 311-20

Stephanopoulos, G., 1999. Metabolic fluxes and metabolic engineering. Metab Eng 1, 1-11

Stephanopoulos, G., Aristidou, A.A. and Nielsen, J., 1998. Metabolic engineering. Principles and Methodologies. Academic Press, San Diego

Stoll, B. and Haussinger, D., 1991. Hepatocyte heterogeneity in uptake and metabolism of malate and related dicarboxylates in perfused rat liver. Eur J Biochem 195, 121-129

Vallino, J.J. and Stephanopoulos, G., 1993. Metabolic Flux Distributions in Corynebacterium-Glutamicum During Growth and Lysine Overproduction. Biotechnology and Bioengineering 41, 633-646

van Gulik, W.M., de Laat, W.T., Vinke, J.L. and Heijnen, J.J., 2000. Application of metabolic flux analysis for the identification of metabolic bottlenecks in the biosynthesis of penicillin-G. Biotechnol Bioeng 68, 602-18

Voet, D. and Voet, J.G., 1995. Biochemistry. John Wiley & Sons, New York

Wang, N.S. and Stephanopoulos, G., 1983. Application of macroscopic balances to the identification of gross measurement errors. Biotechnol Bioeng 25, 2177-2208

Zhou, J., Liu, L., Shi, Z., Du, G. and Chen, J., 2009. ATP in current biotechnology: regulation, applications and perspectives. Biotechnol Adv 27, 94-101

Zhu, H.F. and Shimizu, K., 2005. Effect of a single-gene knockout on the metabolic regulation in Escherichia coli for D-lactate production under microaerobic condition. Metabolic Engineering 7, 104-115

# CHAPTER IV

## DEVELOPMENT OF A HYBRID FRAMEWORK TO MODEL COMPLEX PRODUCT FORMATION IN METABOLIC MODELS

**ADAPTED FROM:**

Carinhas N, Bernal V, Teixeira AP, Carrondo MJT, Alves PM, Oliveira R (2011) Hybrid metabolic flux analysis: combining stoichiometric and statistical constraints to model the formation of complex recombinant products. *BMC Syst Biol* **5**: 34.

# TABLE OF CONTENTS

## 1. SUMMARY

Stoichiometric models constitute the basic framework for fluxome quantification in the realm of metabolic engineering. A recurrent bottleneck, however, is the establishment of consistent stoichiometric models for the synthesis of recombinant proteins or viruses. Although optimization algorithms for *in silico* metabolic redesign have been developed in the context of genome-scale stoichiometric models for small molecule production, still rudimentary knowledge of how different cellular levels are regulated and phenotypically expressed prevents their full applicability for complex product optimization. To address this issue, a hybrid framework was developed combining classical metabolic flux analysis with projection to latent structures to further link estimated metabolic fluxes with measured productivities. We first explored the functional metabolic decomposition of a baculovirus vector-producing insect cell line from experimental data, highlighting the TCA cycle and mitochondrial respiration as pathways strongly associated with viral replication. To reduce uncertainty in metabolic target identification, a Monte Carlo sampling method was used to select meaningful associations with the target, from which 66% of the estimated fluxome had to be screened out due to weak correlations and/or high estimation errors. The proposed hybrid model was then validated using a subset of independent experiments, enabling the accurate prediction of baculovirus productivity. Overall, the results indicate the hybrid metabolic flux analysis framework is an advantageous tool for metabolic identification and quantification in incomplete or ill-defined metabolic networks.

## 2. INTRODUCTION

The biotechnological industry is facing substantial pressure to achieve

global process optimization. Concomitantly, the exploitation of high-throughput cellular data to support metabolic engineering has intensified in recent years (Lee et al., 2005; Otero and Nielsen, 2010). At the top of the various "omic" layers, the metabolic fluxome resides as their integrated functional output, which in turn closely determines the phenotypic portrait of the cell, particularily productivity (Sauer, 2004). Therefore, the estimation of intracellular fluxes in stoichiometric models is essential (Gombert and Nielsen, 2000).

With the emergence of increasingly extensive genome annotations for several organisms, optimization algorithms for genome-wide fluxome estimations have become well popularized. Such estimations are based on flux balance analysis (FBA), which assumes a "metabolic objective" driving the behaviour of the cell (see for instance Kauffman et al., 2003). A set of derived frameworks have since been developed aiming to probe for genomic alterations (knock-outs, knock-ins, down-regulations and over-expressions) expected to yield better performances than the wild-type (Burgard et al., 2003; Patil et al., 2005; Pharkya and Maranas, 2006; Pharkya et al., 2004), and examples of successful FBA-driven predictions are available (Fong et al., 2005; Asadollahi, 2009). However, because fluxes are estimated in a landscape in which the amount of data is not enough to simply use metabolite balancing, as in small-scale metabolic flux analysis (MFA), the need for additional mathematical assumptions when searching for high yielding genetic alterations may render such predictions less dependable.

In spite of their value, and regardless of size, currently available stoichiometric models by-pass a multi-layered web of regulatory events, thus constituting a simplification of cellular function (Oberhardt, 2009). Given the obvious gap between genome and fluxome, mutants "created" *in silico* by linear optimization/inspection may not exhibit the expected

metabolic behaviour *in vivo*. While methods for integration of regulatory and metabolic networks have been reported (Covert et al., 2008; Lee et al., 2008; Kim and Reed, 2010), still fragmentary knowledge of kinetic and regulatory phenomena (e.g. transcriptional, translational, signalling), together with their cumbersome biological specificity (Herrgard, 2004), may preclude their full applicability in metabolic engineering. This is especially relevant when attempting to engineer complex, multi-genic phenotypes, such as improving the yields of recombinant proteins derived from animal cell cultures, for which reason stoichiometric models have been mostly confined to microbial systems producing small molecules (Kauffman et al., 2003). In this respect, an additional important pitfall is the lack of mechanistic knowledge of processing pathways associated with the formation of proteins or viruses; simply lumping the necessary precursors in a set of synthesis reactions has proven a fruitless task since the stoichiometric requirements for these recombinant products are several orders of magnitude below those for host biomass formation, thus making their distinction practically impossible (Sidorenko and Reichl, 2004; Boghigian et al., 2010). As a result, the application of stoichiometric models to complex product formation has been restricted to the evaluation of optimal conditions for cell growth and metabolic efficiency rather than explicitly defining productivity in the models (Quek et al., 2010; Sheikh et al., 2005).

These issues are herein addressed by proposing a hybrid stoichiometric/statistical framework to make sense of fluxome data either from small-scale or genome-scale metabolic models. In order to illustrate this approach, the metabolic behavior of the baculovirus-insect cells system is explored as a case-study for rapid bioprocess optimization. The results obtained in Chapter III are here combined with new data to present a scenario where MFA is employed to reliably estimate intracellular flux distributions in a small-scale network comprising the main pathways of

carbon and nitrogen flow. Then, projection to latent structures (PLS) (Wold et al., 2001) is used to search for correlations between a measured productivity target and the estimated metabolic state, whereby the inclusion of a statistical model allows filling the gaps in our knowledge of global regulation of anabolic processes. The ability of hybrid MFA to assign individual fluxes/pathways of central metabolism to cell-specific functions that cannot be completely defined in a stoichiometric description is demonstrated.

## 3. MATERIALS AND METHODS

Experimental data on infected *Sf*9 cultures used in this Chapter were obtained from Chapter 3. In addition, we simulated nutrient limitations by centrifuging cells prior to infection and ressuspending in a 1:1 dilution of conditioned medium with PBS buffer (adjusted to pH 6.1 and 370 mOsm). For AMP-activated protein kinase (AMPK) activation, aminoimidazole carboxamide ribonucleotide (Sigma Aldrich: A-9978) was added to the culture at 6-8h post-infection to a concentration of 500 μM (Sullivan et al., 1994; Xiao et al., 2009). This kinase is a central energetic sensor in eukaryotic cells. Infections were performed with the recombinant baculovirus *Ac-vp39egfp* as previously described (Chapter III).

### 3.1. Hybrid metabolic flux analysis and Monte Carlo sampling

The input (predictor) data for hybrid MFA are the metabolic fluxes estimated by classical MFA in a well-described metabolic network. After standardization, the decomposition of the predictor matrix $\mathbf{V_e}^T$ (with different culture conditions/steady states as rows, and different fluxes as columns) is

performed iteratively and supervised by maximizing covariance with the target vector $\mathbf{V_t^T}$. The result is the projection of the fluxome space into a "latent space" defined by a set of uncorrelated (orthogonal) latent variables (LVs):

$$\mathbf{T} = \mathbf{V_e^T} \times \mathbf{W}, \quad (4)$$

$$\mathbf{V_e^T} = \mathbf{T} \times \mathbf{Q^T} + \mathbf{E}, \quad (5)$$

where **T** is the matrix with LVs as columns, **W** is a matrix of weights, $\mathbf{Q^T}$ a matrix of "loadings", and **E** a residuals matrix. Similarly, the target vector can also be decomposed using the same latent space as

$$\mathbf{V_t^T} = \mathbf{T} \times \mathbf{P^T} + \mathbf{F}, \quad (6)$$

with $\mathbf{P^T}$ the corresponding loadings vector and **F** a vector of residuals. Finally, the linear model between the predictor and target variables is derived:

$$\mathbf{V_t^T} = \mathbf{V_e^T} \times \mathbf{B} + \mathbf{F}. \quad (7)$$

Here, $\mathbf{B = W \times P^T}$ is the column vector that maximizes the squared sample covariance between $\mathbf{V_t^T}$ and the latent variables in **T** (Boulesteix and Strimmer, 2006). It represents the set of regression coefficients establishing the statistical relationship between fluxome state and the target cellular function, containing quantitative and qualitative information on the potential impact that each flux has on the target variable. The main algorithm for these calculations is part of "The *N*-Way toolbox for MATLAB" (Andersson and Bro, 2000) and is described in Jong (1993).

For the estimation of confidence intervals associated with each regression coefficient, 1000 fluxome states were randomly sampled considering normal error distributions associated with flux estimates that have been propagated in MFA calculations from an initial 16% error in measured exchange fluxes (including cellular growth rate). For the productivity target,

a 22% error was used (Roldão et al., 2009). PLS regression was then performed for the complete generated set of data, resulting in a 1001-sized population of regression coefficients for each flux. Confidence intervals were computed as

$$\mathbf{B} \pm \hat{\sigma}\mathbf{(B)} \times T_{\mathbf{(0.975,dg)}}\,, \qquad (8)$$

with $\hat{\sigma}$ (**B**) the observed standard deviations of coefficients **B** and $T_{(0.975,dg)}$ the two-sided *T*-student distribution value for a 95% confidence level and number of degrees of freedom (dg) equal to 1001 (observations) minus 47 (fluxes). All calculations were implemented by the authors in MATLAB (Version 7.0; Mathworks, USA).

### 3.2. Sensitivity analysis

For the two scenarios where the measurement of product formation rate or cell growth rate are individually omitted from the complete model, the Jacobian of the corresponding overdetermined system (2) was calculated as

$$\mathbf{J}_{\mathbf{V_e}(\mathbf{V_m})} = -\mathbf{A}_{\mathbf{e}}^{\#} \times \mathbf{A}_{\mathbf{m}} = \left\langle \frac{\partial v_{e,i}}{\partial v_{m,j}} \right\rangle_{i,j}\,, \qquad (3)$$

representing the absolute sensitivity of each unknown flux to each metabolic constraint. This is the same equation used in Chapter III and described in Daae and Ison (1999). In order to compute fractional sensitivities for biomass and product synthesis rates, the corresponding (i,j) elements were appropriately factored with an average value of each measured metabolite consumption/production rate and the average value of measured cell growth rate or productivity, respectively, for all metabolic conditions.

### 3.3. Hierarchical clustering

Groups of fluxes sharing similar strengths of association with productivity were hierarchically clustered on the two-dimensional space defined by the pair correlation coefficient/confidence interval. The Euclidian norm was chosen as distance measure. To evaluate if the classification presented in the dendrogram correlates well with the distance measurements between pairs of data objects, the cophenetic correlation coefficient (*c*) was calculated (Sokal and Rohlf, 1962). Values of *c* close to 1 indicate a good representation of the data. Additionally, for each link in the cluster tree, an inconsistency coefficient (*I*) was calculated, which compares the height of each link with that of neighbour links at the same level (Cordes et al., 2002). The higher the value of *I* is, the less similar the objects are. Thus, when plotting the number of emerging tree clusters against decreasing *I* values, a steep discontinuity, along with the appearance of clusters with unacceptable small size, suggest a natural division in the dataset. All calculations were performed using predefined functions available in MATLAB (Statistics Toolbox, Multivariate Statistics section).

## 4. RESULTS

### 4.1. Limitations of classical metabolic flux analysis

Supposing the composition of a recombinant product of interest is known (e.g. protein amino acids sequence or detailed virus structure), a lumped reaction system comprising all metabolic precursors in stoichiometric quantities to synthesize a unit amount of product can be formulated. If the number of measured flux constraints is high enough to yield a determined or overdetermined system, then an estimation of the rate of product

synthesis can be obtained (see Chapter II for a description of MFA). However, this estimation will generally be inaccurate, often lying outside feasible biological boundaries, even for a consistent, overdetermined system with carbon and nitrogen balances closed within experimental error. The problem of the ill-definition of protein/virus formation in a metabolic network is mathematically expressed by its extremely large sensitivity to the measured uptake and production metabolic fluxes. As a corollary, it is only possible to accurately estimate such a rate if all measurements are precisely known, devoid of experimental error. To illustrate this, a comprehensive metabolic model of *Spodoptera frugiperda* cells (*Sf*9) comprising a well-defined central carbon and nitrogen metabolism (Appendix 1; Chapter II and III) was combined with a set of biosynthesis reactions for recombinant baculovirus synthesis (Appendix 3; Bergold and Wellington, 1954; Wellington, 1954). The final system of equations is overdetermined with the same 4 redundant measurements as before. Then, the relative sensitivity of the rate of product formation in this metabolic network was compared to that of the cell growth rate (see Materials and Methods). As presented in Figure 4.1, the existence of measurement errors is significantly dampened when estimating the rate of biomass formation ($\mu$), having sensitivity values lower than 1 (calculated as the fractional variation in $\mu$ produced by an infinitesimal fractional variation in a given measured flux). However, they are amplified when estimating the flux of baculovirus formation (*vBV*), often by several orders of magnitude.

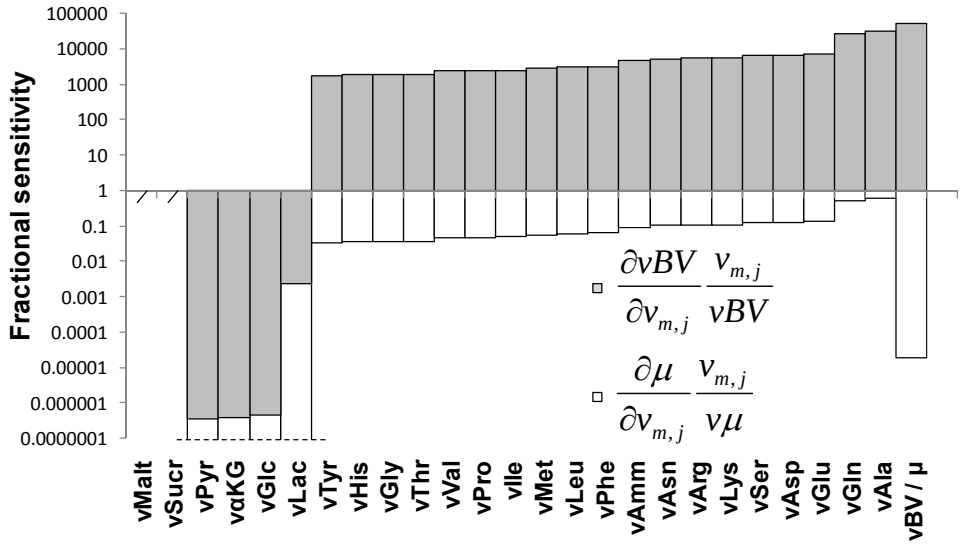


**Figure 4.1.** Sensitivity analysis of virus production and biomass production fluxes. Sensitivity analysis of biomass or product synthesis estimations was performed when the measured value of each of these fluxes was individually omitted from the complete model, yielding an overdetermined system of equations (see text and Materials and Methods section). The estimation of fractional sensitivities was achieved by factoring the appropriate average value of measured metabolite consumption/production rates and average value of measured cell growth rate or productivity, respectively, from all available culture conditions (see Table 4.2). Horizontal axis marks indicate computed sensitivities are zero.

If a representative scenario is chosen, the impact of individually omitting the measurements of *μ* or *rBV*, or of deleting the complete set of biomass or product synthesis reactions, can be assessed in terms of overall fluxome variation in relation to that estimated by the complete model (Table 4.1). As shown, leaving out *μ* has a small effect in the fluxome estimation; moreover, the respective estimated *μ* corresponds roughly to the measurement in the complete model, indicating that the assumed stoichiometry is consistent with experimental data. On the other hand, leaving out *vBV* has a more profound effect in the intracellular flux distribution, evidenced by the considerably higher total fluxome variation.

As expected, the estimated viral replication rate is completely unrealistic, even though the model remained consistent, evidencing that viral replication cannot be directly inferred from the nutrients uptake and metabolites production rates affected by experimental error. This is a result of the negligible requirement of anabolic precursors for viral synthesis as compared to biomass formation. Therefore, it is essentially impossible to accurately estimate how much complex product is being synthesized, per cell and unit time, for a given metabolic state. Finally, taking out reactions associated with virus biosynthesis has a virtually null effect on the remaining fluxes, which contrasts with the massive fluxome variation obtained after deleting reactions for biomass formation. It is important to note that model consistency is independent of incorporating the stoichiometry of virus formation. This clearly shows that the mechanisms of complex product synthesis are ill-defined in a purely stoichiometric description.

**Table 4.1.** Impact of biomass and virus synthesis information on the estimation of *Sf*9 cells post-infection metabolism.

| | **Complete model** | **W/o *μ*** | **W/o *vBV*** | **W/o biomass reactions** | **W/o viral reactions** |
|---|---|---|---|---|---|
| **Fluxome var.** [a] | - | 12.2 | 32.5 | 370.2 | 0.0 |
| ***μ*** [b] | 8.6 | 8.9 | 8.0 | - | 8.6 |
| ***vBV*** [c] | 920.5 | 920.5 | 3995861.2 | 920.6 | - |
| **Redundancies** [d] | 4 | 3 | 3 | 4 | 4 |
| ***h* / $\chi^2$** [e] | 0.3 / 7.8 | 0.0 / 7.8 | 0.0 / 7.8 | 102.0 / 9.5 | 0.3 / 9.5 |

[a]Fluxome variation (%), calculated as the average relative variation of all intracellular fluxes estimated by the model, excluding biosynthetic reactions for biomass or virus formation; [b]Adjusted (underlined) or estimated specific biomass formation rate (/h × 1000); [c]Adjusted (underlined) or estimated specific viral synthesis rate ($10^3$ infectious particles (IP)/$10^6$ cells/h); [d]The number of redundancies in an overdetermined model corresponds to flux measurements in excess of the degrees of freedom of the system (see Materials and Methods); [e]A consistency index (*h*) that is lower than the corresponding $\chi^2$ (95%) value indicates consistency between flux measurements and the assumed network stoichiometry in each case (see Materials and Methods).

### 4.2. Hybrid metabolic flux analysis

In the absence of sufficient mechanistic detail, the unknown or ill-defined part of a metabolic network can be substituted by an empirical (statistical) sub-model bridging the well-defined stoichiometry with a given cellular function, such as the synthesis of a complex recombinant product (Figure 4.2A). The herein proposed hybrid MFA takes advantage of using PLS to find a regression model between input fluxes, $\mathbf{V_e}$ (estimated through classical MFA), and a vector of target productivity, $\mathbf{V_t}$, which is not directly linked with the known part of the network (Figure 4.2B). The result is a vector of regression coefficients (**B**) representing how strongly each flux correlates with the target. This statistical association can be used to derive hypothesis on how to perturb the metabolic network towards increased productivity (refer to Materials and Methods for a detailed mathematical description).

To assess the performance of this methodology, original and previously obtained (Chapter III) MFA data were pooled together, comprising a diverse set of 13 independent infection cultures (Table 4.2). Included are infections performed with a recombinant baculovirus, at different cell densities, in different culture systems and subject to various supplementation and treatment schemes. In all experiments, the *Sf*9 insect cell line was infected at a low multiplicity of infection (number of infectious particles added per cell) in serum-free medium. Fluxes estimated by MFA were used as predictor data for the PLS model. In all cases, the pseudo-steady state hypothesis on intracellular metabolites was assumed, since extracellular metabolite profiles were approximately linear during the initial 48h to 72h productive phase after infection. Data from the end of infection cultures were not taken into account to avoid confounding effects due to cell lysis. As target, specific baculovirus productivities were measured as described in Chapter III, covering on the whole 3 orders of magnitude.

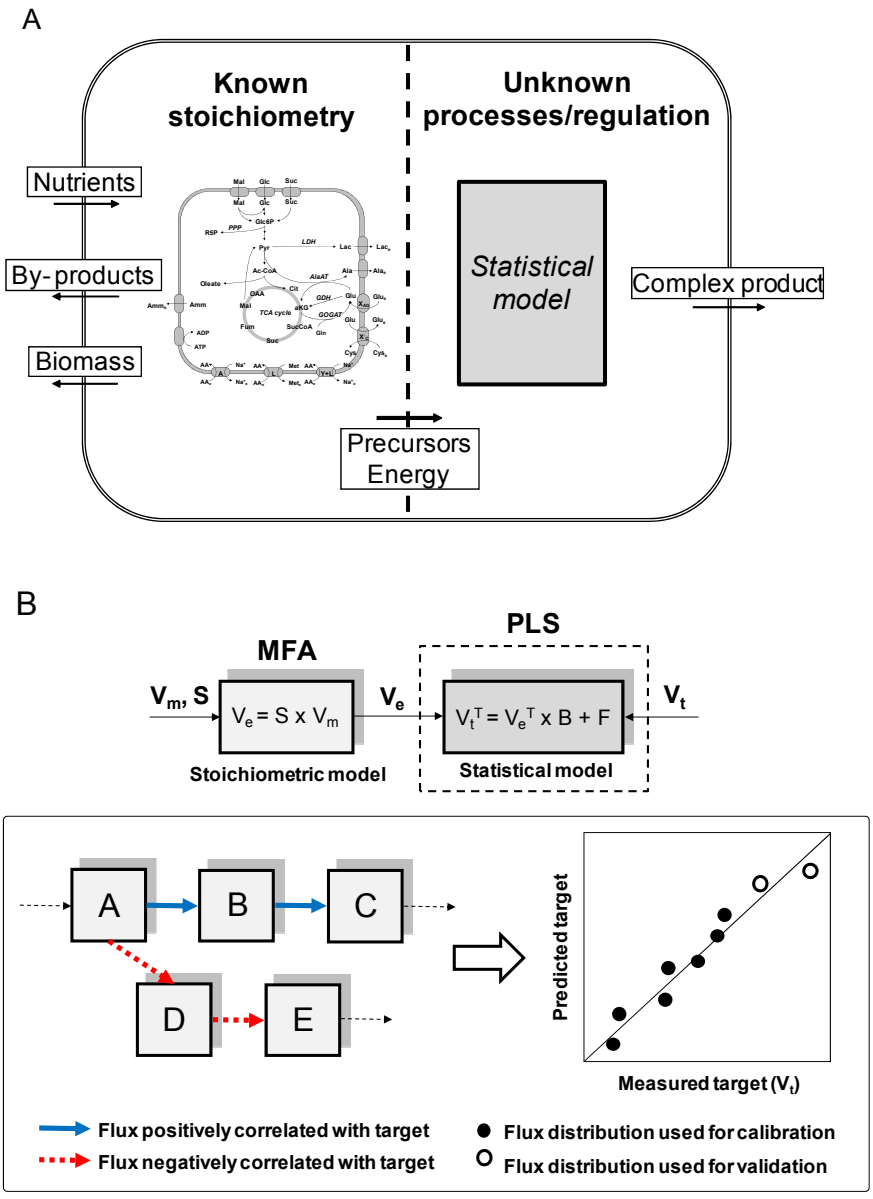


**Figure 4.2.** Data-driven framework for predictive metabolic flux analysis. (A) Schematic representation of a metabolic network with an unknown or ill-defined portion corresponding to the synthesis of a complex recombinant product. These poorly defined pathways are substituted by a statistical sub-model bridging the known well-defined stoichiometry with the target product formation rate. (B) Given a set of measured fluxes ($\mathbf{V_m}$ - usually exchange fluxes of metabolic consumption

and production), metabolic flux analysis is used to estimate the entire flux distribution ($\mathbf{V_e}$) in a predefined metabolic network. Then, PLS is performed to find a linear regression model between the estimated fluxome and the vector of a measured target such as productivity, $\mathbf{V_t}$. As a result, a list of regression coefficients representing how strongly each flux correlates with the target is obtained (**B**), making it possible to predict the productivity of independent cultures after metabolic manipulation.

**Table 4.2.** Experimental cultures used for model establishment.

| # | Virus | CCI[a] | Culture system | Supplementation/ Treatment[b] | Productivity[c] | References |
|---|---|---|---|---|---|---|
| 1 | *Ac-vp39egfp* | 1 | Spinner vessel | - | 1420.7 | Chapter III |
| 2 | | 3 | | - | 117.0 | |
| 3 | | | | Gln | 174.3 | |
| 4 | | | | Amino acids mix | 177.1 | |
| 5 | | | | IMS | 227.3 | |
| 6 | | | | Pyr | 644.2 | |
| 7 | | | | αKG | 920.5 | |
| 8 | | | | Pyr/αKG | 462.4 | |
| 9 | | | | Pyr (24 mM) | 455.2 | |
| 10 | *Ac-vp39egfp* | 3 | Shake flask | - | 23.2 | This work |
| 11 | | | | - | 29.1 | |
| 12 | | | | PBS (50%) | 0.9 | |
| 13 | | | | AICAR | 3.1 | |

In every case, cells were grown to the appropriate cell density in SF900II serum-free medium and infected with 0.1 infectious particles per cell; [a]Cell concentration at infection ($10^6$ cells/mL); "1" and "3" stand for 1-1.5 and 3-4×$10^6$ cells/mL, respectively; [b]Nutrient supplementation and culture treatment were performed as described in Materials and Methods (see indicated references for details). IMS – complete insect medium supplement; [c]Measured specific viral synthesis rate ($10^3$ IP/$10^6$ cells/h).

Our PLS model was able to capture most of the variance in the target productivity, despite using only 3 latent variables to describe the input data (Figure 4.3A). Because in latent variable models, such as PLS, there is no direct relationship between predictor and target variables, the calculation of

reliable confidence intervals for the regression coefficients is not straightforward, limiting their interpretability. Namely, regression coefficients in PLS models have been found to reflect primarily the underlying latent structure of the data, rather than accounting for the error variances of the predictor variables (Burnham et al., 2001). To circumvent this problem, Monte Carlo sampling was used to generate 1000 data matrices based on the error variances of all 47 metabolic fluxes and specific baculovirus productivity. PLS models were then built on the generated data, allowing the estimation of confidence intervals associated with each regression coefficient. The procedure revealed that 31 out of 47 regression coefficients were not statistically meaningful, having strengths of association ($\alpha$ – here defined as the ratio between the regression coefficient and the respective confidence interval) lower than 1 (Figure 4.3B). It should be underlined that the flux discrimination criterion includes both observed correlations with the target and precision of measurement/estimation.

In view of these results, engineering strategies aiming to increase carbon flow through central oxidative pathways, possibly by rearranging flux partitioning at key metabolic nodes or feeding energy-generating metabolites, could potentially be beneficial for virus replication. To this respect, it is possible to find in Table 4.2 a group of cultures that, based on previous empirical inspection, were purposefully designed to increase productivity by the addition of energy-generating metabolites (experiments 6, 7, 8, 9) (Chapter III). Metabolic node rearrangement was not an issue since *Sf*9 cells naturally possess a highly efficient oxidative metabolism (Chapter II and III). Additionally, in face of preliminary simulations, we thought of some treatment to simulate a depressed energetic state and negatively impact productivity, namely through the addition of AICAR (experiment 13), a cell permeable AMP mimetic that strongly binds AMPK, inducing downstream effects typical of ATP starvation such as inhibition of

protein synthesis (Menze et al., 2005). This experiment, together with the substitution of half the culture medium by PBS (experiment 12), comprised the lower segment in the baculovirus productivity range.

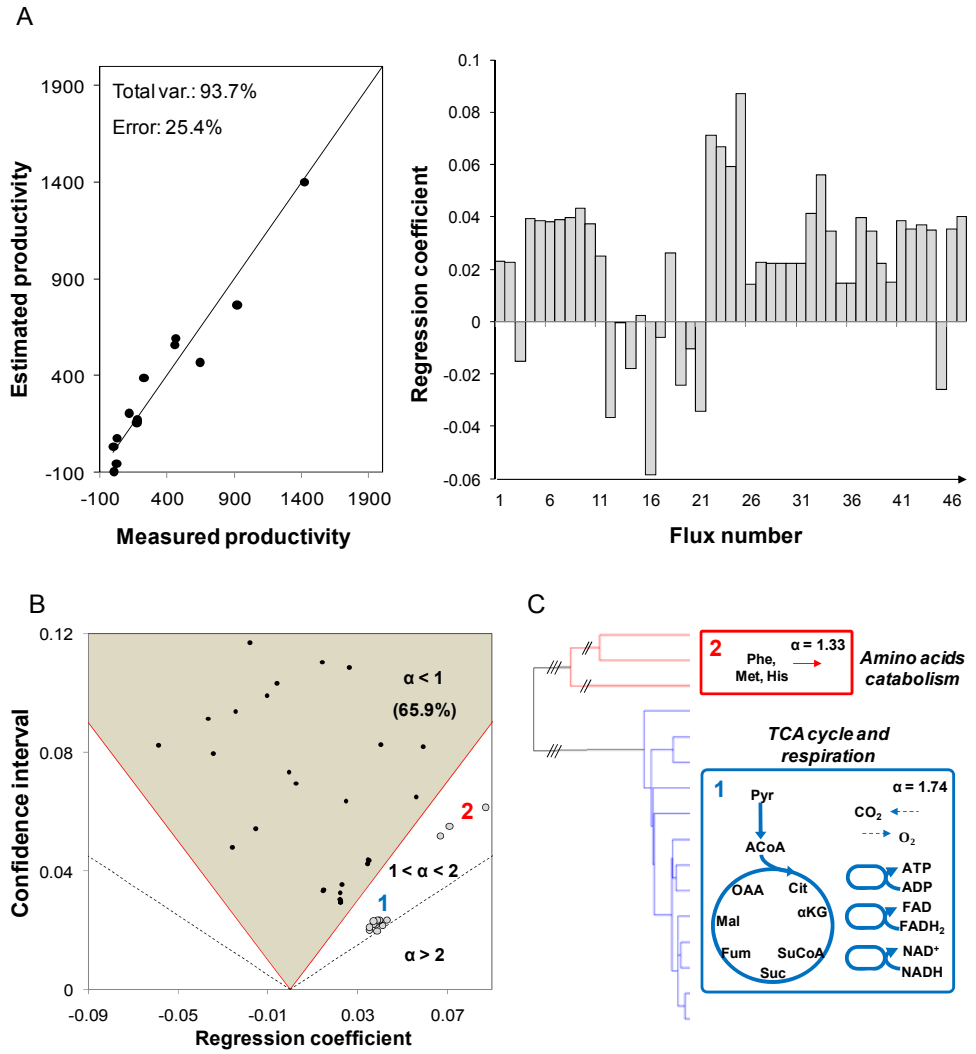


**Figure 4.3.** Functional metabolic decomposition of baculovirus-producing *Sf*9 cells. (A) Performance of hybrid MFA in describing baculovirus productivity based on metabolic data from 13 independent cultures (see Table 4.2). In all cases, *Sf*9 insect cells were infected with a low multiplicity of infection in serum-free medium. A total of 3 latent variables were used to describe the data. Productivity is expressed in $10^3$ IP/$10^6$ cells/h. (B) In order to estimate confidence intervals for the

model regression coefficients, Monte Carlo sampling was used to generate 1000 data matrices based on the error variances of all predictor and target variables (see Materials and Methods section for details). The strength of association ($\alpha$) was defined as the regression coefficient to confidence interval ratio, allowing the exclusion of those fluxes with $\alpha$ values lower than 1. (C) After hierarchical clustering, the TCA cycle and mitochondrial respiration naturally arised as a closely connected group of fluxes strongly correlated with high productivities. With lighter association strengths, one additional cluster corresponds to the catabolization fluxes of the essential amino acids phenylalanine, methionine and histidine. Excluded fluxes ($\alpha$<1) include: glycolysis, pentose-phosphate pathway, by-product formation, pyruvate recycling, amino acids metabolism, biomass synthesis and transhydrogenation.

### 4.3. Predictive power

To validate an empirical model it is mandatory to test its predictive power with new independent experiments not used in the calibration step. We selected the above mentioned subset of experiments (6, 7, 8, 9 and 13) to be used for validation. In a second validation strategy, the three experiments with the highest productivities (1, 6 and 7) were left aside as a means to prevent data interpolation. In both strategies, the number of latent variables was chosen based on maximum total variance explained (calibration and validation) and constrained by a limit of 3. As presented in Figure 4.4A, the productivities of experiments 6, 7, 8, 9 and 13 were reasonably predicted, considering the challenging partition of the data (validation 1), while the results for validation 2 were considerably sounder. More importantly, the hybrid MFA-PLS structure clearly outperformed classical MFA in modeling baculovirus production, as demonstrated by comparing the predicted productivities obtained in both validation data sets with the corresponding values predicted by MFA (Table 4.3).

In terms of metabolic decomposition, these models corroborate our previous conclusions. Indeed, the most important pathways for viral replication previously discriminated, namely TCA cycle and respiration, showed a significant correlation with productivity for both validation strategies (Figure 4.4B). Also for validation strategy 1, the catabolism of phenylalanine, methionine and histidine had again $\alpha$ values higher than 1, though other fluxes with lighter correlations were also selected. Overall, despite the somewhat limited collection of data, these results indicate the hybrid MFA framework should prove a valuable tool in designing metabolic optimization strategies for complex products, with potential applicability to a range of cellular systems.

## 5. DISCUSSION

In this chapter, a cost-effective hybrid methodology is reported to make sense of accessible fluxome data for rapid optimization of complex productivity phenotypes. PLS modelling is used in tandem with classical metabolic flux analysis to establish a link between an estimated metabolic state and system productivity, therefore providing a predictive *in silico* platform to assist genetic/environmental metabolic engineering when a well-defined stoichiometric description of product formation is not available. An important feature of PLS is that it decomposes complex data sets into subsets of uncorrelated vectors, called latent variables, while eliminating redundant information. This permits to address biological problems where the number of variables assessed largely exceeds the number of observations, reason why this method has gathered significance in interpreting “omic” data sets (Boulesteix and Strimmer, 2006). As reviewed in Teixeira et al. (2007), combining such data-mining tools with mechanistic models gives rise to hybrid parametric-nonparametric systems, which

enable cost-effective analysis of complex problems with fragmentary knowledge.

Our method is conceived to perform on the basis of an informative, yet not exhaustive, preliminary set of experiments easily available at laboratory scale. It is especially suited to deal with complex products whose synthesis mechanisms are ill-defined by considering a simple stoichiometric description as part of a global metabolic model, or whose composition is unknown. Productivity enhancement in the case of simpler molecules, for instance amino acids or TCA cycle intermediaries, has been previously achieved by stoichiometric analysis of their respective synthesis pathways (Lee et al., 2007; Zelle et al., 2008). Here, the main output is the global identification of fluxes strongly correlated with a highly productive state, which are discriminated from a background of less significant metabolic reactions contributing to product synthesis. Thus, as opposed to classical MFA, our approach enables predicting the productivity in independent experiments based on a previous calibration, and the identification of metabolic targets for production optimization. This was demonstrated here by replicating the results obtained in Chapter III following a hypothesis-driven metabolic engineering strategy. In this respect, the estimation of reliable confidence intervals for the flux regression coefficients is crucial to remove a large portion of uncertainty in the systematic selection of metabolic targets, considerably improving the odds of successful experimental validation. Methods that assure a higher precision in fluxome estimations, such as isotopic tracer experiments (Sauer, 2006), could in principle expose other targets for manipulation.

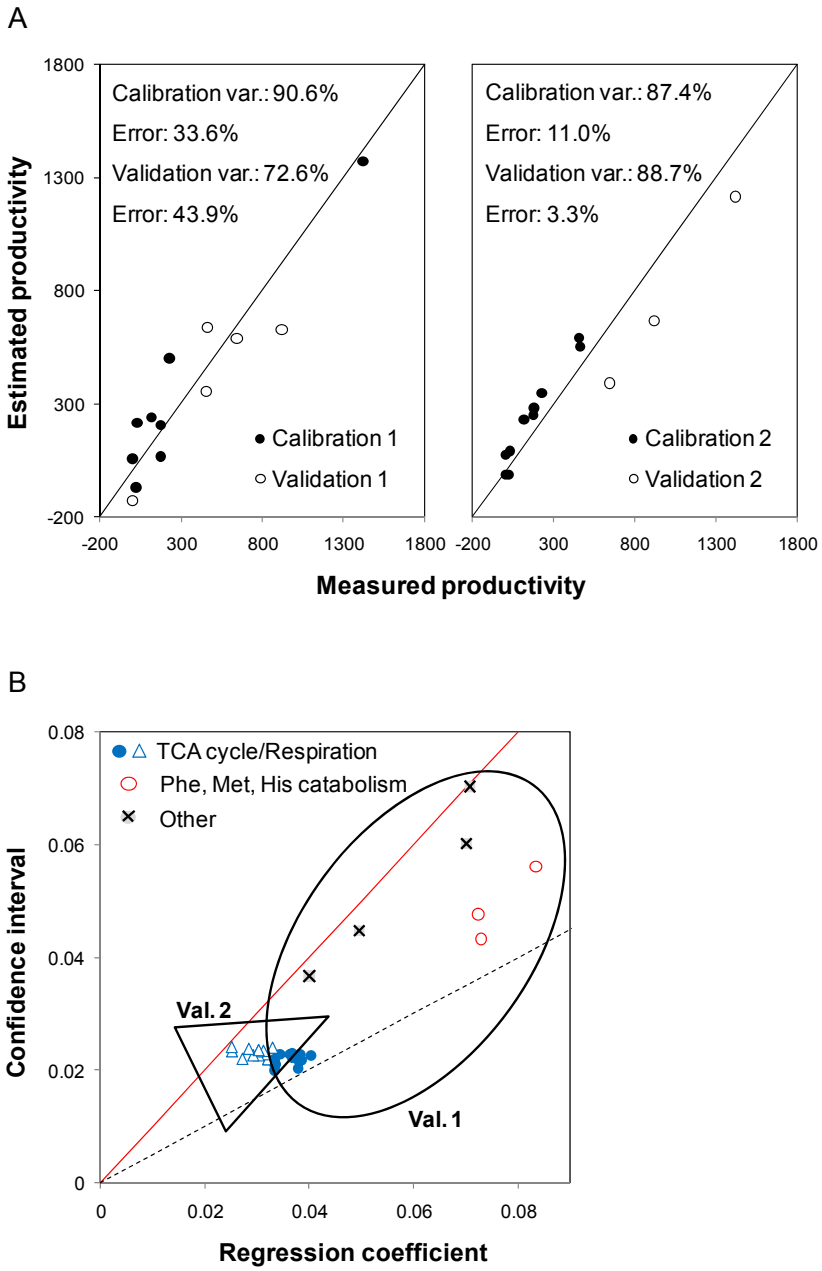


**Figure 4.4.** Validation of predictive MFA for metabolic engineering. (A) To validate our framework as a powerful tool to assign targets for metabolic engineering, the complete set of 13 experiments was purposefully split into calibration and validation subsets in two manners. In strategy 1, experiments 6, 7, 8, 9 and 13, which have

been rationally designed to manipulate the cellular energetic state, were left aside for validation. In strategy 2, the top three producers (experiments 1, 6 and 7) were chosen as validation cultures to avoid data interpolation. The number of latent variables used to build the calibration models in each case was 1 and 3, respectively. Productivity is expressed in $10^3$ IP/$10^6$ cells/h. (B) Metabolic decomposition for each validation strategy, showing the common selection of TCA cycle/respiration as important pathways for viral replication. Also for validation strategy 1, the catabolism of phenylalanine, methionine and histidine had $\alpha$ values higher than 1, as well as other fluxes with lighter correlations with the target (other: catabolism of maltose, proline and tyrosine, formation of alanine).

**Table 4.3.** Predictive power of the hybrid MFA-PLS structure compared to MFA.

| Experiment # | Productivity[a] | MFA prediction | Hybrid MFA prediction |
|---|---|---|---|
| **1** | 1420.7 | 28915535.7 | 1214.6[c] |
| **6** | 644.2 | -15477747.1 | 389.9[c] / 586.4[b] |
| **7** | 920.5 | 3995861.2 | 665.7[c] / 625.6[b] |
| **8** | 462.4 | 18837398.3 | 637.7[b] |
| **9** | 455.2 | 9971383.5 | 353.5[b] |
| **13** | 3.1 | -7199746.4 | -130.8[b] |

[a]Measured specific viral synthesis rate ($10^3$ IP/$10^6$ cells/h); [b]Validation strategy 1; [c]Validation strategy 2.

It should be noted that the predictive capacity for the phenotypic change does not necessarily translate in the ability to predict the means to deliver this change. Specifically, finding a strong statistical correlation between a given metabolic route and productivity does not translate into a direct cause-effect relationship. While this may often be the case for the synthesis of single molecules, production of correctly formed proteins or viruses depends on a complex series of steps ranging from gene transcription to protein secretion or virus assembly, along with their regulation through even less understood signalling events (O'Callaghan and James, 2008). Therefore, the identification of genetic targets may at times be beyond the domain of central metabolic fluxes, which themselves are upstream

regulated along with the productivity phenotype. On this issue, the methodology herein presented could at least allow to hypothesize how different cell pathways/functions are commonly regulated.

Besides providing a list of prospective metabolic targets to be exploited for engineering, the proposed framework adds a functional dimension to previous metabolic decomposition studies based solely on structural properties of the underlying network, namely connectivity (Ma et al., 2004; Guimerà and Amaral, 2005) or pathway feasibility (Schuster et al., 2000; Papin et al., 2004). Here, clusters of fluxes are defined by sharing the same relationship with a given cellular output. As a main drawback, our method is constrained by data availability on cellular fluxome and target phenotype, thus demanding some experimental effort.

As mentioned earlier, when used to handle flux distributions estimated by FBA in genome-scale models, this approach represents an alternative hybrid framework to linear optimization techniques during metabolic target selection, which could significantly surpass existing limitations in modeling complex phenotypes. A recent paper by Melzer et al. (2009) also explores the use of multivariate statistics to correlate stoichiometrically-derived elementary modes in complex networks with stoichiometrically-defined productivity targets, as opposed to common search algorithms for strain improvement. However, our approach differs conceptually to the cited work in that we define a statistical bridge between a well-defined stoichiometry and a complex phenotype, therefore substituting for a metabolic link that may be ill-defined in a purely stoichiometric representation and otherwise hampered by insufficient kinetic and regulatory information. This should prove an advantage in predicting non-obvious metabolic targets associated with the synthesis of more complex recombinant products in animal cells, particularly multimeric proteins, multi-protein particles and viruses, the later

adding an additional degree of complexity due to the virus-coded regulation of cellular machinery.

Finally, from a practical point of view, several issues are worth considering before opting for a genome-scale model. In one respect, the availability of a well sequenced and annotated genome may constitute a major limitation: while accurate metabolic reconstructions are available for un-mutated, standard microorganisms such as *E. coli* and *S. cerevisiae*, in an industrial setting a larger diversity of organisms are used, particularly animal cell systems for which cellular data is much scarcer (Blazeck and Alper, 2010). Another consideration is the cost and time associated with the creation of these models. Even if a comprehensive genome-scale stoichiometric model is already at disposal, a considerable experimental effort is necessary to overlay high-throughput metabolomic and isotopomer flux data for better constraining fluxome estimations (Lee et al., 2006). In particular, the computational power required for $^{13}C$ flux analysis may become prohibitive for very complex networks by today's standards. Overall, our framework could potentially be more useful to steer rapid development of a broad range of organisms on the basis of a representative small-scale metabolic network. As such, it would significantly enhance the quality of information extracted from exploratory experiments compared to traditional metabolic flux analysis.

## ACKNOWLEDGEMENTS

This work was partially supported by the European Project BACULOGENES (FP6 LHSB-CT-2006-037541). Nuno Carinhas acknowledges Fundação para a Ciência e a Tecnologia (FCT) for his Ph.D. grant (SFRH/BD/36676/2007).

# References


Andersson CA, Bro R (2000) The N-way Toolbox for MATLAB. *Chemom Intell Lab Syst* **52**: 1-4

Asadollahi MA, Maury J, Patil KR, Schalk M, Clark A, Nielsen J (2009) Enhancing sesquiterpene production in *Saccharomyces cerevisiae* through *in silico* driven metabolic engineering. *Metab Eng* **11**: 328-334

Bergold GH, Wellington EF (1954) Isolation and chemical composition of the membranes of an insect virus and their relation to the virus and polyhedral bodies. *J Bacteriol* **67**: 210-216

Blazeck J, Alper H (2010) Systems metabolic engineering: genome-scale models and beyond. *Biotechnol J* 5: 647-659

Boghigian BA, Seth G, Kiss R, Pfeifer BA (2010) Metabolic flux analysis and pharmaceutical production. *Metab Eng* **12**: 81-95

Boulesteix A-L, Strimmer K (2006) Partial least squares: a versatile tool for the analysis of high-dimensional genomic data. *Brief Bioinform* **8**: 32-44

Burgard AP, Pharkya P, Maranas CD (2003) OptKnock: a bilevel programming framework for identifying gene knockout strategies for microbial strain optimization. *Biotechnol Bioeng* **84**: 647-657

Burnham AJ, MacGregor JF, Viveros R (2001) Interpretation of regression coefficients under a latent variable regression model. *J Chemometr* **15**: 265-284

Cordes D, Haughton V, Carew JD, Arfanakis K, Maravilla K (2002) Hierarchical clustering to measure connectivity in fMRI resting-state data. *Magn Reson Imaging* **20**: 305-317

Covert MW, Xiao N, Chen TJ, Karr JR (2008) Integrated metabolic, transcriptional regulatory and signal transduction models in Escherichia coli. *Bioinformatics* **24**: 2044-2050

Daae, E.B. and Ison, A.P., 1999. Classification and sensitivity analysis of a proposed primary metabolic reaction network for Streptomyces lividans. Metab Eng 1, 153-65

Fong SS, Burgard AP, Herring CD, Knight EM, Blattner FR, Maranas CD, Palsson BO (2005) In silico design and adaptive evolution of *Escherichia coli* for production of lactic acid. *Biotechnol Bioeng* **91**: 643-648

Gombert AK, Nielsen J (2000) Mathematical modelling of metabolism. *Curr Opin Biotechnol* **11**: 180-186

Guimerà R, Amaral LAN (2005) Functional cartography of complex metabolic networks. *Nature* **433**: 895-900

Herrgard MJ, Covert MW, Palsson BO (2004) Reconstruction of microbial transcriptional regulatory networks. *Curr Opin Biotechnol* **15**: 70-77

Jong S (1993) SIMPLS: An Alternative Approach to Partial Least Squares Regression. *Chemometr Intell Lab* **18**: 251–263

Kauffman KJ, Prakash P, Edwards JS (2003) Advances in flux balance analysis. *Curr Opin Biotechnol* **14**: 491-496

Kim J, Reed JL (2010) OptORF: optimal metabolic and regulatory perturbations for metabolic engineering of microbial strains. *BMC Syst Biol* **4**: 53

Lee JM, Gianchandani EP, Eddy JA, Papin JA (2008) Dynamic analysis of integrated signalling, metabolic, and regulatory networks. *Plos Comput Biol* **4**: e1000086

Lee JM, Gianchandani EP, Papin JA (2006) Flux balance analysis in the era of metabolomics. *Brief Bioinform* **7**: 140-150

Lee KH, Park JH, Kim TY, Kim HU, Lee SY (2007) Systems metabolic engineering of *Escherichia coli* for L-threonine production. *Mol Syst Biol* **3**: 149

Lee SY, Lee D-Y, Kim TY (2005) Systems biotechnology for strain improvement. *Trends Biotechnol* **23**: 349-358

Ma H-U, Zhao X-M, Yuan Y-J, Zeng A-P (2004) Decomposition of metabolic network into functional modules based on the global connectivity structure of reaction graph. *Bioinformatics* **20**: 1870-1876

Melzer G, Esfandabadi ME, Franco-Lara E, Wittmann C (2009) Flux Design: In silico design of cell factories based on correlation of pathway fluxes to desired properties. *BMC Syst Biol* **3**: 120

Menze MA, Clavenna MJ, Hand SC (2005) Depression of cell metabolism and proliferation by membrane-permeable and –impermeable modulators: role for AMP-to-ATP ratio. *Am J Physiol Regul Integr Comp Physiol* **288**: 501-510

O'Callaghan PM, James DC (2008) Systems biotechnology of mammalian cell factories. *Brief Funct Genomic Proteomic* **7**: 95-110

Oberhardt MA, Palsson BO, Papin JA (2009) Application of genome-scale metabolic reconstructions. *Mol Syst Biol* **5**: 320

Otero JM, Nielsen J (2010) Industrial Systems Biology. *Biotechnol Bioeng* **105**: 439-460

Papin JA, Stelling J, Price ND, Klamt S, Schuster S, Palsson BO (2004) Comparison of network-based pathway analysis methods. *Trends Biotechnol* **22**: 400-405

Patil KR, Rocha I, Förster J, Nielsen J (2005) Evolutionary programming as a platform for *in silico* metabolic engineering. *BMC Bioinformatics* **6**: 308

Pharkya P, Burgard AP, Maranas CD (2004) OptStrain: a computational framework for redesign of microbial production systems. *Genome Res* **14**: 2367-2376

Pharkya P, Maranas CD (2006) An optimization framework for identifying reaction activation/inhibition or elimination candidates for overproduction in microbial systems. *Metab Eng* **8**: 1-13

Quek L-E, Dietmair S, Krömer JO, Nielsen LK (2010) Metabolic flux analysis of mammalian cell culture. *Metab Eng* **12**: 161-171

Roldão A, Oliveira R, Carrondo MJT, Alves PM (2009) Error assessment in recombinant baculovirus titration: evaluation of different methods. *J Virol Methods* **159**: 69-80

Sauer U (2004) High-throughput phenomics: experimental methods for mapping fluxomes. *Curr Opin Biotechnol* **15**: 58-63

Sauer U (2006) Metabolic networks in motion: $^{13}$C-based flux analysis. *Mol Syst Biol* **2**: 62

Schuster S, Fell DA, Dandekar T (2000) A general definition of metabolic pathways useful for systematic organization and analysis of complex metabolic networks. *Nature Biotechnol* **18**: 326-332

Sheikh K, Förster J, Nielsen LK (2005) Modeling hybridoma cell metabolism using a generic genome-scale metabolic model of *Mus musculus*. *Biotechnol Prog* **21**: 112-121

Sidorenko Y, Reichl U (2004) Structured model of influenza virus replication in MDCK cells. *Biotechnol Bioeng* **88**: 1-14

Sokal RR, Rohlf FJ (1962) The comparison of dendrograms by objective methods. *Taxon* **11**: 33-40

Sullivan JE, Brocklehurst KJ, Marley AE, Carey F, Carling D, Beri RK (1994) Inhibition of lipolysis and lipogenesis in isolated rat adypocytes with AICAR, a cell-permeable activator of AMP-activated protein kinase. *FEBS Lett* **353**: 33-36

Teixeira AP, Carinhas N, Dias JML, Cruz P, Alves PM, Carrondo MJT, Oliveira R (2007) Hybrid semi-parametric mathematical systems: bridging the gap between systems biology and process engineering. *J Biotechnol* **132**: 418-425

Wellington EF (1954) The amino acid composition of some insect viruses and their characteristic inclusion-body proteins. *Biochem J* **57**: 334-338

Wold S, Sjöström M, Eriksson L (2001) PLS-regression: a basic tool of chemometrics. *Chemometr Intell Lab* **58**: 109-130

Xiao W, Yang Y, Weng Q, Lin T, Yuan M, Yang K, Pang Y (2009) The role of the PI3K-Akt signal transduction pathway in *Autographa californica* multiple nucleopolyhedrosisvirus infection of *Spodoptera frugiperda* cells. Virology **391**: 83-89

Zelle RM, de Hulster E, van Winden WA, de Waard P, Dijkema C, Winkler AA, Geertman JM, van Dijken JP, Pronk JT, van Maris AJ (2008) Malic acid production by *Saccharomyces cerevisiae*: engineering of pyruvate carboxylation, oxaloacetate reduction, and malate export. *Appl Environ Microbiol* **74**: 2766-2777

# CHAPTER V

## EXPLORING BACULOVIRUS-INSECT CELL INTERACTIONS THROUGH QUANTITATIVE PROTEOMICS

**ADAPTED FROM:**

Carinhas N, Robitaille AM, Moes S, Carrondo MJT, Jenoe J, Oliveira R, Alves PM. Quantitative proteomics of *Spodoptera frugiperda* cells during growth and baculovirus infection (in revision).

# TABLE OF CONTENTS

## 1. SUMMARY

Baculovirus infection *of Spodoptera frugiperda* cells is a system of choice to produce a range of recombinant proteins, vaccines and, potentially, gene therapy vectors. While baculovirus genomes are well characterized, the genome of *S. frugiperda* is not sequenced and the virus-host molecular interplay is sparsely known. Herein, we describe the application of stable isotope labeling by amino acids in cell culture (SILAC) to obtain the first comparative proteome quantitation of *S. frugiperda* cells during growth and early baculovirus infection. The proteome coverage was maximized by compiling a search database with protein annotations from insect species. Of interest were differentially proteins related to energy metabolism, endoplasmic reticulum and oxidative stress, yet not investigated in the scope of baculovirus infection. Further, the differential expression of viral-encoded proteins early in the infection cycle is suggested to be related with decreased viral replication in high cell density cultures. These findings have implications for virological research and improvement of baculovirus-based bioprocesses.

## 2. INTRODUCTION

The application of high-throughput omic techniques in cell culture studies can generate hypotheses on how to improve bioprocesses through the design of better cell factories. Among the omic technologies available, quantitative proteomics based on stable isotope labeling by amino acids in cell culture (SILAC) has become a preferred choice for large-scale expression profiling, combining quantitative accuracy with straightforward sample processing and control over culture conditions (Mann, 2006). Not surprisingly, a wealth of information has been gained by investigating how

several mammalian viruses manipulate their host's proteome, including adenovirus (Lam et al., 2010), influenza virus (Coombs et al., 2010) and hepatitis C virus (Mannová et al., 2006), among others.

In spite of the biotechnological interest of the baculovirus expression system, the genomes of insect cell lines susceptible to the prototype *Autographa californica* multicapsid nucleopolyhedrovirus (*Ac*MNPV) have not been sequenced to date. This constitutes a major disadvantage for the use of genome-wide technologies for better understanding this host-pathogen interplay. So far, global expression patterns of *Sf*9 cells at the mRNA level have been recorded at various time-points following infection (Nobiron et al., 2003; Salem et al., 2011). Also, a recent proteomic analysis based on 2D-gel electrophoresis (2DGE) identified 18 (out of 21) proteins differentially expressed 24 h after *Ac*MNPV infection in a different, permissive cell line (Popham et al., 2010). However, a large-scale quantitative proteomic analysis during baculovirus infection has not been tackled to date.

Knowledge on the *Ac*MNPV infection cycle has accumulated over many years of research. Briefly, replication and assembly take place in the nucleus, where viral particles travel by reorganizing the actin cytoskeleton upon cell entry (Ohkawa et al., 2010). The molecular life cycle is broadly divided in three consecutive phases according to gene expression programming. Early genes (0-6 hours post-infection (hpi)), requiring the transcriptional activity of the cell-encoded RNA polymerase II, mainly act as master transactivators essential for both subsequent viral gene expression and subversion of host cell activity by performing tasks common to other DNA viruses, including cell cycle arrest (Prikhod'ko and Miller, 1997; Ramachandran et al., 2001). Block of apoptosis by the viral protein P35 (Beidler et al., 1995) is also a required activity to establish productive

infections. The transition from early to late phase is marked by the onset of viral DNA replication (6-18 hpi) and the activity of a virus-encoded, α-amanitin resistant RNA polymerase (Grula et al., 1981). Concomitant with the onset of the very late phase (18 hpi-), a pronounced down-regulation of host transcriptional activity occurs (Ooi and Miller, 1988), followed by a shut off of most protein synthesis by 24 hpi (Carstens et al., 1979). This phenomenon reflects increased viral autonomy during the later phases of infection, confirmed by the observation that translation of the very-late genes *p10* and *polh* is relatively insensitive to the presence of 5'-cap-binding eukaryotic initiation factor eIF4E (Scheper et al., 1997; van Oers et al., 2001).

In the present work, we investigate proteome expression changes in *Sf*9 cells associated with culture growth and baculovirus infection. Since most of the host proteome is down-regulated at later times in the *Ac*MNPV life cycle, we focused on the transition from early to late phase (around 6 hpi) to investigate the establishment of infection. The lack of a complete genome sequence was overcome by cross-referencing to a database constructed from *S. frugiperda* and related insect species. For quantitation, cells were cultured in the presence of heavy arginine and lysine, commonly used SILAC reagents (Mann, 2006). The adoption of biotechnologically relevant culture conditions in rich medium led to sub-optimal SILAC labelling, from which protein expression ratios were corrected by factoring the experimentally measured isotope incorporation in each protein. A statistical procedure is further described to handle data variability, revealing several proteins regulated by growth and infection that are hereby discussed. Our results provide a data repository that can help the scientific community to accelerate virological research of baculovirus infection and optimization of *S. frugiperda*-based bioprocesses.

# 3. MATERIALS AND METHODS

## 3.1. Stable isotope labeling of *Sf*9 cells and experimental cultures

Maintenance of *Sf*9 cells in culture was done as in the previous chapters. For labeling, customized serum- and protein-free SF900II medium (Invitrogen, Life Technologies) without Arg and Lys was supplemented with ($^{13}$C)-Arg and ($^{13}$C$^{15}$N)-Lys at 1.35 mM each (Cambridge Isotope Laboratories). Cells were cultured in this medium for 5 passages growing as 20 mL flask suspension cultures and then up-scaled to 70 mL for an additional 1-2 passages. In parallel, cells were cultured in light medium containing ($^{12}$C)-Arg and ($^{12}$C$^{14}$N)-Lys at the same concentration. For infection experiments, cells were grown to the desired cell density and inoculated with a recombinant *Ac*MNPV (*Ac-hisgfp*, Chapter I) at a MOI of 5 infectious particles (IP)/cell. Information on virus handling and quantification are provided in Chapter I. About 100 million cells were harvested either before infection (in growth experiments) or at 6 h post-infection and seeded by centrifugation. Cell pellets were washed with ice-cold PBS, instantly frozen and stored at -85ºC until analysis.

## 3.2. Sample processing

Cells were lysed in basic RIPA buffer containing 25 mM Tris (pH 7.6), 150 mM NaCl, 1% NP-40, 1% Na deoxycholate, 1 mM EDTA, and supplemented with 1 mM PMSF and 1× complete protease inhibitor cocktail (Roche, Switzerland). Before further handling, the protein content was quantified for each extract (BCA Protein Assay Kit, Thermo Scientific, USA) and equal protein amounts of labeled and unlabeled material from each culture were pooled. Incorporation of iosotopically labeled amino acids was checked on pooled samples from light and heavy cultures as well as

unmixed samples. For this, proteins from the lysate were precipitated by adding 9 volumes of ice-cold 13.3% trichloroacetic acid/0.07% β-mercaptoethanol (β-ME) in acetone and incubated overnight at -20ºC. Protein content was collected by centrifugation, washed twice with 90% acetone/0.07% β-ME and dissolved in 50 mM Tris-HCL/8 M urea (pH 8). Samples were reduced with 10 mM dithiothreitol and alkylated with 50 mM iodoacetamide, followed by overnight dialysis against 50 mM Tris-HCL/6 M urea (pH 8). Before trypsin digestion, the dialysate was first digested with 20 µg of Lys-C at 30ºC for 2 h and then diluted with 5 volumes of 50mM Tris-HCl (pH 8). Trypsin digestion was carried out overnight at 37ºC using a 50:1 protein to enzyme ratio. The peptide mixtures were acidified and approximately 1 mg of the initial protein content was desalted in 0.1% trifluoroacetic acid (TFA) using MacroSpin Column, Silica C18, 30-300 µg capacity (The Nest Group, Inc., MA, USA). Peptides were biochemically stepwise eluted with 0.1% TFA containing 20%, 40%, and 60% acetonitrile. Before LC-MS/MS analysis, peptide fractions were dried in a speed vac and dissolved in 0.1% TFA.

### 3.3. LC-MS/MS analysis, database searching and isotope ratio quantification

LC-MS/MS analysis was performed on an LTQ-Orbitrap hybrid instrument (Thermo Scientific, San José, CA, USA). 2 µl of peptide digest were injected with an autosampler (CTC Analytics, Agilent Technologies) onto a C18 trapping column (ProteoCol C18 0.15 x 10 mm, SGE, Ringwood, AU) that was connected to a separation column (0.1 mm x 10 cm) packed with Magic 300Å C18 reverse-phase material (5 µm particle size, Michrom Bioresources, Inc., Auburn, CA, USA). A linear 80-min gradient from 2 to 50% solvent B (80% acetonitrile/0.1% acetic acid) in solvent A (2%

acetonitrile/0.1% acetic acid) was delivered with an Agilent 1200 nano pump (Agilent, Basel, Switzerland) at a flow rate of 300 nL/min. The eluting peptides were ionized at 1.7 kV. The LTQ-Orbitrap was operated in data-dependent mode. A survey scan between m/z 400-1600 was acquired in profile mode in the Orbitrap at 60,000 resolution and the 10 most abundant ions were then selected for fragmentation in the LTQ part of the instrument at normalized collision energy of 35%. Singly charged ions were omitted from fragmentation and previously selected ions were dynamically excluded for 25 sec. Scan-to-scan calibration was allowed by setting the lock mass to m/z 445.120025 (Olsen et al., 2005).

The LC-MS/MS data were searched with the SEQUEST search engine (version 3.3.1 SP1) (Eng et al., 1994) against an indexed insect database constructed as a subset of the non-redundant protein database maintained by NCBI (October 2010). The precursor ion and fragment ion mass tolerances were set to 10 ppm and 0.6 Da, respectively. Two missed cleavages were allowed. Dynamic modification was set for oxidized methionine, while cysteine carbamidomethylation was set as a fixed modification. The results were filtered for Xcorr values of 1.5 for single-, 2.0 for double-, 2.5 for triple-, and 3.0 for quadruple-charged peptides, respectively. Delta CN was set to 0.1, and the peptide and protein probabilities were set to 0.5 and 0.01, respectively.

For SILAC ratio quantification, the area of those precursor ions that had been identified by SEQUEST were integrated by the PepQuan option of Bioworks (Thermo Scientific, version 3.3.1 SP1). Precursor ion and fragment ion mass tolerances were set to 10 ppm and 0.6 Da, respectively. Searched files corresponding to different fractions of the same sample were merged together. Relative abundances were calculated as area ratios of heavy and light peptides, and the protein ratios were calculated as

averages of all quantified peptides. The mass shift tolerance of “Arg 6” and “Lys 8” was set to 0.02 Da.

### 3.4. Data analysis

The corrected unlabeled/labeled culture ratio for each protein was derived from Liao et al. (2008) as follows:

$$Rc = \frac{Ri - R}{(Ri + 1) \times R}, \text{ for all Ri > R,} \qquad (1)$$

where R represents the heavy/light isotope ratio from a 1:1 mixed sample and Ri the heavy/light isotope ratio from the corresponding unmixed labeled sample. The error propagation from R and Ri into Rc is based on the unbiased standard deviation from triplicate experiments and was calculated according to the equation:

$$S.D.(Rc) = \sqrt{\left(\frac{\partial Rc}{\partial R}\right)^2 \times S.D.^2(R) + \left(\frac{\partial Rc}{\partial Ri}\right)^2 \times S.D.^2(Ri)}\,. \qquad (2)$$

Sensitivity analysis of equation (1) was performed by calculating the relative gradient with respect to R and Ri:

$$rel.\nabla Rc = \sqrt{\left(\frac{\partial Rc}{\partial R}\right)^2 \times R^2 + \left(\frac{\partial Rc}{\partial Ri}\right)^2 \times Ri^2} \times \frac{1}{Rc}\,. \qquad (3)$$

The corrected SILAC ratio distributions were symmetrized around 0 through logarithmic transformation. Using the natural logarithm (*ln*) has the advantage of preserving data dispersion by only dividing each S.D. (Rc) by the respective Rc to yield S.D. (*ln* Rc). Maximum S.D. (*ln* Rc) cutoffs were

then applied to each data set resulting in more focused normal distributions. The two-tailed Student's *t*-test was performed assuming unequal variances and unequal sample sizes.

# 4. RESULTS

## 4.1. A draft *Sf*9 proteome

The major challenge for a large-scale assessment of the *Sf*9 proteome is the lack of an annotated genome sequence for protein identification. After experimental analysis of the cellular proteome, this missing knowledge was overcome by compiling a search database with available annotations from insect species, constructed as a subset of the non-redundant protein database maintained by the National Center for Biotechnology Information (NCBI). The proteome coverage was further maximized by enriching raw datasets with MS spectra recorded from different experimental conditions, biological replicates and biochemical fractionation of samples. When analyzing these MS spectra, a total of 648 high-confidence hits were identified as protein homologs from 31 species and 2 baculovirus genomes (Figure 5.1A). In this database, protein sequence redundancy is defined such that the same *Sf*9 or baculovirus protein may be identified multiple times in closely related insect organisms or viruses. Thus, to provide an estimation of interspecies redundancy, the Protein Information Resource SuperFamily (PIRSF) classification system was adopted to group proteins sharing homology (common ancestry) and homeomorphy (full-length sequence and domain architecture similarity) (Wu et al., 2004). 233 out of 418 proteins could be assigned to unique PIRSF designations, indicating a total of 56% different proteins (approximately 361 out of 648).

Among the organisms with the highest number of identifications are the only sequenced lepidopteran, the silkworm *Bombyx mori* (Mita et al., 2004), and the model insects *Drosophila melanogaster* and *Anopheles gambiae*. Genomic information on *S. frugiperda* derives primarily from constructed EST libraries of larval hemocyte, fat body and midgut tissues, as well as the *Sf*9 cell line (Landais et al., 2003; Nègre et al., 2006). As for viral genes, we identified 8 known early/late proteins from the related *Bm*NPV, which shares an average 90% homology with *Ac*MNPV (Acharya et al., 2002): P143 (helicase), DBP (DNA-binding protein), ME53, LEF3 (late expression factor 3), P35, HE65, 39K and GP64. In addition, 3 hits from the *Spodoptera litura* NPV correspond to the same P35 and the large (RR1) and small (RR2b) subunits of ribonucleotide reductase, a virally encoded enzyme involved in synthesizing deoxyribonucleotides (Pang et al., 2001). However, the latter two genes are known not to be present in the *Ac*MNPV genome and the pronounced homology with their eukaryotic counterparts indicates they originate from the cellular proteome (Pang et al., 2001, van Strien et al., 1997); their expression ratios could be quantified in uninfected samples at different cell concentrations (data not shown).

Figure 5.1B, C and D represent the overall proteome classification according to the gene ontology (GO) vocabulary. For an unbiased compilation, GO terms for the 648 protein identifications were directly retrieved from the online resource *i*ProClass (Wu et al., 2001) and the 15 most abundant terms in each class are shown without further curation. 576 were assigned to at least one molecular function, 408 to at least one cellular component and 497 to one biological process, while 368 were retrieved that belong to three categories. On the whole, the assigned categories are dominated by components of the translation machinery (ribosomal proteins, translation factors), followed by metabolic enzymes. Noteworthy, the proteome distribution across molecular functions and

cellular components is substantially more heterogeneous than in the GO Process category, highlighting the higher degree of hierarchization in the former classes. Also, the number of different biological processes retrieved is much higher, mirroring the total number of terms available to date in each class. This indicates that the proteome here presented, though certainly incomplete, achieves a certain level of comprehensiveness.

Unfortunately, an enrichment analysis of GO annotations across the different database species is hindered by incomplete sequence information. For example, it is assumed that the *S. frugiperda* EST libraries contain at least 35% of the potential total gene number (Nègre et al., 2006); however, it is the ribosomal proteins that have mostly been confidently annotated (Landais et al., 2003), explaining why 51 of the 69 identified proteins in this study are ribosomal. The complete set of proteins with NCBI identifiers, species, PIRSF and GO assignments will be published as electronic supplementary material to the accompanying paper.

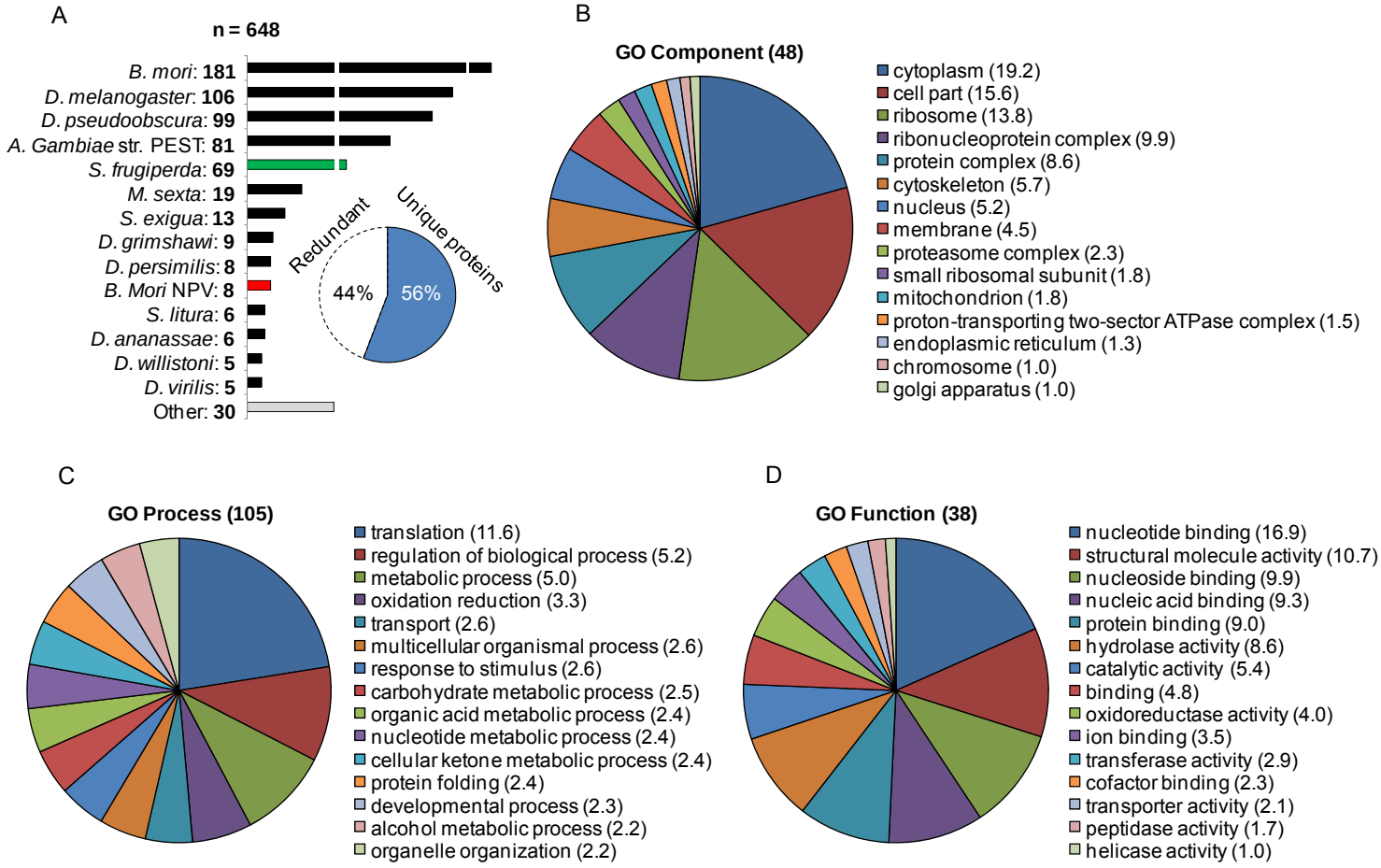
A
n = 648
B. mori: 181
D. melanogaster: 106
D. pseudoobscura: 99
A. Gambiae str. PEST: 81
S. frugiperda: 69
M. sexta: 19
S. exigua: 13
D. grimshawi: 9
D. persimilis: 8
B. Mori NPV: 8
S. litura: 6
D. ananassae: 6
D. willistoni: 5
D. virilis: 5
Other: 30
Redundant
Unique proteins
44%
56%
B
GO Component (48)
cytoplasm (19.2)
cell part (15.6)
ribosome (13.8)
ribonucleoprotein complex (9.9)
protein complex (8.6)
cytoskeleton (5.7)
nucleus (5.2)
membrane (4.5)
proteasome complex (2.3)
small ribosomal subunit (1.8)
mitochondrion (1.8)
proton-transporting two-sector ATPase complex (1.5)
endoplasmic reticulum (1.3)
chromosome (1.0)
golgi apparatus (1.0)
C
GO Process (105)
translation (11.6)
regulation of biological process (5.2)
metabolic process (5.0)
oxidation reduction (3.3)
transport (2.6)
multicellular organismal process (2.6)
response to stimulus (2.6)
carbohydrate metabolic process (2.5)
organic acid metabolic process (2.4)
nucleotide metabolic process (2.4)
cellular ketone metabolic process (2.4)
protein folding (2.4)
developmental process (2.3)
alcohol metabolic process (2.2)
organelle organization (2.2)
D
GO Function (38)
nucleotide binding (16.9)
structural molecule activity (10.7)
nucleoside binding (9.9)
nucleic acid binding (9.3)
protein binding (9.0)
hydrolase activity (8.6)
catalytic activity (5.4)
binding (4.8)
oxidoreductase activity (4.0)
ion binding (3.5)
transferase activity (2.9)
cofactor binding (2.3)
transporter activity (2.1)
peptidase activity (1.7)
helicase activity (1.0)

**Figure 5.1.** Species distribution and classification of a draft *Sf*9 proteome. (A) A total of 648 protein hits were retrieved from an insect subset of the NCBI non-redundant database. Due to high interspecies homology, some hits correspond to the same protein identified from different organisms. An estimated 56% correspond to unique PIRSF designations, indicating approximately 361 different proteins. (B) (C) (D) Proteome classification according to the gene ontology (GO) vocabulary. A total of 48 Component, 105 Process and 38 Function terms were manually retrieved from the online resource *i*ProClass. The 15 most abundant terms in each class are shown. As each protein is generally assigned to more than one term, the percentage of proteins in each term is shown instead of total number to avoid redundancy.

### 4.2. Stable isotope labeling and quantitative analysis of protein expression ratios

*Sf*9 cells were cultured for at least 6 passages in customized medium where Arg and Lys have been replaced by their respective heavy isotope counterparts ($^{13}$C)-Arg ("Arg 6") and ($^{13}$C$^{15}$N)-Lys ("Lys 8"). In parallel, cultures in light media were maintained as a control. The feasibility of performing SILAC in this cell line was confirmed by comparable average duplication times (22-24 h), high viability (>90%) and normal morphology. To assess the effect of culture growth and recombinant *Ac*MNPV infection on the cellular proteome, a full factorial design of 2×2 comparisons was applied, whereby cells were grown and infected with a high MOI at both low (1.5-2×10$^6$ cell/mL; LCC) and high (4-4.5×10$^6$ cell/mL; HCC) cell concentrations (Figure 5.2). In infection experiments, cells were harvested at 6 hpi.

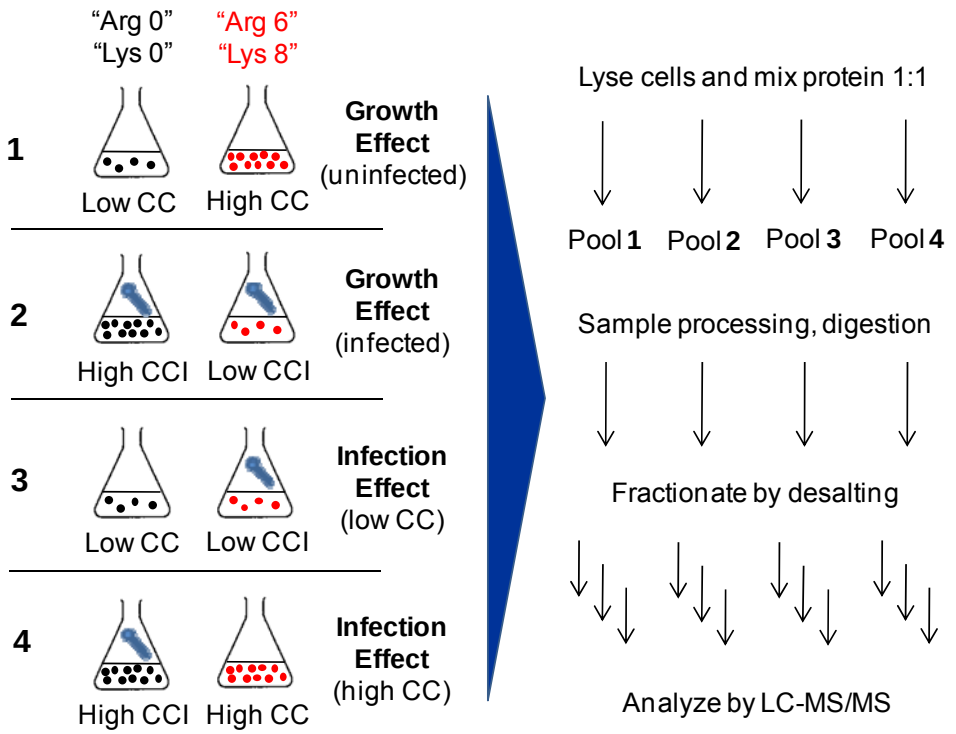


**Figure 5.2.** Schematic representation of the SILAC experimental design. For each comparison, cells maintained in unlabeled medium and medium labeled with heavy Arg ("Arg 6") and heavy Lys ("Lys 8") were grown to the desired cell density (CC) and infected (CCI) when appropriate. Protein extracts were mixed in equal amounts and subject to further processing until LC-MS/MS analysis.

A preliminary analysis of expected mass shifts of "Arg 6" and "Lys 8" clearly revealed the presence of unlabelled peptides. This was further confirmed by monitoring isotope incorporation into the proteome of the unmixed protein extracts Figure 5.3A). Incorporation efficiency was, on average, slightly over 50% after 21 cell duplications, and did not improve by an additional passage, suggesting that equilibrium was reached. We also performed cultures in media lacking Arg, Lys or both amino acids, and observed that the cells maintained high viability and the growth rates achieved in all media were comparable to those obtained when using

medium containing both amino acids at 1.35 mM (data not shown). However, there is a possibility that the culture medium contains undefined amino acid sources derived from plant or yeast hydrolysates, which are essential for cell growth and infection efficiency. In view of this, the primary heavy-to-light isotope ratios (R) were mathematically corrected with the measured ratios of incorporated label (Ri) in a protein-specific manner, adapting the method described in Liao et al. (2008). With this procedure (outlined in Figure 5.3B), the distribution of the resulting set of corrected SILAC ratios (Rc) can be centered around 1 (for simplicity, this is shown only for the comparison between uninfected and infected cultures at LCC, Figure 5.3C). Deviations of individual proteins are more likely to reflect biological variability than different turnover rates, given the high number of cell duplications. Between 68% and 75% of the proteins quantified in each of the 4 comparisons could be covered by this procedure. The remaining proteins were excluded to preserve quantitative accuracy.

Since all cultures were performed in triplicates, for each average R and Ri an associated standard deviation (S.D.) was calculated for most of the proteins. Naturally, each of these ratios constitutes a source of experimental error and biological variability in the calculation of Rc. The question therefore is whether the previously applied mathematical correction of the SILAC ratios introduces additional data variability by means of error amplification. It could lead one to assume that a statistical outlier has biological significance, or produce a distribution of corrected ratios that is too spread out, hampering the identification of differentially expressed proteins. To investigate this, a sensitivity analysis of Rc with respect to R and Ri was performed (Figure 5.3D). It can be seen that the lower the efficiency of label incorporation is, the more the error amplifies in the corrected ratios, increasing asymptotically for very low R, while being negligible for very high values. This heterogeneity is given by the

non-linearity of the correction and correlates well with the experimentally propagated S.D. of Rc.

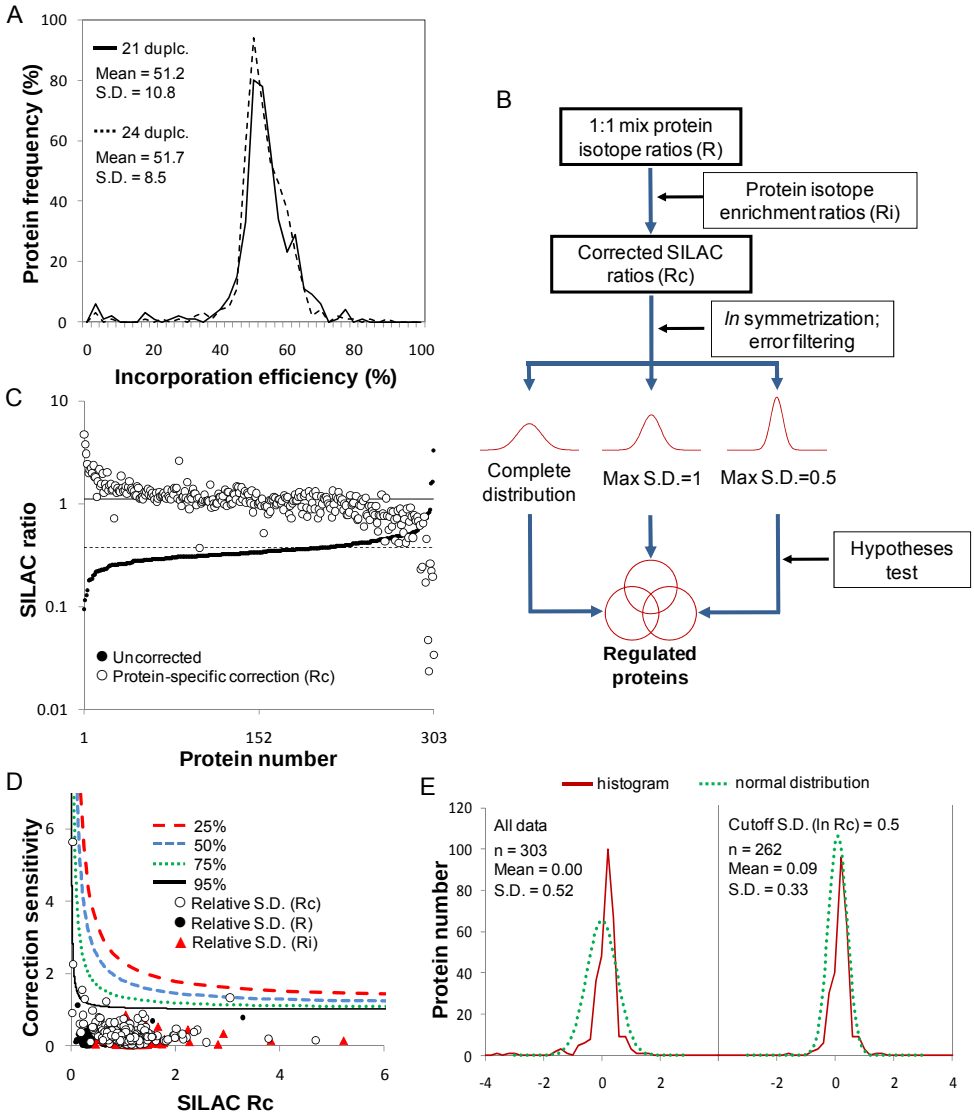


**Figure 5.3.** Correction and statistical analysis of SILAC ratios based on suboptimal label incorporation. (A) The proteome enrichment with heavy Arg and Lys was monitored after 21 and 24 cell duplications by analyzing unmixed protein extracts from labeled cultures. (B) Flow chart of the data analysis methodology. Briefly,

protein isotope ratios directly obtained from LC-MS/MS analysis of 1:1 mixed labeled/unlabeled cultures (R) are corrected in a protein-specific manner with the respective isotope enrichment ratios (Ri). The resulting set of corrected SILAC ratios (Rc) reflecting differential expression within each experimental comparison is symmetrized by logarithmic transformation and fitted with a Gaussian curve. In parallel, the unbiased standard deviations (S.D.) from triplicate experiments of R and Ri are propagated into standard deviations of Rc. Data distributions are then constructed by filtering out ratios with S.D. (*ln* Rc) values larger than 1 or 0.5, yielding more focused Gaussian fittings. For each distribution, differentially expressed proteins are defined as being different than the average by a *t*-test with at least 95% confidence. The combined set of proteins arising from the 3 distributions is considered to be regulated in the particular experimental comparison. (C) Protein-specific and global correction of ratios obtained from uninfected and infected cultures at LCC. (D) The introduction of data variability by the mathematical operation was investigated by performing a sensitivity analysis of Rc. (E) Added variability in the final *ln*-transformed distribution of Rc is substantially reduced after applying a 0.5 maximum S.D. cutoff (shown for the uninfected/infected comparison at LCC). Equations and definitions are available in Materials and Methods.

As hypothesized, the distribution of *ln*-transformed ratios after correction in the uninfected/infected comparison at LCC is too outspread (Figure 5.3E, left panel). In order to obtain a more focused normal fitting, the original data distribution was successfully decomposed by considering only proteins with S.D. (*ln* Rc) values lower than 1 or 0.5 (Figure 5.3B and E, right panel). For the proteins that lacked an experimental S.D. in R, Ri or both, an estimation was calculated considering the average relative S.D. of the remaining proteins. This error filtering methodology allowed a considerable reduction in data variability, with comparable results obtained for the other 3 experimental comparisons.

For each transformed SILAC ratio distribution, a protein was considered to be differentially expressed when *ln* Rc was different from the average by a *t*-test with at least 95% confidence. This definition accounts simultaneously for the overall dispersion of the data as well as for the propagated S.D. associated with each corrected protein ratio, thus avoiding arbitrary definitions based only on location (Coombs et al., 2010; Lam et al., 2010; Liao et al., 2008; Mannová et al., 2006). For each protein, a different number of replicates (*n*) exists for uncorrected and incorporation ratios, those proteins that pass the test for the higher *n* value, but not for the lower one, were considered differentially expressed only if they lie outside of the bulk 95% of the data (Average ± 1.96 S.D.). This was also done for those proteins lacking a replicate for either R, Ri or both. Only protein ratios lying outside 68% of the distribution were considered to have biological relevance (Average ± S.D.). The combined set of proteins with statistically significant expression changes from the unfiltered and filtered distributions is considered to be the regulated sub-proteome for each experimental comparison (Figure 5.3B).

### 4.3. Global assessment of growth- and infection-regulated proteins

As previously stated, two experimentally different sources of information regarding the impact of growth and infection on the cellular proteome are available. Yet, infection and growth constitute physiological “treatments” with substantially different strengths (comparing for instance the viral-induced halt in cell division with the cell density-associated decrease of growth rate). In the presence of experimental error and biological variability, their interacting effect can significantly obscure the assessment of how growth affects the cell proteome when comparing two infected cultures at different cell densities, for which reason we considered only

uninfected cells in this case. Direct comparison of two infected cultures at different cell densities was carried out to discriminate possible changes in the expression levels of early baculovirus proteins. On the other hand, the infection effect was evaluated not just separately for LCC and HCC cultures, but also globally by pooling together as “infection replicates” the six experimental comparisons performed in both conditions. Those proteins identified as differentially expressed from this pool will form a subset that has higher associated confidence.

According to the statistical analysis described, a total of 13, 14, 14 and 9 proteins had significantly changed expression caused by culture growth, infection (globally), infection at LCC and infection at HCC, respectively (detailed quantitative and statistical information will be published electronically as supplementary material to the accompanying paper). Not surprisingly, some proteins only emerged as differentially expressed after applying S.D. filters to the distributions, hidden by the high variability in the original data sets (Figure 5.4). In addition, the only viral protein with significantly changed expression levels detected in this study was the late expression factor LEF3, found to be more expressed following infection at LCC than at HCC.

We also carried out a comparative analysis of the overall quantification results in the various experimental settings. The subsets of corrected SILAC ratios simultaneously quantified for the “treatment” pairs Growth/Infection (globally) and Infection (LCC)/Infection (HCC) were standardized and plotted against each other (Figure 5.5A and B). It is clear that proteins considered to be regulated only by one condition either have large S.D. values or locate close to the average, hence suggesting they were regulated in only one case. This is particularly interesting when infections at LCC and HCC are contrasted, since the absence of statistical

significance in one of the conditions that is not due to high associated S.D. suggests an underlying cell density effect on baculovirus infection. Nevertheless, viral infection is not expected to have an opposed effect on expression of any given protein at different cell densities. This is confirmed by our data since when a protein is less expressed at LCC, it is not significantly over expressed at HCC, and *vice versa*.

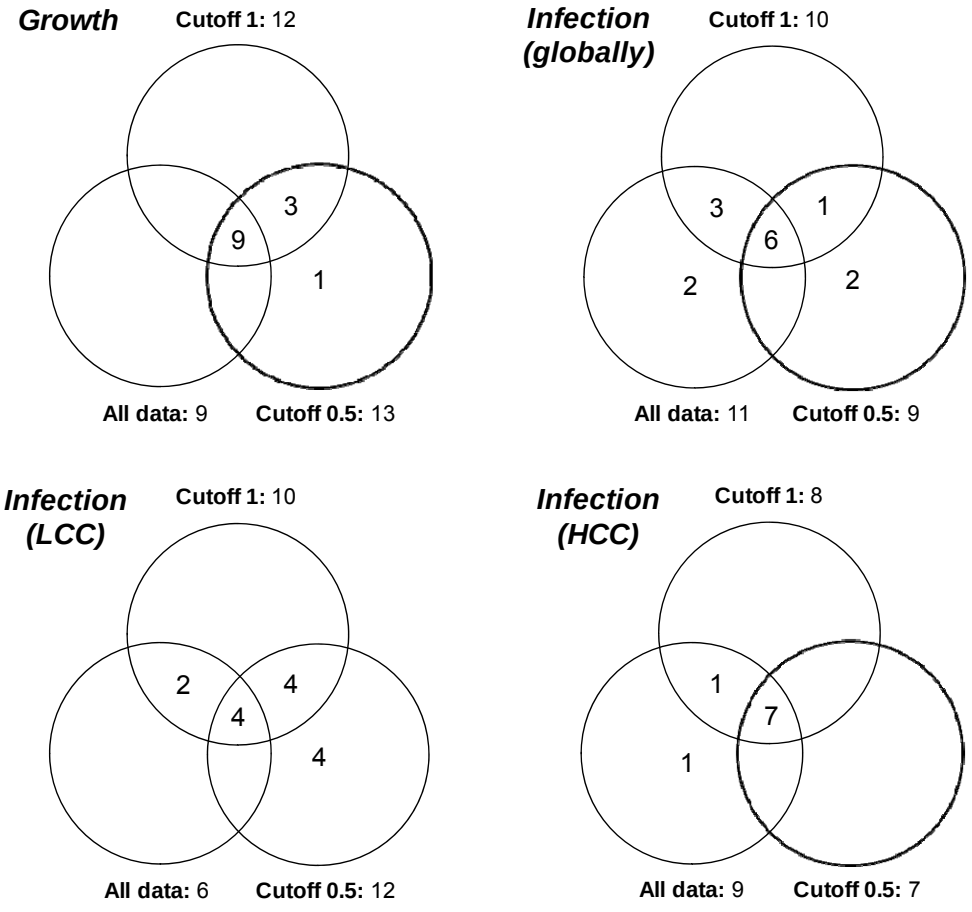


**Figure 5.4.** Allocation of differentially expressed proteins for each experimental comparison after the application of S.D. (*ln* Rc) cutoffs to data distributions.

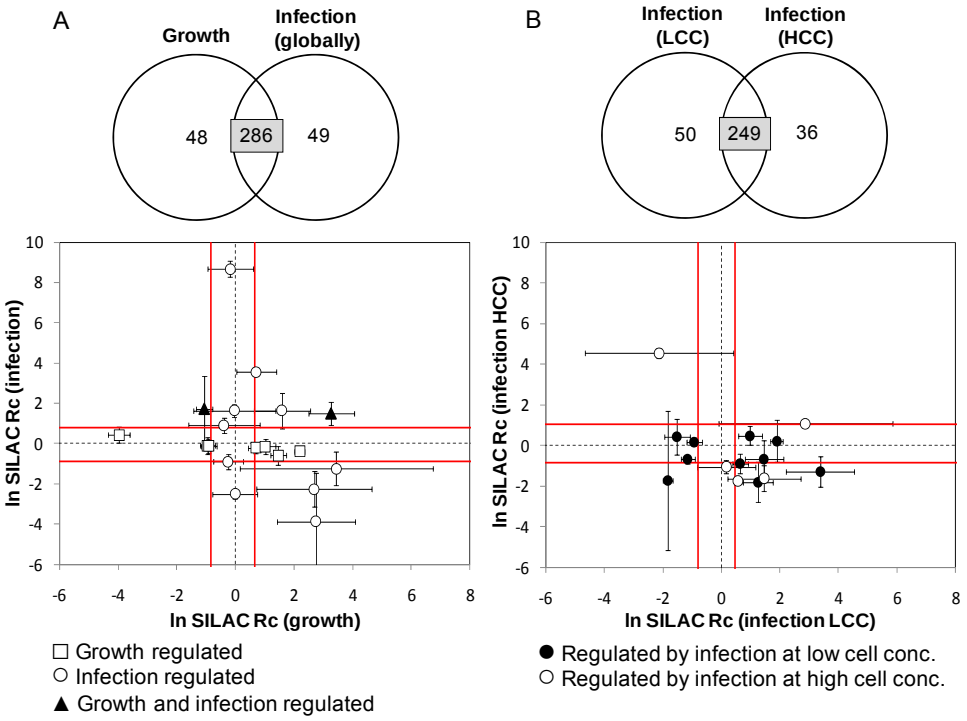


**Figure 5.5.** Comparative analysis of simultaneously quantified proteins in the various experimental settings. Standardization of the *ln*-transformed corrected ratios was performed against the respective unfiltered distributions. Error bars presented for differentially expressed proteins correspond to propagated S.D. values from triplicate experiments. The vicinity of the average distributions is delimited by Average ± S.D. of the more focused distribution in each case (cutoff S.D. (*ln* Rc) = 0.5), after standardizing as above. (A) (B) Comparative analyses of 286 and 249 proteins simultaneously quantified for the treatment pairs Growth/Infection (globally) and Infection (LCC)/Infection (HCC), respectively. Proteins considered to be regulated only by one condition are highlighted so they can be easily tracked in the other condition. For simplicity, statistically unmeaning or unregulated proteins are not shown.

### 4.4. Regulatory modulations associated with culture growth and early baculovirus infection

Cellular proteins with changed expression levels across the 4 experimental comparisons were grouped according to their potential physiological roles in growth and infection (Figure 5.6). In conformity with the statistical analysis described, evaluating the relative strength of regulation among different proteins based directly on the corrected SILAC ratios could be misleading, due to the associated S.D. values. Thus, a simple code indicating up- or down-regulation was chosen to reflect the directional change.

Of the metabolic enzymes suggested to be regulated during culture growth, dihydrolipoyl dehydrogenase (E3 subunit of the mitochondrial PDH complex) and aldehyde dehydrogenase (ALDH, conversion of alcohols to carboxylic acids) are known to fuel energetic metabolism and were overexpressed at high cell densities. In contrast, several enzymes involved in different metabolic pathways were less expressed at HCC (6-phosphogluconate dehydrogenase – PGDH, malic enzyme - ME, S-adenosyl-L-homocysteine hydrolase – SAHCH and hydroxysteroid dehydrogenase - HSDH), consistent with the typical slowdown of growth along culture time. In particular, decreased fluxes through ME were already observed in Chapter II. Also relevant was the increased expression of the 70-KDa heat shock protein 5 (HSP70-5 or BiP), a resident ER factor that is up-regulated during the unfolded protein response (UPR) triggered by various cell stresses. Other changes associated with signaling pathways include down-regulation of a GTPase, the catalytic subunit of protein phosphatase 1 (PP1c) and the increased expression of tumor necrosis factor receptor (TNFR)-associated protein 1, the later being involved in the transmission of apoptotic signals. Changes were also observed in some ribosomal proteins.

A total of 11 cellular proteins were differentially expressed at the same time for the global infection assessment and either of the LCC or HCC infection conditions, showing consistent regulation in all cases. This indicates that gross quantitative errors are not present in our study. In terms of metabolic enzymes, PDH-E3 and ALDH were upregulated in at least one infection condition, underlying the importance of the energetic metabolism for baculovirus replication assessed in Chapter II and III. In opposition to culture growth, SAHCH was overexpressed after infection, an enzyme involved in methionine degradation and possibly associated with increased viral replication (Chapter IV). An interesting observation was the down-regulation of glycogen phosphorylase (GP) upon viral expression, an enzyme responsible for glycogen degradation and thus potentially important as an additional energy source. However, the apparent contradiction is in agreement with the fact that GP is repressed by dephosphorylation through PI3K-Akt signaling, a pathway stimulated very early in infection and shown to be essential for replication of baculoviruses and other DNA viruses (Buchkovich et al., 2008; Xiao et al., 2010). This suggests a compromise between positive and negative outcomes from viral manipulation of functionally branched cellular pathways.

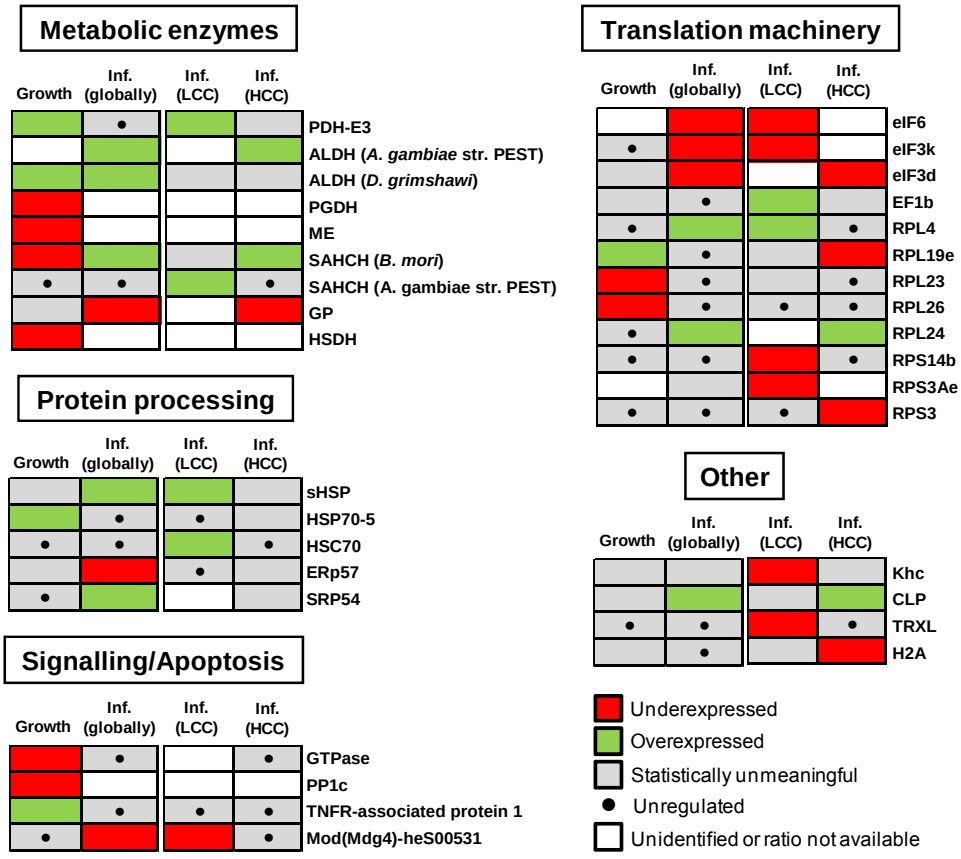


**Figure 5.6.** Differentially expressed proteins during growth and baculovirus infection. Under- or over-expression imply statistical significance as described in the text. Proteins suggested to be unregulated locate within Average ± S.D of the respective distributions (cutoff S.D. (*ln* Rc) = 0.5).

In terms of protein processing pathways, the up-regulation of HSP chaperones (sHSP, HSC70) has been associated with several viral infections, including *Ac*MNPV (Nobiron et al., 2003; Salem et al., 2011), most likely as a result of UPR initiation. Strikingly, our data indicates that central UPR effectors HSP70-5 and ERp57 are not over-expressed after infection, the later being even repressed, suggesting a previously unknown active role of *Ac*MNPV genes in the modulation of ER stress. This is

consistent with the observed up-regulated signal recognition particle SRP54, involved in targeting newly synthesized polypeptides for processing in the ER. The protein Mod(Mdg4)-heS00531, under expressed in this study, is part of the gypsy chromatin insulator complex and can trigger apoptosis by a specific pathway known to be blocked by baculovirus IAP and P35 proteins (Harvey et al., 1997). Other interesting discoveries concern the modulation of proteins involved in cytoskeleton motility, underscoring its importance for the viral life cycle, and the down-regulation of a thioredoxin-like protein (TRXL) involved in oxidative stress, among histone H2B and several translation initiation factors.

Finally, of the proteins suggested to be only regulated by infection at LCC, the physiological roles of HSC70, Mod(Mdg4)-heS00531 and TRXL may imply limitations to baculovirus replication during high cell density culture. Moreover, the lower levels of LEF3 detected following infection at HCC, compared to cells infected at LCC, are consistent with the lower baculovirus progeny produced after infection at HCC when compared with LCC (Chapters I-III): LEF3 is one of 6 virally encoded genes (called replicative LEFs) that essential for DNA replication (Okano et al., 2006).

## 5. DISCUSSION

In this work, a comprehensive SILAC-based proteome analysis of the popular *Sf*9 cell factory was presented. The effect of baculovirus infection and culture growth on the cellular proteome was investigated to gain insights into regulatory modulations associated with a productive infection cycle, thus relevant from both the virological and bioprocess points of view. Despite not having a complete genome sequence for this insect species, homology-based mass spectra interpretation gave the framework for

genome-wide data extraction from limited knowledge. Inarguably, reanalyzing the data generated against a complete *S. frugiperda* database would unravel many more important players in this complex molecular interaction.

The analysis of differentially expressed proteins in SILAC experiments is straightforward when an almost complete incorporation (>95%) of heavy amino acids in cellular proteins is possible. However, atypical growth behavior of certain cellular types may complicate or completely prevent this ideal scenario (Gruhler et al., 2005; Liao et al., 2008). Compared to mammalian cells, the metabolic capacity for amino acids biosynthesis in insect cell lines is less known, with reports pointing to a greater flexibility (Adam et al., 2005; Doverskog et al., 1997). Our results are not conclusive on this point given the presence of undefined amino acids sources in serum-free culture medium. Alternative chemically defined media for growth of *S. frugiperda* cell lines require supplementation with serum or yeastolate. Cell adaptation to a minimal supplementation of these components could be cumbersome and induce alterations to normal culture behavior, affecting the infection cycle. Furthermore, serum dialysis was recently shown to induce marked changes in the proteomes and phosphoproteomes of several mammalian cell lines, despite the generalized practice (Imami et al., 2010). Instead of invasive cell culture manipulation, the mathematical correction of the primary SILAC ratios with experimentally measured enrichment ratios can be profitably applied to analyze industrially relevant culture conditions, while preserving quantitative accuracy. Further, the statistical implications of this procedure were thoroughly analyzed and a process to circumvent added variability in the final data sets caused by error amplification was described, which would otherwise preclude the identification of several proteins with changed expression levels. This bears

relevance for studies where for various reasons complete protein labeling is not attainable.

Our study was conducted at 6 hpi to assess cellular proteomic modulations associated with the establishment of infection, which will ultimately determine the outcome in terms of viral replication and recombinant protein expression. At this stage in the infection cycle, Nobiron et al. (2003) and Salem et al., (2011) showed most host transcript levels are not pronouncedly changed (an exception is HSC70, which was increased), suggesting a post-translational regulation. Here we report protein expression changes in several cellular pathways. For example, three metabolic enzymes are shown to be up-regulated after infection, emphasizing the dependency of baculovirus replication on cell metabolism. In particular, a higher TCA cycle activity driven by an efficient glycolytic bridge (PDH-E3) and anaplerotic feeding of carboxylic acids (ALDH) is important for efficient energy generation and diversion of substrates to lipid biosynthesis. This agrees with the increased productivities obtained when organic acids are supplemented to the culture along with infection (Chapter III). Other viruses were also found to actively modulate energetic and anabolic pathways (Diamond et al., 2010; Munger et al., 2008), collectively contributing to the view that viruses behave as natural metabolic engineers, instead of representing a simple metabolic burden (Maynard et al., 2010).

The induction of energetic metabolism as a response to culture growth was also observed, a phenomenon previously described to be associated with a low proliferative, quiescent physiological state (Heiden et al., 2009), and which represents an apparent paradox in relation with the mentioned negative cell density effect on baculovirus replication. However, this can be explained by a concomitant growth-associated repression of anabolic processes (for instance PGDH and ME decreased in this study) and

reduced substrate uptake rates as can be seen in Chapter I and II, consistent with an overall lower metabolic rate.

The early up-regulation of HSC70 and the related sHSP after LCC infection (but not HCC) indicate a disturbance of ER homeostasis known to be associated with viral infection. Interestingly, we observed expression changes in two proteins that together are counterintuitive with an activation of UPR, namely decreased levels of the chaperone ERp57, a central UPR effector also involved in $Ca^{2+}$ homeostasis, and the polypeptide transporter SRP57. These findings suggest that, through unknown mechanisms, baculoviruses are able to take advantage of ER stress while avoiding negative effects associated with UPR, probably in different ways than already described for other viruses (Lucas et al., 2001; Tardif et al., 2005). Failure to induce HSC70 expression at HCC infection can mean less ER capacity for viral protein processing and thus less baculovirus progeny.

Also interesting are the decreased levels of TRXL (only after LCC infection), since human thioredoxin (TRX) related proteins are known to integrate signals and prevent apoptosis from ER, oxidative and mitochondrial stresses. This complexity draws further curiosity into the strategies that different viruses have evolved to manipulate the cell for their advantage. For instance, the endogenous human T-cell leukemia retrovirus type I was shown to promote cell growth through elevation of TRX levels, while the apoptotic HIV infection is associated with decreased TRX expression (Masutani et al., 2005). In contrast, Popham et al. (2010) observed unaltered levels of TRXL in the lepidopteran *Heliothis virescens*, although at very late times after *Ac*MNPV infection. More relevant, however, is the discovery that the multifaceted early P35 protein also acts as an antioxidant by quenching ROS (Sah et al., 1999), reinforcing the fact that an induction of oxidative stress is only observed late in infection (Wang

et al., 2001). One hypothesis is that this additional role of P35 compensates for decreased TRXL levels in preventing oxidative stress-induced apoptosis early in infection. Alternatively, the possibility of a direct viral-mediated regulation of TRXL levels concurs with unaltered levels of this protein following HCC infection, when viral replication is less efficient. An involvement of P35 in the modulation of TRXL, as it seems conclusive in the case of Mod(Mdg4)-heS0053, remains to be elucidated.

The role of LEF3 as a key determinant of a productive infection cycle is suggested by its lower expression at HCC compared to LCC infections. Noteworthy, a recent study has demonstrated that silencing of the replicative LEFs (including LEF3) during AcMNPV infection not only blocks viral DNA replication and late gene expression, but also prevents the induction of apoptosis and shutoff of cellular protein synthesis in *S. frugiperda* cells (Schultz and Friesen, 2009). Hence, this protein can be a potential target to overcome the negative cell density effect on baculovirus production (Chapters I-III). Moreover, one may speculate a link between energetic metabolism and the differential accumulation of other viral-encoded proteins in regulating the level of baculovirus replication and recombinant protein expression.

Finally, among changed expression levels in several translation factors and ribosomal proteins, we found diminished levels of kinesin heavy chain (Khc), a tubulin motor protein, and up-regulation of a calponin-like protein (CLP), an inhibitor of myosin ATPase activity, which in turn is an actin motor protein. These observations suggest baculoviruses reorganize the cytoskeleton not only through actin polymerization (Goley et al., 2006; Ohkawa et al., 2010), but possibly also by regulating other proteins to enhance their own intracellular transport.

In conclusion, as a hypotheses generation tool, this proteomic study offers new insights and potential research targets for a better understanding of the complex *Ac*MNPV infection cycle. One exciting point remains to be discriminating active modulations induced by the virus and the natural cellular response to infection. The complete resolution of this puzzle will probably require complementary information from targeted, scale-down experiments and other high-throughput assessments of protein-protein, protein-DNA and protein phosphorylation networks. From a distinct perspective, our data highlights possible regulatory bottlenecks associated with the described cell density effect on viral replication. This is one of few examples where large-scale quantitative proteomics was used with a focus on improved performance of an animal cell factory, in the scope of Systems Biotechnology. In a broader sense, this work provides a case-study of the application of advanced omic technologies in poorly characterized organisms.

## ACKNOWLEDGEMENTS

The authors want to acknowledge Marco Patrone, André Almeida, Vicente Bernal, Ana Teixeira and Catarina Brito for fruitful discussions and for revising the paper. This work was partially supported by the European Project BACULOGENES (FP6 LHSB-CT-2006-037541) and CLINIGENE-NoE (FP6 LSHB-CT-2004-018933). NC acknowledges Fundação para a Ciência e a Tecnologia (FCT) for his Ph.D. grant (SFRH/BD/36676/2007).

## REFERENCES

Acharya A, Sriram S, Sehrawat S, Rahman M, Sehgal D, Gopinathan KP (2002) *Bombyx mori* nucleopolyhedrovirus: Molecular biology and biotechnological applications for large-scale synthesis of recombinant proteins. *Curr Sci* **83**: 455-465

Adam P, Gütlich M, Oschkinat H, Bacher A, Eisenreich W (2005) Studies of the intermediary metabolism in cultured cells of the insect *Spodoptera frugiperda* using $^{13}C$- or $^{15}N$-labelled tracers. *BMC Biochem* **6**: 24

Beidler DR, Tewari M, Friesen PD, Poirier G, Dixit VM (1995) The baculovirus p35 protein inhibits Fas- and tumor necrosis factor-induced apoptosis. *J Biol Chem* **270**: 16526-16528

Buchkovich NJ, Yu Y, Zampieri CA, Alwine JC (2008) The TRORrid affairs of viruses: effects of mammalian DNA viruses on the PI3K-Akt-mTOR signaling pathway. *Nat Rev Microbiol* **6**: 266-275

Carstens EB, Tija ST, Doerfler W (1979) Infection of *Spodoptera frugiperda* cells with *Autographa californica* nuclear polyhedrosis virus. I. Synthesis of intracellular proteins after virus infection. *Virology* **99**: 386-396

Coombs KM, Berard A, Xu W, Krokhin O, Meng X, Cortens JP, Kobasa D, Wilkins J, Brown EG (2010) Quantitative analyses of influenza virus-infected cultured human lung cells. *J Virol* **84**: 10888-10906

Diamond DL, Syder AJ, Jacobs JM, Sorensen CM, Walters K-A, Proll SC, McDermott JE, Gritsenko MA, Zhang Q, Zhao R, Metz TO, Camp II DG, Waters KM, Smith RD, Rice CM, Katze MG (2010) Temporal proteome and lipidome profiles reveal hepatitis C virus-associated reprogramming of hepatocellular metabolism and bioenergetics. *PLoS Pathog* **6**: e1000719

Doverskog M, Ljunggren J, Öhman L, Häggström L (1997) Physiology of cultured animal cells. *J Biotechnol* **59**: 103-115

Eng JK, McCormack AL, Yates III JR (1994) An approach to correlate tandem mass spectral data of peptides with amino acid sequences in a protein database. *J Am Soc Mass Spectrom* **5**, 976-989

Goley ED, Ohkawa T, Mancuso J, Woodruff JB, D'Alessio JA, Cande WZ, Volkman LE, Welch MD (2006) Dynamic nuclear actin assembly by Arp2/3 complex and a baculovirus WASP-like protein. *Science* **314**: 464-467

Gruhler A, Schulze WX, Matthiesen R, Mann M, Jensen ON (2005) Stable isotope labeling of *Arabidopsis thaliana* cells and quantitative proteomics by mass spectrometry. *Mol Cell Proteomics* **4**: 1697-1709

Grula M, Buller PL, Weaver RF (1981) α-Amanitin-resistant viral RNA synthesis in nuclei isolated from nuclear polyhedrosis virus-infected *Heliothis zea* larvae and *Spodoptera frugiperda* cells. *J Virol* **38**: 916-921

Harvey AJ, Bidwai AP, Miller LK (1997) Doom, a product of the *Drosophila mod(mdg4)* gene, induces apoptosis and binds to baculovirus inhibitor-of-apoptosis proteins. *Mol Cell Biol* **17**: 2835-2843

Heiden MGV, Cantley LC, Thompson CB (2009) Understaning the Warburg effect: the metabolic requirements of cell proliferation. Science **324**: 1029-1033

Imami K, Sugiyama N, Tomita M, Ishihama Y (2010) Quantitative proteome and phosphoproteome analyses of cultures cells based on SILAC labeling without requirement of serum dialysis. *Mol Biosyst* **6**: 594-602

Lam YW, Evans VC, Heesom KJ, Lamond AI, Mathews DA (2010) Proteomics analysis of the nucleolus in adenovirus-infected cells. *Mol Cell Proteomics* **9**: 117-130

Landais I, Ogliastro M, Mita K, Nohata J, López-Ferber M, Duonor-Cérutti M, Shimada T, Fournier P, Devauchelle G (2003) Annotation pattern of ESTs from *Spodoptera frugiperda* Sf9 cells and analysis of the ribosomal protein genes reveal insect-specific features and unexpectedly low codon usage bias. *Bioinformatics* **19**: 2343-2350

Liao L, Park SK, Xu T, Vanderklish P, Yates III JR (2008) Quantitative proteomic analysis of primary neurons reveals diverse changes in synaptic protein content in *fmr1* knockout mice. *Proc Natl Acad Sci* **105**: 15281-15286

Lucas M, Karrer U, Lucas A, Klenerman P (2001) Viral espace mechanisms – escapology taught by viruses. *Int J Exp Pathol* **82**: 269-286

Mann M (2006) Functional and quantitative proteomics using SILAC. *Nat Rev Mol Cell Biol* **7**: 952-958

Mannová P, Fang R, Wang H, Deng B, McIntosh MW, Hanash SM, Beretta L (2006) Modification of host lipid raft proteome upon hepatitis C virus replication. *Mol Cell Proteomics* **5**: 2319-2325

Masutani H, Ueda S, Yodoi J (2005) The thioredoxin system in retroviral infection and apoptosis. *Cell Death Differ* **12**: 991-998

Maynard ND, Gutschow MV, Birch EW, Covert MW (2010) The virus as a metabolic engineer. *Biotechnol J* **5**: 686-694

Mita K, Kasahara M, Sasaki S, Nagayasu Y, Yamada T, Kanamori H, Namiki N, Kitagawa M, Yamashita H, Yasurochi Y, Kadono-Okuda K, Yamamoto K, Ajimura M, Ravikumar G, Shimomura M, Nagamura Y, Shin-i T, Abe H, Shimada T, Morishita S, et al. (2004) The genome sequence of the silkworm, *Bombyx mori*. *DNA Res* **11**: 27-35

Munger J, Bennett BD, Parikh A, Feng X-J, McArdle J, Rabitz HA, Shenk T, Rabinowitz JD (2008) Systems-level metabolic flux profiling identifies fatty acid biosynthesis as a target for antiviral therapy. *Nat Biotechnol* **26**: 1179-1186

Nègre V, Hôtelier T, Volkoff A-N, Gimenez S, Cousserans F, Mita K, Sabau X, Rocher J, López-Ferber M, d'Alençon E, Audant P, Sabourault C, Bidegainberry V, Hilliou F, Fournier P (2006) SPODOBASE: an EST database for the lepidopteran crop pest *Spodoptera*. *BMC Bioinformatics* **7**: 322

Nobiron I, O'Reilly DR, Olszewski JA (2003) *Autographa californica* nucleopolyhedrovirus infection of *Spodoptera frugiperda* cells: a global analysis of host gene regulation during infection, using a differential display approach. *J Gen Virol* **84**: 3029-3039

Ohkawa T, Volkman LE, Welch MD (2010) Actin-based motility drives baculovirus transit to the nucleous and cell surface. *J Cell Biol* **190**: 187-195

Okano K, Vanarsdall AL, Mikhailov VS, Rohrmann GF (2006) Conserved molecular mechanisms of the Baculoviridae. *Virology* **344**: 77-87

Olsen JV, de Godoy LM, Li G, Macek B, Mortensen P, Pesch R, Makarov A, Lange O, Horning S, Mann M (2005) Parts per million mass accuracy on an Orbitrap mass spectrometer via lock mass injection into a C-trap. *Mol Cell Proteom* **4**: 2010–2021

Ooi BG, Miller LK (1988) Regulation of host RNA levels during baculovirus infection. *Virology* **166**: 515-523

Pang Y, Yu J, Wang L, Hu X, Bao W, Li G, Chen C, Han H, Hu S, Yang H (2001) Sequence analysis of the *Spodoptera litura* multicapsid nucleopolyhedrovirus genome. *Virology* **287**: 391-404

Popham HJR, Grasela JJ, Goodman CL, McIntosh AH (2010) Baculovirus infection influences host protein expression in two established insect cell lines. *J Insect Physiol* **56**: 1237-1245

Prikhod'ko EA, Miller LK (1997) Role of baculovirus IE2 and its RING finger in cell cycle arrest. *J Virol* **72**: 684-692

Ramachandran A, Bashyam MD, Viswanathan P, Ghosh S, Kumar MS, Hasnain SE (2001) The bountiful and baffling baculovirus: the story of polyhedrin transcription. *Curr Sci* **81**: 998-1010

Sah NK, Taneja TK, Pathak N, Begum R, Athar M, Hasnain SE (1999) The baculovirus antiapoptotic p35 gene also functions via an oxidative-dependent pathway. *Proc Natl Acad Sci USA* **96**: 4838-4843

Salem TZ, Zhang F, Xie Y, Thiem S (2011) Comprehensive analysis of host gene expression in *Autographa californica* nucleopolyhedrovirus-infected *Spodoptera frugiperda* cells. *Virology* **412**: 167-178

Scheper GC, Vries RGJ, Broere M, Usmany M, Voorma HO, Vlak JM, Thomas AAM (1997) Translational properties of the untranslated regions of the p10 messenger RNA of *Autographa californica* multicapsid nucleopolyhedro-virus. *J Gen Virol* **78**: 687–696

Schultz KLW, Friesen PD (2009) Baculovirus DNA replication-specific expression factors trigger apoptosis and shutoff of host protein synthesis during infection. *J Virol* **83**: 11123-11132

Tardif KD, Waris G, Siddiqui A (2005) Hepatitis C virus, ER stress, and oxidative stress. *Trends Microbiol* **13**: 159-163

van Oers MM, van der Veken LTJN, Vlak JM, Thomas AAM (2001) Effect of baculovirus infection on the mRNA and protein levels of the *Spodoptera frugiperda* eukaryotic initiation factor 4E. *Insect Mol Biol* **10**: 255-264

van Strien EA, Faktor O, Hu ZH, Zuidema D, Goldbach RW, Vlak JM (1997) Baculoviruses contain a gene for the large subunit of ribonucleotide reductase. *J Gen Virol* **78**: 2365-2377

Wang Y, Oberley LW, Murhammer DW (2001) Evidence of oxidative stress following the viral infection of two lepidopteran insect cell lines. *Free Radic Biol Med* **31**: 1448-1455

Wu CH, Nikolskaya A, Huang H, Yeh L-SL, Natale DA, Vinayaka CR, Hu Z-Z, Mazumder R, Kumar S, Kourtesis P, Ledley RS, Suzek BE, Arminski L, Chen Y, Zhang J, Cardenes JL, Chung S, Castro-Alvear J, Dinkov G, Barker WC (2004) PIRSF: family classification system as the Protein Information Resource. *Nucleic Acids Res* **32**: 112-114

Wu CH, Xiao C, Hou Z, Huang H, Barker WC (2001) *i*ProClass: an integrated, comprehensive and annotated protein classification database. *Nucleic Acids Res* **29**: 52-54

Xiao W, Yang Y, Weng Q, Lin T, Yuan M, Yang K, Pang Y (2010) The role of the PI3K-Akt signal transduction pathway in *Autographa californica* multiple nucleopolyhedrovirus infection of *Spodoptera frugiperda* cells. *Virology* **391**: 83-89

# Discussion

## TABLE OF CONTENTS

## 1. BACULOVIRUS VECTORS BIOPROCESSING AND THE CELL DENSITY EFFECT

The work presented in this thesis focuses on the optimization of baculovirus vectors (BV) productivity in *Sf*9 cultures. Optimization of virus-based bioprocesses is a daunting task due to the number of culture parameters affecting product delivery. When to infect, how many infectious particles to be added and what medium composition to use are amongst the important questions that need to be answered to achieve an efficient bioprocess.

Our results support previous observations that, in order to obtain a productive infection, cells must be infected at an early stage of growth if no additional manipulations are performed, owing to the so-called cell density effect (Chapter I). In the literature, the optimal inflection point in the culture growth curve, referred to as the optimal peak cell density, is defined as the cell density which gives the greatest product formation under synchronous (high MOI) infection (Aucoin et al., 2010; Wong et al., 1996). Since infections at low MOI lead to subsequent culture growth, the peak cell density is higher than the actual CCI, explaining why the cell density effect is apparently "delayed" when infections are performed at high MOI. In these conditions, we could obtain the highest specific BV yield at CCI $2\times10^6$ cells/mL (2475 IP/cell), decreasing thereafter at CCI $3\times10^6$ cells/mL to 2060 IP/cell; otherwise, a step decline in BV specific yields was observed already at CCI $2\times10^6$ cells/mL with a low MOI.

In strike contrast to previous suggestions (Bédard et al., 1994; Weiss et al., 1992), nutrient depletion could not explain the decrease in productivity associated with high cell density infections, even though medium exchange significantly improved BV yields. In fact, neither of the analysed medium components (including sugars and amino acids) was depleted during infected cultures, whereas toxic by-product accumulation has been shown

not to be an issue in *Sf*9 cells (Bédard et al., 1993; Drews et al., 2000; Öhman et al., 1995; Öhman et al., 1996). These observations clearly indicate more complex mechanisms underlie the cell density effect, probably a means to control population size that is regulated by constitutively secreted autocrine/paracrine factors, which are screened out after medium replenishment (Doverskog et al., 1997; Doverskog et al., 2000). An in-depth analysis of cellular metabolism during culture growth and its response to infection is therefore needed.

Although specific aspects of *Sf*9 cells physiology in culture can be found dispersed among several reports (Bhatia et al., 1997; Doverskog et al., 1997; Drews et al., 2000; Ferrance et al., 1993; Ikonomou et al., 2003), to date a comprehensive analysis of cellular metabolism and its response to infection has not been conducted. To gain a quantitative understanding, a metabolic flux analysis (MFA) model of this cell line capable of describing metabolic shifts occurring at different cell densities and also as a result of baculovirus infection was developed (Chapter II). Supported by extensive experimental data, the model revealed metabolic modulations associated with cellular energetics and the redox state; namely, a decrease in central metabolic activity (glycolysis, tricarboxylic acids (TCA) cycle) and energetic output (cellular respiration and ATP synthesis) was observed along culture growth. In terms of post-infection metabolism, it was found that viral infection exerts a positive effect on the metabolic activity at an early stage of culture growth, which fails to occur when infections are performed at high cell densities. Furthermore, a positive dose-response trend could be observed for different MOIs at low cell density; for instance, cellular respiration increased only 6% after low MOI infection but soared 63% when a high MOI was used. This suggests that the post-infection metabolic state is actively regulated during the BV life-cycle at low cell density. Overall, these findings correlated well with our previous production results, pointing

for a strong association between per cell BV yields and the cellular energetic state.

Hypothesizing that the energetic state of the cells is a feasible controlling constraint for the production of BVs, we engaged in the selection of targeted strategies to improve BV productivity at high cell density, attempting to meet viral vector delivery requirements associated with clinical gene therapy (Chapter III). It was demonstrated that one-time supplementation of 12 mM pyruvate or 12 mM α-ketoglutarate, along with infection of 0.1 IP/cell, is able to boost an increase in specific viral yields at high cell density of up to 7 fold, reaching volumetric quantities of infectious particles significantly higher than those obtainable by infection at a lower cell concentration ($12.2\pm3.6\times10^7$ IP/mL and $6.6\pm2.8\times10^7$ IP/mL, respectively). A low MOI was used since it allows for the highest BV amplification, at the same time minimizing the expenditure of viral stocks. The intrinsic mechanism of this cost-effective approach comprised the direct stimulation of energetic pathways as demonstrated by MFA, while the supplementation of amino acids, lipids or even a complete medium additive did not restore cell specific productivity. Together with our previous observations, this further brings down the classical nutrient exhaustion explanation for the cell density effect. Also, because carboxylic acids supplementation bypasses most of the peripheral nutrient utilization routes, it is consistent with the possible negative regulation of metabolic activity by cell secreted factors. Finally, since a stimulation of energetic output is oxygen demanding, the positive results obtained in spinner vessels demonstrate that oxygen was not the primary cause for poor productivities at high cell densities.

Other biological systems have been affected by a negative cell density effect on productivity, including viral-based systems (Nadeau and Kamen,

2003; Ferreira et al., 2005) and microorganisms (Yoon et al., 2003). Interestingly, in Ferreira et al. (2005), the cell density effect on a human 293 cell line producing a recombinant adenovirus was assessed in oxygen-controlled bioreactors and productivity could not be enhanced by the simple replenishment of limiting nutrients, whereas it could be improved by changing to non-ammoniagenic medium. Considering the highly efficient carbon utilisation and physiological robustness of *Sf*9 cells, the work developed in this thesis demonstrates that the complexity of the cell density effect goes beyond the basic bioprocess variables, nutrient availability and by-product formation, and was successful in generating an hypothesis leading to a dramatic increase in specific productivity. However, the direct extrapolation of this strategy to other animal cell systems, including those used in stable expression, should be considered with care, as it depends on an efficient glycolysis-TCA cycle bridge, which is significantly impaired in the majority of mammalian cell lines (Doverskog et al., 1997; Petch and Butler, 1994). Beyond previous efforts in alleviating this bottleneck through cell engineering strategies (Chen et al., 2001; Irani et al., 1999), a complete reprogramming of carbon usage would be a significant breakthrough for mammalian cell culture, possibly leading to unprecedented levels of specific productivity.

One important question that was not addressed in the previous chapters but that was also analyzed in this thesis is the effect of energetic stimulation on recombinant protein production. Given that virus replication is correlated with viral gene expression, supplementation of pyruvate or α-ketoglutarate should in principle exert a positive effect on protein production as well. However, our results with a BV expressing the recombinant vp7 rotavirus capsid glycoprotein show a very modest effect when compared to the improvement seen in BV specific yields (Figure D.1). These results are likely related to the very-late, *polh*-driven expression of

the recombinant proteins, overlapping a phase prior to cell lysis during which most of the cell activity, including protein processing pathways, is quickly deteriorating (Chapter V; van Oers et al., 2001).

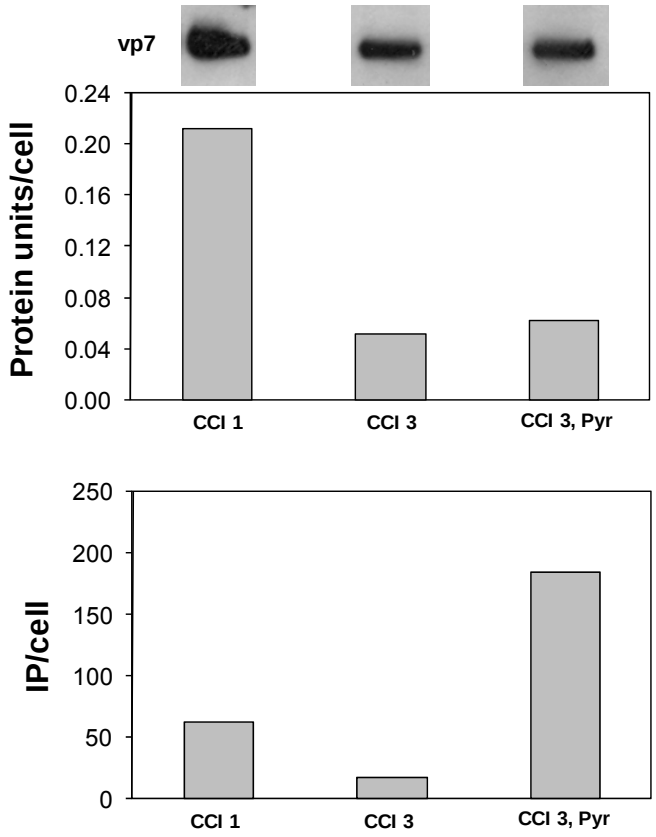


**Figure D.1.** Effect of cell density and pyruvate supplementation on recombinant vp7 and BV production. Cultures were infected at a concentration of $1\times10^6$ cells/mL (CCI 1) or $3\times10^6$ cells/mL (CCI 3) with a MOI of 0.1 IP/cell. 12 mM of pyruvate were added at infection time as previously described (Chapter III).

## 2. THE BACULOVIRUS-*SF*9 CELL AS A SYSTEM: HYBRID METABOLIC MODELING AND OMIC-BASED HYPOTHESES GENERATION

The need to understand and manipulate cellular systems for increased biosynthesis of target products has been a consistent focus of research, more recently supported supported by the huge flows of data being obtained at different cellular levels. Likely the near future will witness a substantial growth in cell-wide resources for a variety of organisms with biotechnological interest (Otero and Nielsen, 2010); in particular, the expansion of annotated genomes and omic technologies downstream of gene expression profiling should progressively close the gap with the phenotype, enabling combined analysis of different layers of information. At the same time, it is clear that simply accumulating data will not directly translate into dependable strategies for optimization, since the link between the molecular traits and the desired phenotypic properties would still remain a black box. The real challenge will be to incorporate these data into mechanistic systems enabling accurate prediction of cell behaviour in response to perturbations, which can be exploited for forward cell engineering. However, our knowledge so far only grants us the possibility to have 'hybrid cellular models', as detailed mechanistic understanding of specific cell processes can only be connected at a higher level by multivariate statistical/mining methods, filling the gaps in our understanding of regulatory phenomena (Ideker and Lauffenburger, 2003; Ortega et al., 2008; Teixeira et al., 2007; Tomita, 2001).

In the context of the present thesis, we were interested in the possibility of developing a predictive tool able to quantitatively link metabolic flux distributions and BV production beyond simple empirical inspection. This was attempted by integrating MFA with partial least squares (PLS) regression into a hybrid (statistical) metabolic flux analysis framework as a

valuable complement to purely stoichiometric models for the optimization of complex productivity phenotypes (Chapter IV). This modeling effort was applied to the same small-scale metabolic network developed in Chapter II, although being readily scalable to genome-wide metabolic reconstructions, when available. Model calibration was based on the data accumulated in the previous chapters, and we were able to predict the importance of the TCA cycle fluxes and mitochondrial respiration as pathways strongly associated with viral replication. This was then validated using only a subset of preliminary experiments to pinpoint the same determinant pathways, while predicting the productivity of independent cultures within measurement error. Therefore, the positive effect of supplementing pyruvate or α-ketoglutarate could have been suggested not by an observational hypothesis, but as a result of model prediction. Though still far from the ultimate objective of developing a comprehensive global cellular model, the contribution presented herein proved to be valuable in harnessing the central metabolism for improved productivity in this system. Given a preliminary set of experimental data, hybrid MFA should also be straightforwardly applicable to other insect and mammalian production systems, including stable recombinant protein expression, for the design of customized optimization strategies.

Taking a different Systems Biology approach, Chapter V describes an attempt to apply advanced omic technologies in the baculovirus-*Sf*9 cell system as high-throughput hypotheses generating tools. As briefly mentioned in the Introduction section, there is a “macroscopic” gap between genomic annotation, gene expression profiling and cell function, whereby regulatory phenomena at multiple levels modulate the information flow inside the cell. For instance, quantitative inconsistencies between mRNA and protein levels have been reported before (Liao et al., 2008; Seth et al., 2007). For this reason, we opted to quantitatively analyze the *Sf*9

proteome during culture growth and as a response to BV infection. The challenge here was not only to identify a large-scale *Sf*9 proteome, constrained by the unavailability of a genome sequence and annotation for *S. frugiperda*, but also to assure the accuracy of protein expression changes. In fact, quantitative accuracy is a fundamental issue in the generality of large-scale or high-throughput measurement techniques, particularly in the context of the omic sciences (see Wolfinger et al., 2001). Overall, homologs of 361 non-redundant proteins were identified from 31 insects and 2 baculoviruses, representing the opening block for an organized *S. frugiperda* proteome. Through stable isotope labelling with amino acids in cell culture (SILAC) and a thorough statistical analysis of biological replicates, we were able to confidently discriminate differentially expressed proteins due to growth or infection, including several proteins related to energy metabolism, endoplasmic reticulum stress and oxidative stress, which can be effective targets for the design of improved bioprocesses. In particular, the viral-induced up-regulation of enzymes involved in energy metabolism (dihydrolipoyl dehydrogenase and aldehyde dehydrogenase) further confirmed the induction of these pathways found in terms of reaction flux at low cell density (Chapter II). Another meaningful result of this study was the suggestion that, based on the relative quantification of the viral protein LEF3, the differential accumulation of BV-encoded proteins early in infection at different cell densities could play a role in the cell density effect. The mechanism involved is that the expression of early proteins determines the level of viral DNA replication and recombinant protein expression later in the infection cycle (Lin et al., 2001; Ramachandran et al., 2001).

The collective proteome data generated does not clarify the overall molecular mechanisms underlying the cell density effect, but complement our previous findings in providing a few target proteins whose expression is

influenced by culture growth and baculovirus infection, which can in turn determine viral replication and recombinant protein expression. Some unanswered question are 1) what and how cell secreted factors influence the energetic state and the growth/productivity phenotypes?; 2) What are the virus-host molecular protein-protein and protein-DNA interaction networks established upon infection? Certainly the needed fundamental understanding of these questions will depend on creating a cell-wide integration of multi-level information. As such, we expect this work to constitute a catalyst for further developments, of which a full genomic characterization would represent a major achievement. This would allow the generation of more comprehensive, genome-scale omic data, the reconstruction of a genome-scale metabolic model with increased predictive capacity, and the development of tailored molecular tools for biological discovery and cell engineering.

## 3. SYSTEMS BIOTECHNOLOGY OF ANIMAL CELLS: A COMPROMISE BETWEEN WHAT IS POSSIBLE AND WHAT IS DOABLE

The application of systems biology in bioprocess optimization has been previously set forth by several authors. For instance, Lee et al. (2005) described it in this way: “Systems biotechnology will have an increasing impact on industrial biotechnology in the future. All steps of biotechnological development, from up-stream (strain, cell and organism development) and mid-stream (fermentation and other unit operations) to down-stream processes, will benefit significantly by taking systems biotechnological approaches.” Since such an all-inclusive approach for the systematic improvement of bioprocesses is significantly beyond what we have been accustomed to, doubts are likely not confined to the most skeptical minds; in particular, Systems Biology currently faces unsolved

challenges regarding the integrative tasks (Stephanopoulos et al., 2004). A positive argument in this regard is that computer aided design is today routinely used in other manufacturing industries, such as electrical, automotive and aircraft. Though biological systems are not a human mechanic construction, it is worth noticing that engineering systems have begun to have almost comparable complexity levels, judging by the number of components (Csete and Doyle, 2002). It is therefore expectable that the building blocks of life may also one day be simulated in their complex systems environment.

Besides these inherent challenges facing the systems biologist, a critical question in the biopharmaceutical context is the cost-effectiveness of these endeavors. In particular, the application of systems approaches in animal cells bioprocessing is constrained by the availability of database resources and the increased complexity of recombinant products, requiring deeper and wider cell state characterization (regulation of gene expression, protein processing and secretion, host-virus interactions, etc.). As pointed out in the Introductory section to this thesis, R&D spending on generating systems-level knowledge for bioprocess improvement competes for financial resources with other activities, including the development of new investigational biologicals and clinical testing, where acceptable returns on investment have been achieved to date. Even for the biosimilars business, the benefits of systems biotechnology have to clearly outpace the overall manufacturing costs pressured by market competition. Therefore, it is envisaged that companies will keep following systems biology developments mostly from the sidelines, leveraging on academic collaborations where expertise is available without taking full risk. Future breakthroughs will probably blossom first in the fields of biomedicine and drug discovery, as suggested by the recently issued “Strategic Priorities 2011-2015: Responding to the Public Health Challenges of the 21$^{st}$

Century" by the Food and Drug Administration. Nevertheless, the Systems Biotechnology laggard should also cross the end line.

## REFERENCES


Aucoin MG, Mena JA, Kamen AA (2010) Bioprocessing of baculovirus vectors: a review. *Curr Gene Ther* **10**: 174-186

Bédard C, Kamen A, Tom R, Massie B (1994) Maximization of recombinant protein yield in the insect cell/baculovirus system by one-time addition of nutrients to high-density batch cultures. *Cytotechnology* **15**: 129-38

Bédard C, Tom R, Kamen A (1993) Growth, nutrient consumption, and end-product accumulation in Sf-9 and BTI-EAA insect cell cultures: insights into growth limitation and metabolism. *Biotechnol Prog* **9**: 615-24

Bhatia R, Jesionowski G, Ferrance J, Ataai MM (1997) Insect cell physiology. *Cytotechnology* **24**: 1-9

Chen K, Liu Q, Xie L, Sharp PA, Wang DIC (2001) Engineering of a mammalian cell line for reduction of lactate formation and high monoclonal antibody production. *Biotechnol Bioeng* **72**: 55-61

Csete ME, Doyle JC (2002) Reverse engineering of biological complexity. *Science* **295**: 1664-1669

Doverskog M, Bertram E, Ljunggren J, Öhman L, Sennerstam R, Häggström L (2000) Cell cycle progression in serum-free cultures of Sf9 insect cells: modulation by conditioned medium factors and implications for proliferation and productivity. *Biotechnol Prog* **16**: 837-846

Doverskog M, Ljunggren J, Öhman L, Haggstrom L (1997) Physiology of cultured animal cells. *J Biotechnol* **59**: 103-115

Drews M, Doverskog M, Ohman L, Chapman BE, Jacobsson U, Kuchel PW, Haggstrom L (2000) Pathways of glutamine metabolism in *Spodoptera frugiperda* (Sf9) insect cells: evidence for the presence of the nitrogen assimilation system, and a metabolic switch by 1H/15N NMR. *J Biotechnol* **78**: 23-37

Ferrance JP, Goel A, Ataai MM (1993) Utilization of glucose and amino acids in insect cell cultures: Quantifying the metabolic flows within the primary pathways and medium development. *Biotechnol Bioeng* **42**: 697-707

Ferreira TB, Ferreira AL, Carrondo MJT, Alves PM (2005) Effect of reefed strategies and non-ammoniagenic medium on adenovius production at high cell densities. *J Biotechnol* **119**: 272-280

Ideker T, Lauffenburger D (2003) Building with a scaffold: emerging strategies for high- to low-level cellular modeling. *Trends Biotechnol* **21**: 255-262

Ikonomou L, Schneider YJ, Agathos SN. 2003. Insect cell culture for industrial production of recombinant proteins. *Appl Microbiol Biotechnol* **62**: 1-20

Irani, N., Wirth, M., van Den Heuvel, J. and Wagner, R., 1999. Improvement of the primary metabolism of cell cultures by introducing a new cytoplasmic pyruvate carboxylase reaction. Biotechnol Bioeng 66, 238-46

Lee SY, Lee D-Y, Kim TY (2005) Systems biotechnology for strain improvement. *Trends Biotechnol* **23**: 349-358

Liao L, Park SK, Xu T, Vanderklish P, Yates III JR (2008) Quantitative proteomic analysis of primary neurons reveals diverse changes in synaptic protein content in *fmr1* knockout mice. *Proc Natl Acad Sci* **105**: 15281-15286

Lin G, Li G, Granados RR, Blissard GW (2001) Stable cell lines expressing baculovirus P35: resistance to apoptosis and nutrient stress, and increased glycoprotein secretion. *In Vitro Cell Dev-An* **37**:293-302

Nadeau I, Kamen A (2003) Production of adenovius vector for gene therapy. *Biotechnol Adv* **20**: 475-489

Öhman L, Alarcon M, Ljunggren J, Ramqvist A-K, Häggström L (1996) Glutamine is not an essential amino acid for Sf-9 insect cells. *Biotechnol Lett* **18**: 765-70

Öhman L, Ljunggren J, Häggström L (1995) Induction of a metabolic switch in insect cells by substrate-limited fed-batch cultures. *Appl Microbiol Biotechnol* **43**: 1006-13

Ortega F, Sameith K, Turan N, Compton R, Trevino V, Vannucci M, Falciani F (2008) Models and computational strategies linking physiological response to molecular networks from large-scale data. *Phil Trans R Soc A* **366**: 3067-3089

Otero JM, Nielsen J (2010) Industrial systems biology. *Biotechnol Bioeng* **105**: 439-460

Petch D, Butler M (1994) Profile of energy metabolism in a murine hybridoma: glucose and glutamine utilization. *J Cell Physiol* **161**: 71–76

Radford KM, Reid S, Greenfield PF (1997) Substrate limitation in the baculovirus expression vector system. *Biotechnol Bioeng* **56**: 32-44

Ramachandran A, Bashyam MD, Viswanathan P, Ghosh S, Kumar MS, Hasnain SE (2001) The bountiful and baffling baculovirus: the story of polyhedrin transcription. *Curr Sci* **81**:998-1010

Seth G, Philp RJ, Lau A, Jiun KY, Yap M, Hu W-S (2007a) Molecular portrait of high productivity in recombinant NS0 cells. Biotechnol Bioeng 97: 933-951

Stephanopoulos G, Alper H, Moxley J (2004) Exploiting biological complexity for strain improvement through systems biology. *Nat Biotechnol* **22**: 1261-1267

Teixeira AP, Carinhas N, Dias JML, Cruz P, Alves PM, Carrondo MJT, Oliveira R (2007) Hybrid semi-parametric mathematical systems: bridging the gap between systems biology and process engineering. *J Biotechnol* **132**: 418-425

Tomita M (2001) Whole-cell simulation: a grand challenge for the 21st century. *Trends Biotechnol* **19**: 205-210

van Oers MM, Thomas AAM, Moormann RJM, Vlak JM (2001) Secretory pathway limits the enhanced expression of classical swine fever virus E2 glycoprotein in insect cells. *J Biotechnol* **86**: 31-38

Weiss SA, Whitford WG, Godwin GP, Reid S (1992) Media design: optimizing of recombinant proteins in serum free culture. In: Vlak JM, Schlaeger E-J, Bernard AR, editors. Workshop on Baculovirus and Recombinant Protein Production Processes, March 29-April 1, Interlaken, Switzerland

Wolfinger RD, Gibson G, Wolfinger ED, Bennett L, Hamadeh H, Bushel P, Afshari C, Paules RS (2001) Assessing gene significance from cDNA microarray expression data via mixed models. *J Comput Biol* **8**: 625-637

Wong KTK, Peter CH, Greenfield PF, Reid S, Nielsen LK (1996) Low multiplicity infection of insect cells with a recombinant baculovirus: the cell yield concept. *Biotechnol Bioeng* **49**: 659-666

Yoon SH, Han M-J, Lee SY, Jeong KJ, Yoo J-S (2003) Combined transcriptome and proteome analysis of *Escherichia coli* during high cell density culture. *Biotechnol Bioeng* **81**: 753-767

# APPENDIX

# TABLE OF CONTENTS

# 1. BIOCHEMICAL REACTIONS OF *SPODOPTERA FRUGIPERDA´*S METABOLISM

**Passive transport/diffusion**

$Glc_e$ = Glc ("e" denotes extracellular metabolite)
Lac = $Lac_e$
$Malt_e$ = Malt
$Sucr_e$ = Sucr
$Pyr_e$ = Pyr (reaction only considered in Chapter III)
$\alpha KG_e$ = αKG (reaction only considered in Chapter III)
Amm = $Amm_e$
Ala = $Ala_e$
$O_{2,e} = O_2$
$CO_2 = CO_{2,e}$

**Active (ATP-dependent) transport**

*$X_{AG}$ Transport System:*
$Asp_e$ + 1 ATP = Asp + 1 ADP
$Glu_e$ + 1 ATP = Glu + 1 ADP
*A/L Transport System:*
$Gln_e$ + 0.33 ATP = Gln + 0.33 ADP
*A Transport System:*
$Ser_e$ + 0.33 ATP = Ser + 0.33 ADP
$Asn_e$ + 0.33 ATP = Asn + 0.33 ADP
$Gly_e$ + 0.33 ATP = Gly + 0.33 ADP
$Thr_e$ + 0.33 ATP = Thr + 0.33 ADP
$Pro_e$ + 0.33 ATP = Pro + 0.33 ADP
$Met_e$ + 0.33 ATP = Met + 0.33 ADP
*L Transport System:*
$His_e$ + 0.33 ATP = His + 0.33 ADP
$Tyr_e$ + 0.33 ATP = Tyr + 0.33 ADP
$Val_e$ + 0.33 ATP = Val + 0.33 ADP
$Ile_e$ + 0.33 ATP = Ile + 0.33 ADP
$Leu_e$ + 0.33 ATP = Leu + 0.33 ADP
$Phe_e$ + 0.33 ATP = Phe + 0.33 ADP
*y+L Transport System:*
$Arg_e$ + 0.33 ATP = Arg + 0.33 ADP
$Lys_e$ + 0.33 ATP = Lys + 0.33 ADP
*$X^-_C$ Transport System:*
$Cys_e$ + 1 ATP = Cys + 1 ADP

**Glycolysis and Pentose-phosphate pathway**

Malt = Glc + G6P
Sucr + 2 ATP = G6P + F6P
Glc + ATP = G6P + ADP *(hexokinase, HK)*
G6P = F6P *(6-phospho-D-glucose isomerase, PGI)*
F6P + ATP = 2 GAP
GAP + $NAD^+$ + ADP = NADH + ATP + PEP
ADP + PEP = Pyr + ATP *(pyruvate kinase, PK)*
3 G6P + 6 $NADP^+$ = 3 $CO_2$ + 3 R5P + 6 NADPH *(pentose-phosphate pathway, PPP)*

**Pyruvate node**

Pyr + NADH = Lac + $NAD^+$ *(lactate dehydrogenase, LDH)*
Pyr + Glu = Ala + αKG *(alanine aminotransferase, AlaAT)*
Pyr + $NAD^+$ = $CO_2$ + ACoA + NADH *(pyruvate dehydrogenase, PDH)*
Mal = Pyr + $CO_2$ *(malic enzyme, ME)*

**TCA Cycle**

ACoA + OAA = Cit *(citrate synthase, CS)*
Cit + $NAD^+$ = $CO_2$ + αKG + NADH
αKG + $NAD^+$ = $CO_2$ + SuCoA + NADH (*αKG dehydrogenase, αKGDH)*
SuCoA + ADP = Suc + ATP *(SuCoA synthetase, SuCoAS)*
Suc + FAD = Fum + $FADH_2$ *(Succinate dehydrogenase, SucDH)*
Fum = Mal *(fumarase, Fum)*
Mal + $NAD^+$ = OAA + NADH *(malate dehydrogenase, MDH)*

**Amino acids metabolism**

αKG + Gln + NADH = 2 Glu + $NAD^+$ *(glutamate synthase, GOGAT)*
Glu + $NAD^+$ = αKG + Amm + NADH *(glutamate dehydrogenase, GDH)*
2 Gly + $NAD^+$ = $CO_2$ + Amm + Ser + NADH
Ser = Pyr + Amm
2 αKG + Lys + 4 $NAD^+$ + NADPH + FAD = 2 $CO_2$ + 2 Glu + 2 ACoA + 4 NADH + NADP + $FADH_2$
αKG + Leu + $NAD^+$ + ATP + FAD = $CO_2$ + Glu + 2 ACoA + NADH + ADP + $FADH_2$ + mevalonate
αKG + Ile + 2 $NAD^+$ + ATP + FAD = $CO_2$ + Glu + ACoA + SuCoA + 2 NADH + ADP + $FADH_2$
αKG + Arg + $NAD^+$ = 2 Glu + NADH + urea
Glu + OAA = αKG + Asp *(aspartate aminotransferase, AspAT)*
Thr + $NAD^+$ = ACoA + Gly + NADH

αKG + Val + 3 $NAD^+$ + ATP + FAD = $CO_2$ + Glu + SuCoA + 3 NADH + ADP + $FADH_2$
Ser + Met + $NAD^+$ + ATP = SuCoA + Amm + Cys + NADH + 2 ADP
Phe + NADH + $O_2$ = Tyr + $NAD^+$
αKG + Tyr + $O_2$ = $CO_2$ + Glu + ACoA + Fum
His = Glu + Amm
Asn = Amm + Asp (asparaginase, Asnase)
Pro + $NADP^+$ + 0.5 $O_2$ = Glu + NADPH
Cys = Pyr + Amm

**Energy Production** (respiration, ATP expenditure and redox balance)

NADH + 2.5 ADP + 0.5 $O_2$ = $NAD^+$ + 2.5 ATP
1.5 ADP + $FADH_2$ + 0.5 $O_2$ = 2.5 ATP + FAD
ATP = Energy (unidirectional flux for cell maintenance and futile cycles)
$NAD^+$ + NADPH = NADH + $NADP^+$ *(transhydrogenase, TransH*)

**Biomass Synthesis**

1000 Protein + 111 FA + 89.5 DNA + 224.7 RNA = Biomass

*Nucleic Acids*

0.5 $CO_2$ + R5P + 1.9 Gln + 1.3 Ser + 1.3 Asp + 0.7 $NAD^+$ + NADPH + 9 ATP = 1.9 Glu + 0.8 Fum + 0.8 Gly + DNA + 0.7 NADH + $NADP^+$ + 9 ADP
$CO_2$ + R5P + 1.9 Gln + Ser + 1.3 Asp + $NAD^+$ + ATP = Glu + 0.8 Fum + 0.5 Gly + RNA + NADH + ADP

*Protein Synthesis*

0.417 Ala + 0.251 Glu + 0.315 Gln + 0.432 Gly + 0.348 Ser + 0.344 Lys + 0.410 Leu + 0.213 Ile + 0.301 Arg + 0.238 Asp + 0.290 Thr + 0.305 Val + 0.109 Met + 0.162 Phe + 0.131 Tyr + 0.109 His + 0.266 Pro + 0.223 Asn + 0.142 Cys + 10.014 ATP = 1 Protein + 10.014 ADP

*Lipids metabolism*

9 AcoA + 7 NADPH + 26 ATP + 10 NADH + 1 $O_2$ = 1 FA + 7 $NADP^+$ + 26 ADP + 10 $NAD^+$

**Metabolite abbreviations**

ACoA - acetyl-coenzyme A
ADP - adenosine diphosphate
Ala - alanine
Amm - ammonia
Arg - arginine
Asn - asparagine
Asp - aspartate
ATP - adenosine triphosphate

Cit - citrate
$CO_2$ - carbon dioxide
Cys - cysteine
DNA - deoxyribonucleic acids
F6P - fructose-6-phosphate
FA - fatty acids
$FAD/FADH_2$ –-flavin adenine dinucleotide
Fum - fumarate
G6P - glucose-6-phosphate
GAP - glyceraldehyde-3-phosphate
Glc - glucose
Gln - glutamine
Glu - glutamate
Gly - glycine
His - histidine
Ile - isoleucine
Lac - lactate
Leu - leucine
Lys - lysine
Mal - malate
Malt - maltose
Met - methionine
$NAD^+$/NADH - nicotinamide adenine dinucleotide
$NADP^+$/NADPH - nicotinamide adenine dinucleotide phosphate
$O_2$ - oxygen
OAA - oxaloacetate
PEP - phosphoenolpyruvate
Phe - phenylalanine
Pro - proline
Pyr - pyruvate
R5P - ribose-5-phosphate
RNA - ribonucleic acids
Ser - serine
Suc - succinate
SuCoA - succinyl-coenzyme A
Sucr - sucrose
Thr - threonine
Tyr - tyrosine
Val - valine
αKG - α-ketoglutarate

## 2. CALCULATION OF METABOLIC PARTITIONING COEFFICIENTS AT THE PYRUVATE AND A-KETOGLUTARATE NODES

***Pyruvate node.*** To analyze flux partitioning at the pyruvate node, all intracellular fluxes leading to pyruvate formation or utilisation were considered, as estimated by metabolic flux analysis. The pyruvate uptake rate was not considered to allow comparable coefficients between the different cultures. From these reactions, only the most representative in terms of total contribution are shown.

| | | | |
|---|---|---|---|
| **Incoming fluxes** | PEP (glycolysis) | *Pyruvate kinase* (PK) | $\frac{v_{PK}}{v_{PK} + v_{ME} + v_{other}}$ |
| | Malate | *Malic enzyme* (ME) | $\frac{v_{ME}}{v_{PK} + v_{ME} + v_{other}}$ |
| **Outgoing fluxes** | Lactate | *Lactate dehydrogenase* (LDH) | $\frac{v_{LDH}}{v_{LDH} + v_{AlaAT} + v_{PDH} + v_{other}}$ |
| | Alanine | *Alanine aminotransferase* (AlaAT) | $\frac{v_{AlaAT}}{v_{LDH} + v_{AlaAT} + v_{PDH} + v_{other}}$ |
| | ACoA | *Pyruvate dehydrogenase* (PDH) | $\frac{v_{PDH}}{v_{LDH} + v_{AlaAT} + v_{PDH} + v_{other}}$ |

***α-Ketoglutarate node.*** To analyze flux partitioning at the αKG node, all fluxes leading to αKG formation or utilisation were considered. The αKG uptake rate was not considered to ensure comparable coefficients between cultures. Only the most representative in terms of total contribution are shown.

| | | | |
|---|---|---|---|
| **Incoming fluxes** | Isocitrate | *Isocitrate dehydrogenase* (ICDH) | $\frac{v_{Isocit}}{v_{ICDH} + v_{AlaAT} + v_{other}}$ |
| | Alanine | *Alanine aminotransferase* (AlaAT) | $\frac{v_{AlaAT}}{v_{ICDH} + v_{AlaAT} + v_{other}}$ |
| **Outgoing fluxes** | Glutamate | *Glutamate dehydrogenase* (GDH) | $\frac{v_{GDH}}{v_{GDH} + v_{\alpha KGDH} + v_{GOGAT} + v_{other}}$ |
| | Succinyl-CoA | *α-Ketoglutarate dehydrogenase* (αKGDH) | $\frac{v_{\alpha KGDH}}{v_{GDH} + v_{\alpha KGDH} + v_{GOGAT} + v_{other}}$ |
| | Glutamate | *Glutamate synthase* (GOGAT) | $\frac{v_{GOGAT}}{v_{GDH} + v_{\alpha KGDH} + v_{GOGAT} + v_{other}}$ |

Isocitrate and the enzyme ICDH are not explicitly considered in the metabolic model, being lumped in the following reaction: Cit + $NAD^+$ = $CO_2$ + αKG + NADH

## 3. VIRAL SYNTHESIS REACTIONS USED FOR COMPLETE MFA MODEL ESTABLISHMENT

Insect baculoviruses were considered to be composed of 77% protein and 8% DNA (Bergold and Wellington, 1954; see full reference in Chapter IV). Molar percentages of amino acids in insect viruses were taken as the average values from Wellington (1954; see full reference in Chapter IV). Each viral particle was considered to weight $1.07\times10^{-17}$ g and has a circular genome of 262000 deoxyribonucleotides.

**Lumped reaction for baculovirus synthesis**

0.000435 bvDNA + 0.001 bvProtein = 1 bvMass

("bv" denotes baculovirus component; 1 bvMass represents $10^6$ particles; the coefficients represent the nmol content of each component in $10^6$ particles)

*Viral protein synthesis*

0.00305 Ala + 0.00371 Glu + 0.00231 Gln + 0.00388 Gly + 0.00703 Ser + 0.00226 Lys + 0.00513 Leu + 0.00374 Ile + 0.01229 Arg + 0.00603 Asp + 0.00449 Thr + 0.0028 Val + 0.00167 Met + 0.0037 Phe + 0.00385 Tyr + 0.00095 His + 0.00431 Pro + 0.00336 Asn + 0.00057 Cys = 1 bvProtein

(1 bvProtein represents the pmol content of protein amino acids present in $10^6$ particles; ATP utilization was not taken into account.)

*Viral DNA synthesis*

0.5 $CO_2$ + R5P + 1.9 Gln + 1.3 Ser + 1.3 Asp + 0.7 NAD + NADPH + 9 ATP = 1.9 Glu + 0.8 Fum + 0.8 Gly + bvDNA + 0.7 NADH + NADP + 9 ADP

(1 DNA represents 1 "average" deoxyribonucleotide, considering a G/C content of 40% (The International Lepidopteran Genome Project).)

*Measured outflux of viral particles*

vBV